MAREES TERRESTRES

BULLETIN D'INFORMATIONS

INTERNATIONAL CENTER FOR EARTH TIDES
CENTRE INTERNATIONAL DES MAREES TERRESTRES

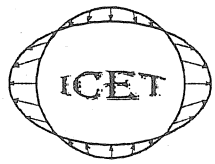

Federation of Astronomical and Geophysical Data Analysis Services
(FAGS)

International Association of Geodesy - International Gravity Field Service
(IAG – IGFS)

Publié avec le soutien de l'Observatoire Royal de Belgique

BIM
1 3 7

15 OCTOBRE 2002

Editeur: Dr. Bernard DUCARME
Observatoire Royal de Belgique
Avenue Circulaire 3
B-1180 Bruxelles

BIM 137

15 octobre 2002

Meeting of the ETC-Working Group 7 on Analysis of Environmental Data (end)

Additional Scientific Paper

Seasonal Variations of Hydrological Influences on Gravity Measurements at Wettzell

Martina Harnisch, Günter Harnisch
formerly Bundesamt für Kartographie und Geodäsie (BKG)
Richard-Strauss-Allee 11, D-60598 Frankfurt am Main

1. Introduction

During the first years of gravimeter recordings at Wettzell hydrological influences were assumed to be unimportant. Arguments were: station on a mountain top, rocky underground, water circulation only in clefts etc. However, at least since R. FALK [7] found a clear correlation between absolute gravity measurements and groundwater, there is no doubt about the presence of hydrological influences on the gravity at Wettzell (fig. 1). If the influence of groundwater variations is corrected, the scattering range of the measured absolute values decreases from more than 100 nm s^{-2} to about 50 nm s^{-2}, which much better corresponds to the expected accuracy of the FG5.

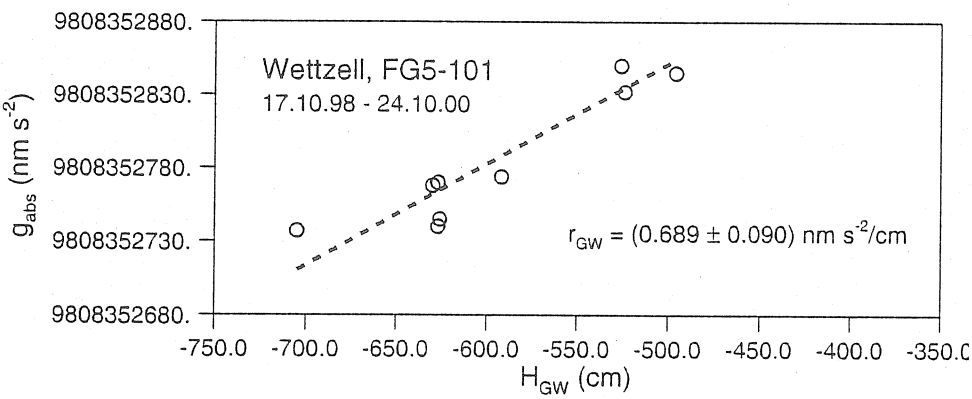

Fig. 1: Correlation between changes of the groundwater level and gravity variations, measured with the absolute gravimeter FG5-101 at Wettzell.

The changes of the groundwater level at Wettzell may reach about 4 m (fig. 2). The formal fit of a sinusoidal wave with a period of 365.25 days to the groundwater data results in an amplitude of 57.02 cm. Using a groundwater regression coefficient of 0.689 nm s^{-2}/cm (the value which was derived from the comparisons with absolute gravity measurements), the corresponding gravity variations would be near ±40 nm s^{-2}. It is clear that variations of such an amount are very dangerous for investigations of long-term gravity phenomena and that they must be taken into account and eliminated very carefully.

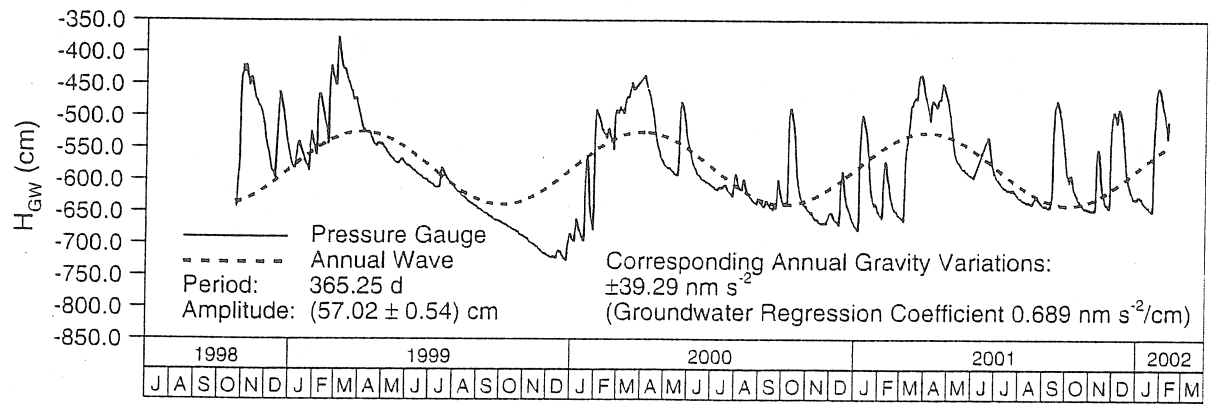

Fig. 2: Long-term changes of the groundwater level at Wettzell and the corresponding annual gravity variations.

2. Some problems of hydrological modeling in gravimetry

The infiltration of water into the underground and its redistribution are very complex processes. Because of the great economical importance there are many attempts of hydrological modeling, which aim at the estimation of water resources. Generally the fundamental equation of hydrology (equation of the water balance) is valid

$$P = R_0 + E + (A - C) \quad (1)$$

where P = precipitation, R_0 = run-off at the earth's surface, E = evaporation, A = accumulation (= increase of water in a certain area during a certain time) and C = consumption (= decrease of water in a certain area during a certain time). Each of the constituents of this equation may be influenced by different factors in different ways.

First of all the accumulation of water depends on the rocks in the underground, their state of weathering and tectonic influences (formation of clefts and cavities of different size). The run-off depends on the properties of the superficial material, the evaporation on meteorological parameters (air temperature, humidity of the air, wind) and on the plant cover, etc. In hydrologic modeling generalized input data and parameters are commonly used, which are representative for a certain area or a certain period of time.

In contrast, models for gravimetric purposes should describe with high accuracy the actual hydrologic situation in the area under consideration and its variation with time.

In view of the multitude of factors influencing the hydrologic modeling, which themselves stand for different complex processes, the following conclusions may be drawn:

- It seems to be nearly impossible to develop physically based models, which describe very accurate the actual distribution of water and soil moisture in the underground and which moreover may be realized in practice (especially with regard to the input data to be measured). Therefore for gravimetric purposes statistic models are preferred. However, such models may also be improved if basic principles of the deterministic hydrologic modeling are incorporated.

- Many of the factors mentioned above, which influence the infiltration of water and its distribution in the underground, change seasonally (e.g. precipitation, air temperature, plant cover). Therefore not only seasonal changes of the groundwater level and of the soil moisture measured at single points are to expect. Varying influences on the resulting gravimetric signal, i.e. seasonal variations of the corresponding regression coefficients are also possible.

3. Meteorological and Hydrological Data at Wettzell

Meteorological data are gathered at Wettzell since 1986. A small meteorological station continuously records air temperature, air pressure, humidity of the air, precipitation (since 1.4.1998), direction and velocity of the wind. In August 2000 a second rain sensor was added, and since December 2000 soil moisture is also recorded continuously. The soil moisture sensor (Type TRIME-EZ, accuracy ±1%) was placed in a depth of about 50 cm beneath the earth's surface. The position of the measuring points as well as that of the gravimeter building is shown in fig. 3.

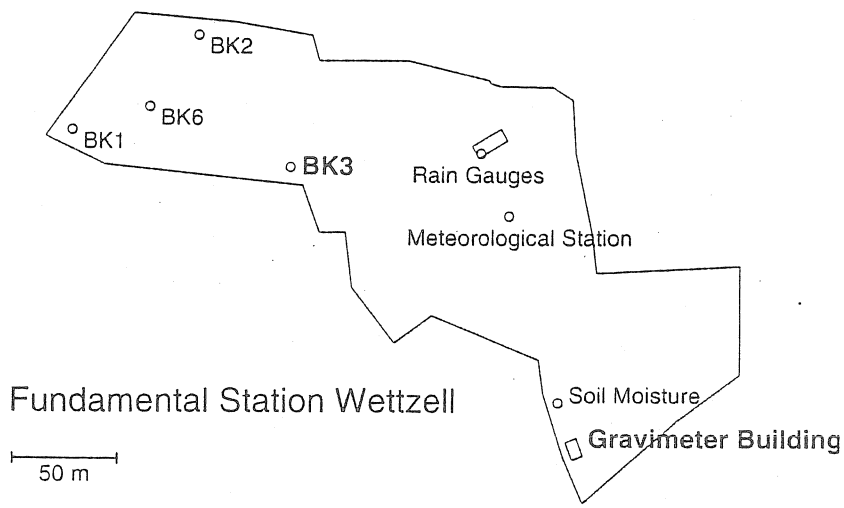

Fig. 3: Schematic map of the Fundamental Station Wettzell (Bavarian Forest, Germany).

As a part of the site investigation for the installation of the 4 × 4 m ring laser at Wettzell, several bore-holes were drilled within the station area in 1998. The first groundwater data were measured "by hand" with a light gauge. In October 1998 an automatically recording pressure gauge was installed in the bore-hole BK3. The variations of the groundwater level in the bore-holes BK1, BK2, BK3 and BK6 between August 1998 and November 1999 are shown in fig. 4. From the data of BK3 (lowermost frame) it may be seen, that there is no significant difference between the measurements by hand (small circles) and the data from the pressure gauge (solid line).

The variations of the water level in all the bore-holes are similar but not identical. The water level has its deepest position in BK1 (between -12.5 and -8.5 m) and the highest in BK6 (between -5.0 and -2.0 m). The maximum amplitudes of the level changes are also different (about 4.0 m at BK1 and 2.0 m at BK2). Finally it has to be mentioned that the most detailed variations of the groundwater level occur in BK3, while the changes in BK1 are very smooth. From these more or less general facts alone it may be concluded, that the distribution of soil moisture and groundwater in the area of the station Wettzell is very inhomogeneous and that it should be very problematic to describe the corresponding gravity effect and its variation in time by a simple deterministic (physical) model.

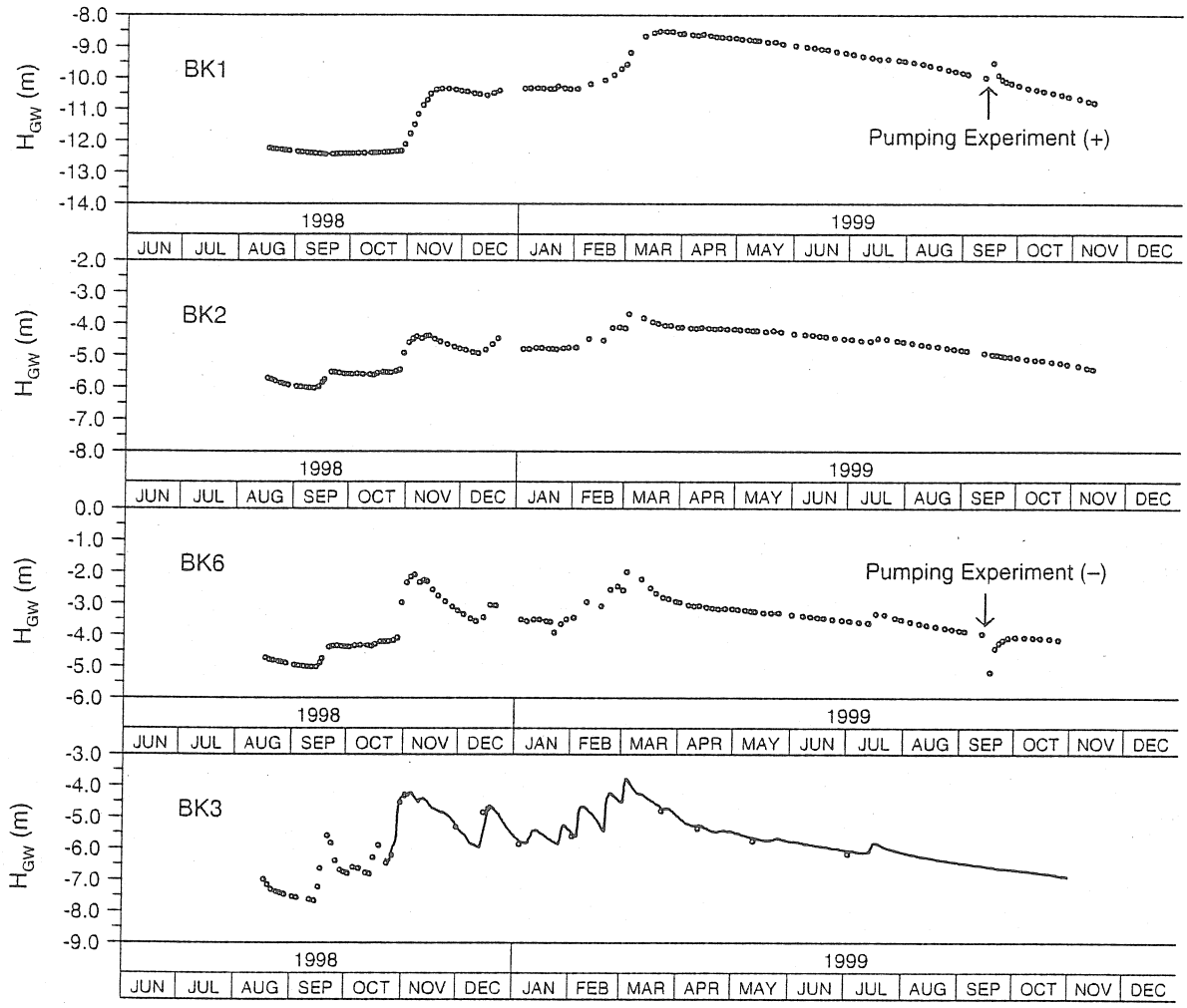

Fig. 4: Groundwater variations in the bore-holes BK1, BK2, BK3 and BK6, measured between August 1998 and November 1999 with the light gauge.

A pumping experiment gives also an idea of the complicated hydrologic situation at Wettzell. Between 15.9.1999, 13:00 CEST and 16.9.1999, 14:00 CEST about 100 m^3 water were pumped out from BK6 and injected into BK1. The pumping rate decreased from 1.2 l/s in the beginning to 1.0 l/s at the end of the experiment. After one day the water level in BK6 returned again to its original position. The gravity variations recorded by the CD029 show a clear influence of the pumping experiment. The distance from BK6 is 250 m. With a delay of 12 hours the residual gravity decreased by about 10 nm s^{-2}. On the other hand, in a distance of only 70 m from BK6 and nearly in the same direction as to the gravimeter, no clear changes of the water level occurred in BK3. If a groundwater regression coefficient r_{GW} =

0.689 nm s^{-2}/cm is assumed (derived from the absolute measurements, see above) about 15 cm had to be expected. The downward directed bulge in the air pressure is not related to the pumping experiment.

A summary of all the precipitation, groundwater and soil moisture data available at Wettzell from the beginning of the recordings up to the end of January 2002 is given in fig. 6. The groundwater data measured with the light gauge (see fig. 4) as well as the data from rain gauge RE2 were not included in the figure. The series of the rain data starts in April 1998, the groundwater data followed in October of the same year (BK3, pressure gauge). The measurements of the soil moisture started more than two years later in the end of December 2000.

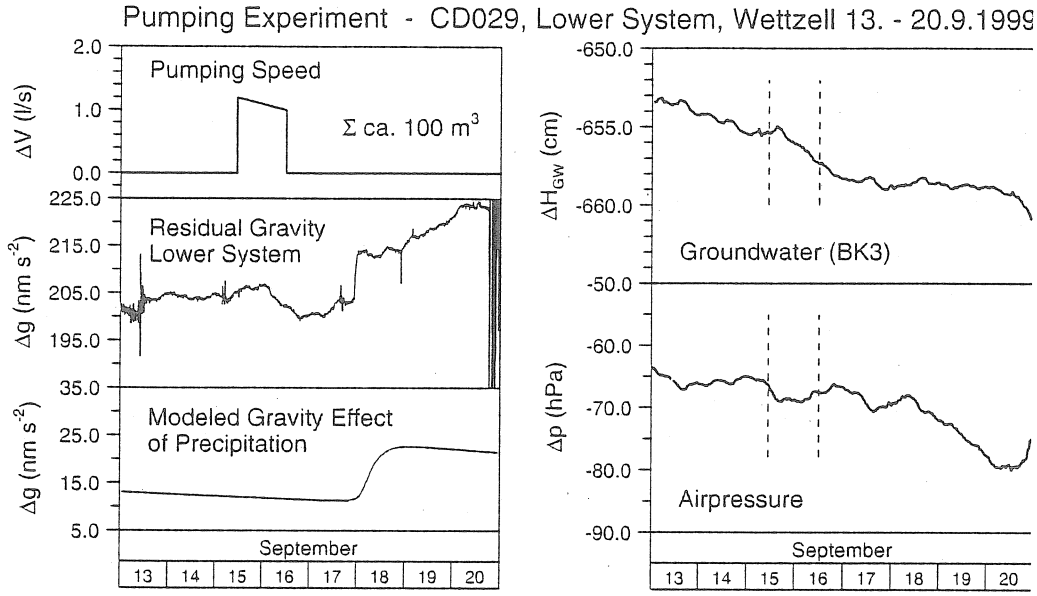

Fig. 5: Pumping experiment. In the two frames at the right the vertical broken lines mark the time of the pumping experiment.

Within the precipitation data two small sections are marked by rectangles. In both cases gaps in the precipitation data occurred which are filled up with data from the nearby power station at the Hoellenstein reservoir (in a valley about 2 km to the south-west from Wettzell, elevation difference about 200 m). Such manipulations are problematic from different points of view, but better than data gaps.

4. Preparation of the SG-Data

The investigations concerned with the influence of groundwater variations on the gravity are based on the residual gravity, derived from the recordings of the superconducting gravimeter CD029 at Wettzell. "Residual gravity" means that from the observed gravity data several "disturbing" influences are eliminated. It is of great importance, that the "right" influences are eliminated. In our case these are

- **Tides**. In the period range greater than one month the amplitude factor 1.16 has to be used, regardless of the results of the tidal analysis of local gravity data. Otherwise there is a risk, that the groundwater effect under study is partly eliminated together with the tides.
- **Air pressure**. The influence of varying air density in the atmosphere is eliminated by a linear regression model, using the local air pressure variations at the gravimeter site and an regression coefficient derived by the standard tidal analysis. More details of the air pressure model (e.g. regional air pressure distribution, deviations from the standard atmosphere) are not included.
- **Polar motion**. The gravity effect of polar motion has to be eliminated before any estimates of the instrumental drift are made. To this end IERS pole co-ordinates and the amplitude factor of 1.16 have to been used.
- **Instrumental drift**. Different constituents of the instrumental drift have to be taken into account. The exponential drift, occurring in the initial phase after the initialization of the gravimeter, has to be eliminated by fitting an exponential model. After the exponential constituents have been eliminated, the remaining long-term drift in most cases may be described by a linear model. If a suffi-

cient number of absolute measurements is available, they may be used to check the drift model derived alone from the data of the superconducting gravimeter. Commonly there is a good agreement. In the case of discrepancies the residual gravity of the SG may be fitted linearly to the AG data and in this way a corrected value of the drift rate may be found.

The data series of the CD029 is interrupted by a gap of about 6 weeks (May 5 – June 12, 1999), caused by total loss of the Helium. In the first section before the gap a strong linear drift of -136.15 nm s^{-2}/month occurred in the lower system. After a careful re-initialization the drift-rate reduced to a very low value in the section after the gap. Altogether 9 absolute measurements were available, which could be used to correct the instrumental drift. The result is shown in the uppermost frame of figure 7. Especially in the second section of the data series a clear correlation between gravity variations and changes of the groundwater level at BK3 can be recognized. Anomalies in the residual gravity can now be explained simply by strong groundwater variations, e.g. the large peak of the residual gravity in the first half of 2000.

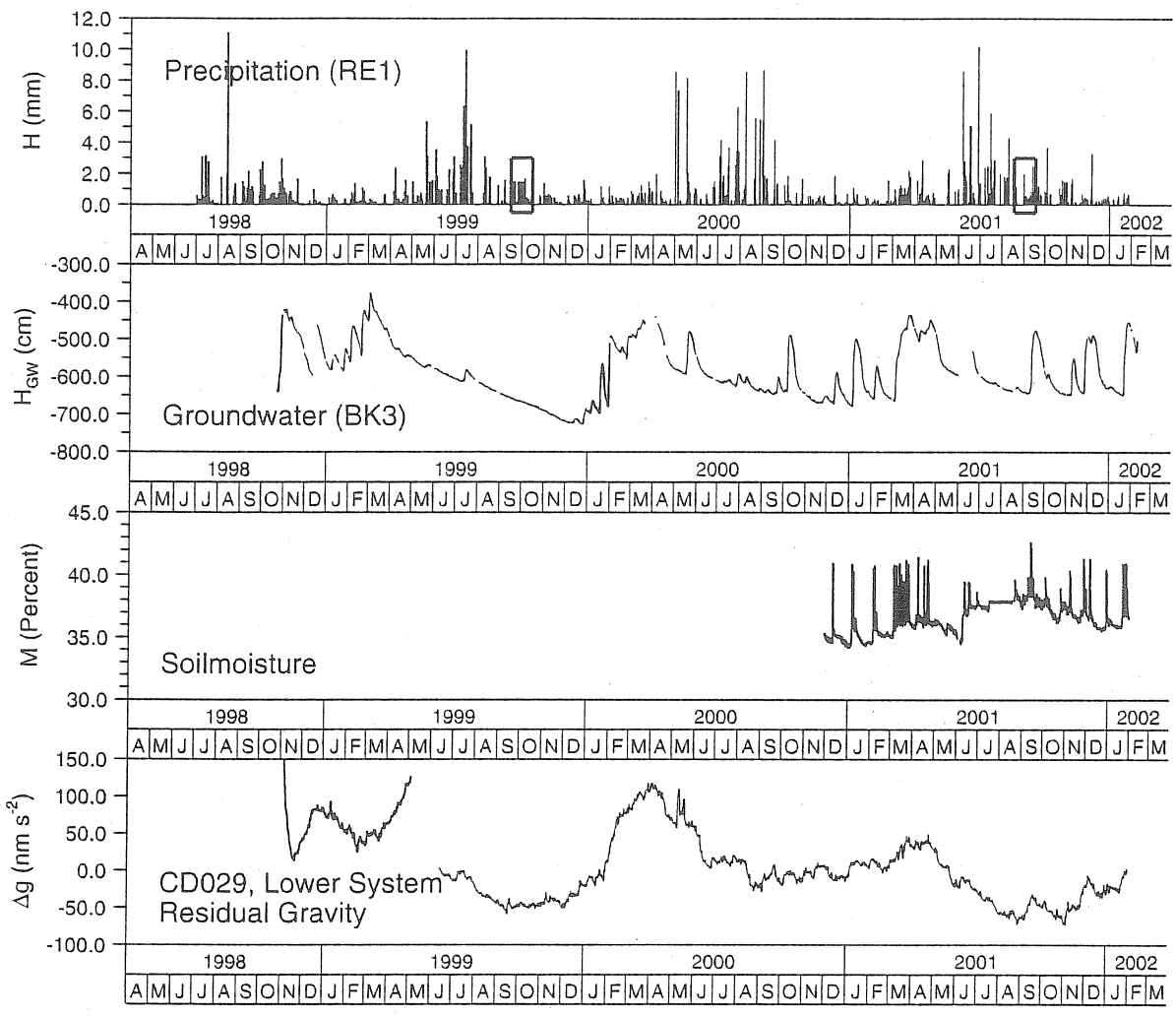

Fig. 6: Precipitation, groundwater and soil moisture at Wettzell from the beginning of the recordings up to the end of January 2002. The rectangles mark gaps in the precipitation data, which have been filled up with data from the nearby power station at the Hoellenstein reservoir.

Unfortunately the first section of the data series recorded by the CD029 is supported only by two absolute measurements. Considering moreover the very strong linear drift and the remaining residuals of the exponential constituents, it may be concluded that the gravity data before the gap are very unreliable and therefore unsuited for further investigations.

5. Correlation between precipitation and gravity

From equation (1) follows that in a closed hydrological system precipitation is the only input of water. The precipitation infiltrates and distributes in the ground. In this way changes of the groundwater level

and of the soil moisture arise. Inflow and run-off of water in the underground may change the situation in detail. However, precipitation measurements in principle provide the most important input data of hydrological modeling.

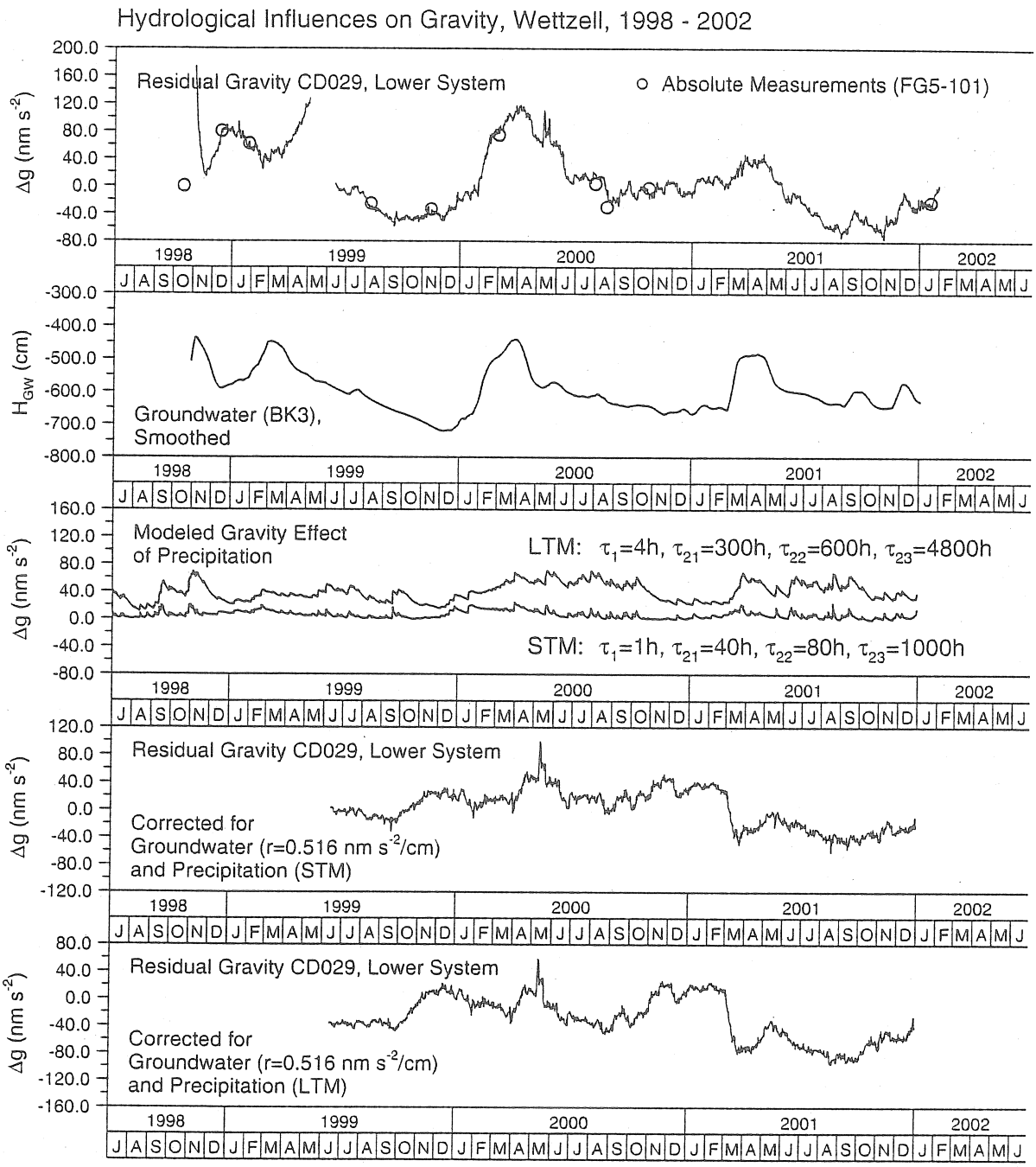

Fig. 7: Corrections for the influences of precipitation and groundwater, applied to the residual gravity of the gravimeter CD029 at Wettzell.

The rain-meter used at Wettzell counts ticks of a rocker arm. However, there is always the problem to discern from the distance between "no rain" and "no data due to a malfunction of the instrument". In every case precipitation sensors must be maintained very carefully.

Generally precipitation data may not be correlated directly with gravity changes. At first the precipitation (measured in height or volume per unit of time) has to be converted into the corresponding gravity effect. For that purpose the simple formula

$$\delta g_i = 2\pi G\rho\, r_j (1 - e^{-(i-j)/\tau_1})\, e^{-(i-j)/\tau_2} \qquad (2)$$

was used, which was proposed and very successfully applied by D. CROSSLEY et al. [2] to correct a data series recorded at Boulder. δg_i is the contribution of the precipitation r_j at the time j to the gravity change at the time i (i j). To get the total time dependent gravity effect the single δg_i have to be summed up over i and j. The time constants τ_1 and τ_2 stand for a multitude of different influences. According to the balance equation (1) τ_1 describes the accumulation, i.e. the infiltration of the precipitation into the underground, and τ_2 the consumption, i.e. the disappearance of the moisture due to evapotranspiration and downward migration. Numerical values of τ_1 and τ_2 representative for a certain station are derived by fitting the mathematical model to the observed gravity data. In [2] the values τ_1 = 4 hours and τ_2 = 91 days are given, which are valid for the local hydrological situation at Boulder. First attempts of hydrological modeling at Wettzell were done using the modified values τ_1 = 4 hours and τ_2 = 30 days [5,6 [1]].

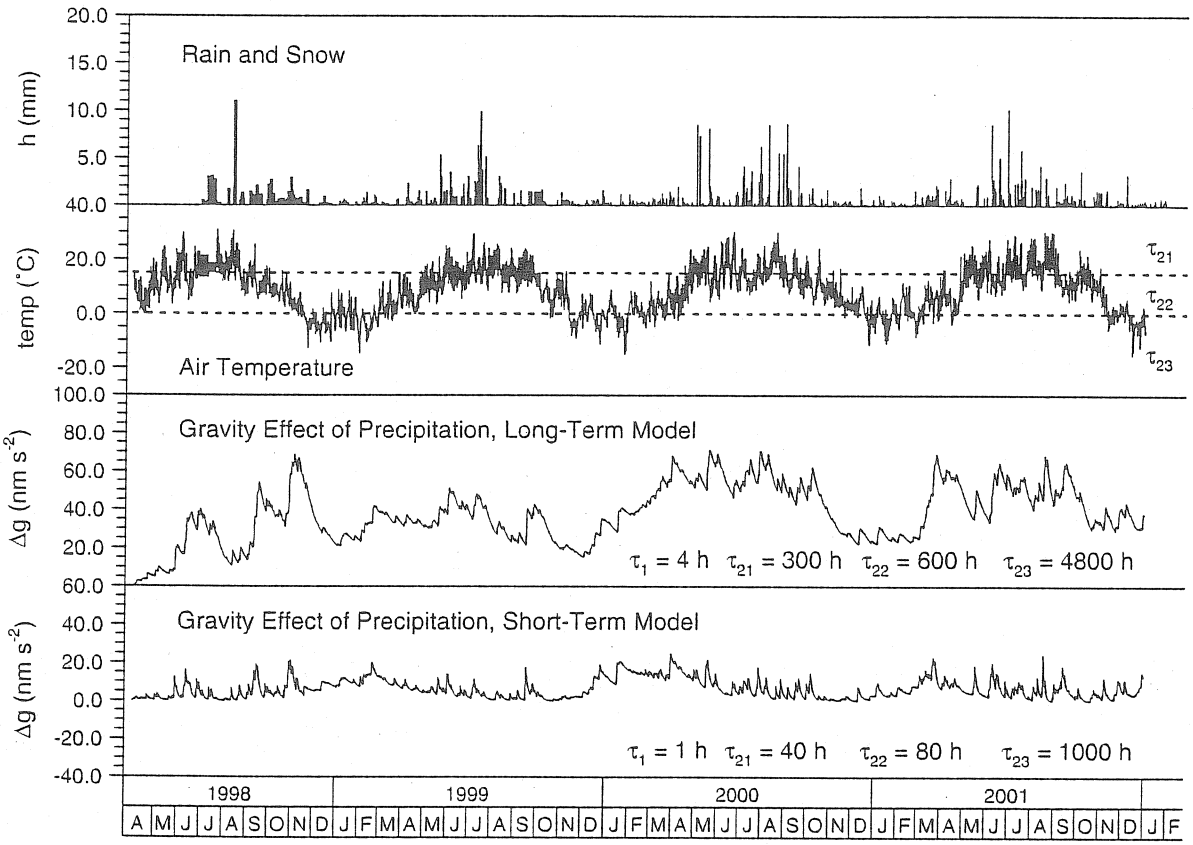

Fig. 8: Precipitation and air temperature at Wettzell, 1.4.1998 – 30.6.2001. Modeled gravity effect of precipitation according to equation (2). First frame: precipitation. Second frame: air temperature. Three different values of the time constant τ_2 were used in dependence of the air temperature. Third frame: long-term model (LTM). Fourth frame: short-term model (STM).

Many of the influences themselves vary during the year and as a consequence seasonal variations of the time constants are to be expected too. A very expressive example are the variations of temperature which not only influence the direct evaporation and the evapotranspiration (which additionally includes the contribution of the vegetation), but are also responsible for the kind of precipitation (rain or snow) and for the state of the underground (frozen or not). Therefore the attempt was made to introduce time constants τ_{21}, τ_{22} and τ_{23}, being valid for the temperature ranges above 15°C, between 0 and 15°C, and below 0°C respectively. Examples of the gravity effect of precipitation modeled in this way are given in the third and the fourth frame of fig. 8. As may be seen from a comparison of both examples, the time constants influence the amplitude of the modeled gravity effect. However, it has to be considered that no irreversible long-term accumulation occurs. The greater values used in the long-term model (fig. 8, third frame), result in more pronounced gravity anomalies as compared with the short-term model (fig. 8, fourth frame). Another example is given in fig. 12. There it could be shown,

[1] In [6] the false value τ_2 = 91 days is given instead of the right value 30 days

that the short-term model is equivalent to corrections derived from the directly measured changes of the groundwater level and variations of the soil moisture.

The relation between precipitation and gravity variations changes during the year. The correlogram is similarly muddled like that of the groundwater influence (fig. 10, upper left frame), however it looks even less clear. At first for the relation between precipitation and groundwater as well as for the relation between precipitation and gravity changes regression coefficients were estimated over fortnightly periods. Similarly to the considerations with concern to the groundwater influence (as described in the next paragraph) these fortnightly values were stacked with an annual period and averaged over the years (fig. 9). In a last step moving averages over every three neighboring values were derived. In this way the thick solid lines result, which more or less clearly show the seasonal variations of the regression behavior.

Due to the fact that precipitation cannot be directly correlated with changes of groundwater or gravity, the interpretation of the resulting regression coefficients differs slightly from that of the corresponding groundwater regression coefficients. With regard to the influence of precipitation on gravity the regression coefficients describe the deviations from the respective model and its parameters.

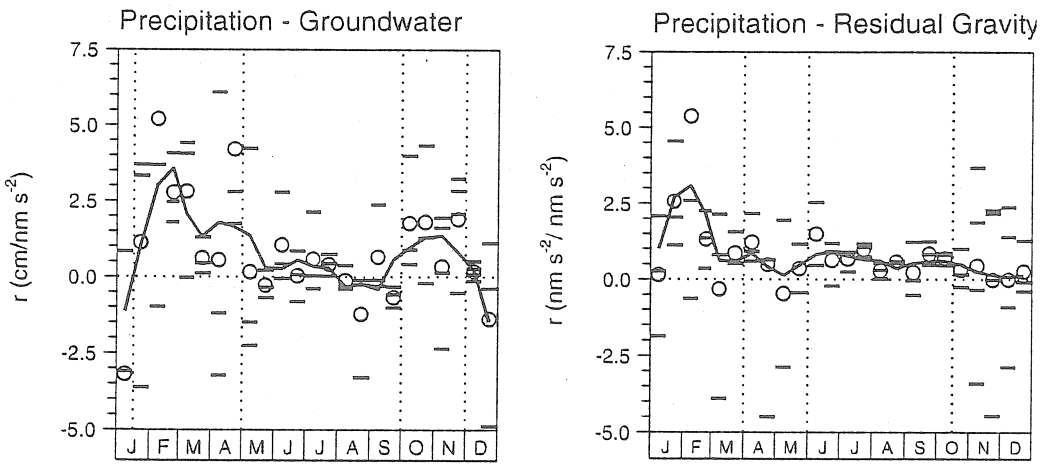

Fig. 9: Correlation between the modeled gravity effect of precipitation, groundwater and residual gravity. Stacked representation of the regression coefficients. Horizontal bars: regression coefficients estimated over fortnightly periods in the different years. Circles: mean values of the fortnightly regression coefficients over the years. Solid line: moving average of the fortnightly mean values. The vertical dotted lines separate the periods of high and low correlation.

As may be seen from the left frame of fig. 9 during the cold first months of the year as well as in the rainy autumn a strong correlation between precipitation and changes of the groundwater level occurs (upward curved sections of the solid line), while in the remaining time of the year the influence nearly vanishes. The right frame shows, that the influence of precipitation on the gravity has also a maximum in the cold season (snow cover, persistent frost), i.e. the modeled gravity effect during this time is too low. Due to increased run-off and evaporation the influence of precipitation is less in the remaining time of the year. While in summer the observed values nearly correspond to the modeled effect (regression coefficient near 1.0), for two short periods in spring and in the early winter the influence is very low (regression coefficient near zero).

6. Correlation between groundwater and gravity

At the end of 2000 a first attempt was made to estimate the dependency of groundwater variations and gravity. This investigation was spread over the period 13.6.1999 – 31.12.2000. The result was the clear proof of a varying regression behavior during the year. From February to August groundwater variations have a strong influence on the gravity, while from September to January the influence is weak.

At the end of 2001 a similar investigation was started on the basis of an enlarged data set. All data of the second part of the CD029 series having been available up to that time were included (i.e. all data after the large gap in May 1999). At first sight the result was disappointing. The correlogram looks like

a chaotic muddle of lines, obviously caused by residuals of incompletely eliminated systematic influences (fig.10, upper left frame). However, if the correlogram is studied more in detail (especially during the period when its visualization develops step by step on the screen of the computer), the visual impression alone suggests to distinguish between sections with weak slope and steeper ones. A separation of these sections results in the graphic representations shown in the upper right and the lower left frame of fig. 10. The different slopes being characteristic for both subsets of the correlogram are clearly seen. However, like in the total data set, the data of both subsets are not homogeneous. Therefore regression lines were separately derived for each uninterrupted section of the correlograms. The results are given in the lower right frame of fig. 10. The solid lines relate to the weak sloped sections, the broken lines to the steep sections. The averaged regression coefficients are (0.248 ± 0.028) and (0.933 ± 0.048) nm s^{-2}/cm respectively. These numbers very clearly confirm the visual impression of different slopes being characteristic for both subsets of the correlogram. If the fact of different slopes is neglected, the adjustment of the total data set (upper left frame) would result in a regression coefficient of (0.516 ± 0.003) nm s^{-2}/cm. This value is near to the weighted mean of 0.476 nm s^{-2}/cm derived from the both seasonal values. The weights were set proportional to the respective range of validity. The directly estimated total value as well as the weighted mean correspond to the value of (0.689 ± 0.090) nm s^{-2}/cm, derived from absolute measurements (fig. 1). However, due to the use of only 9 separate absolute gravity values this first estimation of the groundwater regression coefficient is less reliable than the later values on the basis of the continuous CD029 data series.

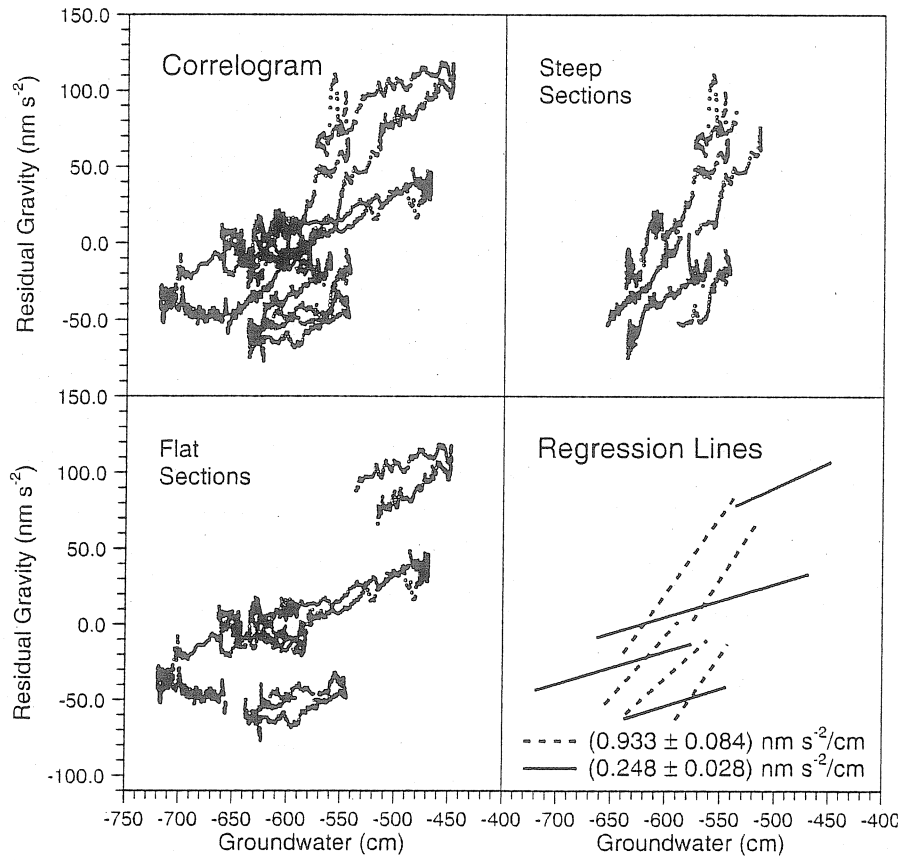

Fig.10: Correlation between groundwater and residual gravity. Seasonal variations of the groundwater regression coefficient

Generally correlograms have no relation to time. However, if the data are transferred to the time scale, the sections with different regression behavior (described by the different regression coefficients) may be related to different times of the year. From this kind of representation it becomes clear, that the periods with similar regression line slope repeat very regularly from year to year. Therefore in a last step the data were stacked over a yearly period. The result is given in fig.11, which very clearly shows the strong influence of groundwater changes from mid-May to mid-September (high regression coefficients, broken lines) and the weak influence from mid-September to mid-May (low regression coefficients, solid lines). The short sections of broken lines in February and November/December are related to the marginal sections of the data set and therefore may be ignored.

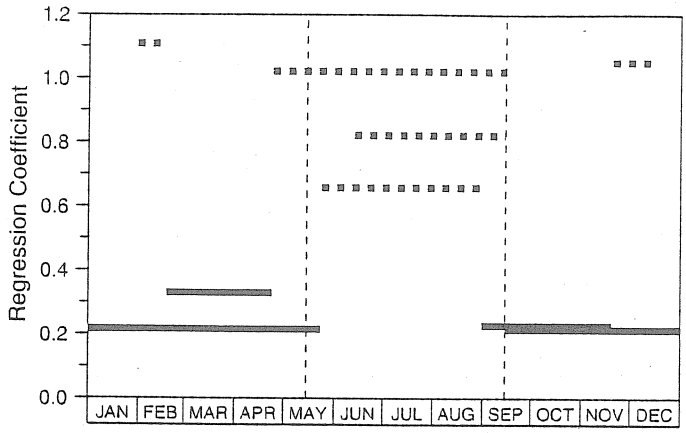

Fig. 11: Wettzell, 13.6.1999 – 31.12.2002. Stacked time intervals with similar regression behavior. The vertical dotted lines separate the period of strong groundwater influence (from mid-May to mid-September) from that of weak groundwater influence (from mid-September to mid-May).

7. Examples of corrected gravity data

The change of soil moisture and groundwater after rainfall and the response of the gravimeter are clearly to be recognized, if short sections of the data series are studied. An example is given in fig. 12, covering the two monthly period from October 1 to November 30, 2001. Between November 6 and 9 numerous rainfalls occurred (the plot is based on the precipitation sums over 15 minutes each), which are followed by clear signals of the soil moisture as well as the groundwater level. The vertical dotted line at November 7, 2001, 15:00 UT marks a steep rise of the soil moisture immediately after the beginning of the rainfall. The groundwater level changes with a time delay of about two days. After the rainfall both signals go down, the soil moisture more rapidly than the groundwater.

The residual gravity (fifth frame from above) is also influenced by the rainfall. A clear peak is to be seen similar to the change of the soil moisture. At last it has to be pointed out, that the modeled gravity effect of the precipitation corresponds very well to the change of the residual gravity, especially to its amplitude. However, it decreases more slowly than the residual gravity. - In the lowermost frame two attempts of corrections are shown.

In the first variant the modeled gravity effect of precipitation is subtracted from the residual gravity (short-term model, second frame from above). However, for better approximation additionally a factor c_{rain} = 1.5 was used. Due to the fact, that the modeled gravity represents the total effect of precipitation, in this way changes of the soil moisture as well as those of the groundwater level are corrected (assuming that the parameters of the model are chosen correctly). As may be seen from the lowermost frame, the result of this correction is a clear diminution of the roughness of the curve. However, a total elimination of the precipitation influence could not be achieved.

In the second variant instead of the modeled gravity effect of precipitation the directly measured changes of soil moisture and of the groundwater level are used. The corrections are based on the groundwater regression coefficient 0.150 nm s^{-2}/cm, valid for the time between mid-September and mid-May, while for the soil moisture a value of 2.5 nm s^{-2}/percent is assumed (roughly estimated from the graphical representations).

If the results of both correction procedures are compared, no significant differences are to be recognized, i.e. both variants are equivalent. Strictly this is valid only for the example under consideration (1.10. – 30.11.2001, fig. 12). From other examples a similar visual impression results. However, details and the numerical values may differ.

The residual gravity during the total recording period of the CD029 at Wettzell is shown in fig. 13 (lowermost frame). The two curves beneath are corrected for the influence of groundwater changes and additionally for the influence of precipitation (short-term model, instead of a soil moisture correction). As already mentioned, caused by certain reasons the first section of the record (before the gap in May, 1999) is unfavorably affected, and therefore it cannot be included in the detailed studies. The second section is dominated by the large anomaly in the first half of 2000, clearly caused by an anomaly of the groundwater (uppermost frame). A similar behavior repeats in the first half of 2001. After the groundwater correction was applied, the large anomaly in 2000 reduces considerably. Only a part of the second half of the anomaly remains. In contrast to that, the correspondent anomaly in 2001 seems to be overcompensated. As may be seen from the third curve below, the correction for precipitation has only

a small influence. There are two exceptions. At first the overcompensated groundwater anomaly in 2001 seems to be increased. The second exception concerns the sharp double anomaly in May 2000. While the second spike unambiguously is caused by a heavy rainfall, the first spike has no correspondence to rainfall, soil moisture or groundwater. Therefore only the second spike vanishes after the data have been corrected for the influence of precipitation. The first spike remains unchanged. To sum up it can be said that the greatest part of the hydrological influences is eliminated by the groundwater correction on the basis of smoothed data, while details are covered by corrections for the influence of precipitation (modeled gravity effect of precipitation, STM). Residuals of the anomalies may remain or overcompensation may arise if the seasonal changes of the regression behavior are neglected.

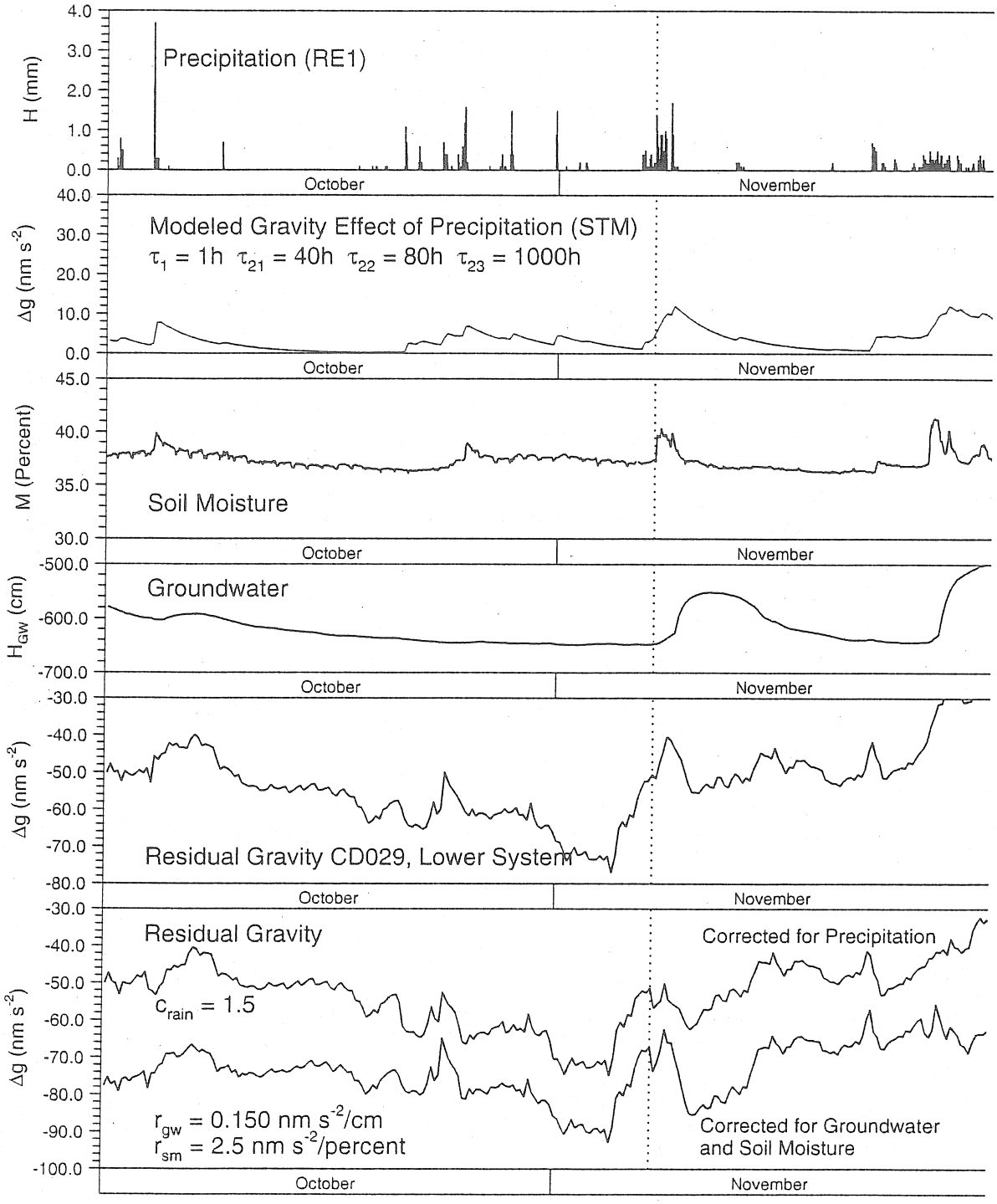

Fig. 12: Hydrological influences at Wettzell, 1.10. – 30.11.2001. Groundwater values not smoothed. The vertical dotted line marks the date November 7, 2001, 15:00 UT. In the lowermost frame two different ways of hydrological corrections are compared: firstly the modeled gravity effect of precipitation, secondly corrections derived from measured values of the groundwater level and of the soil moisture.

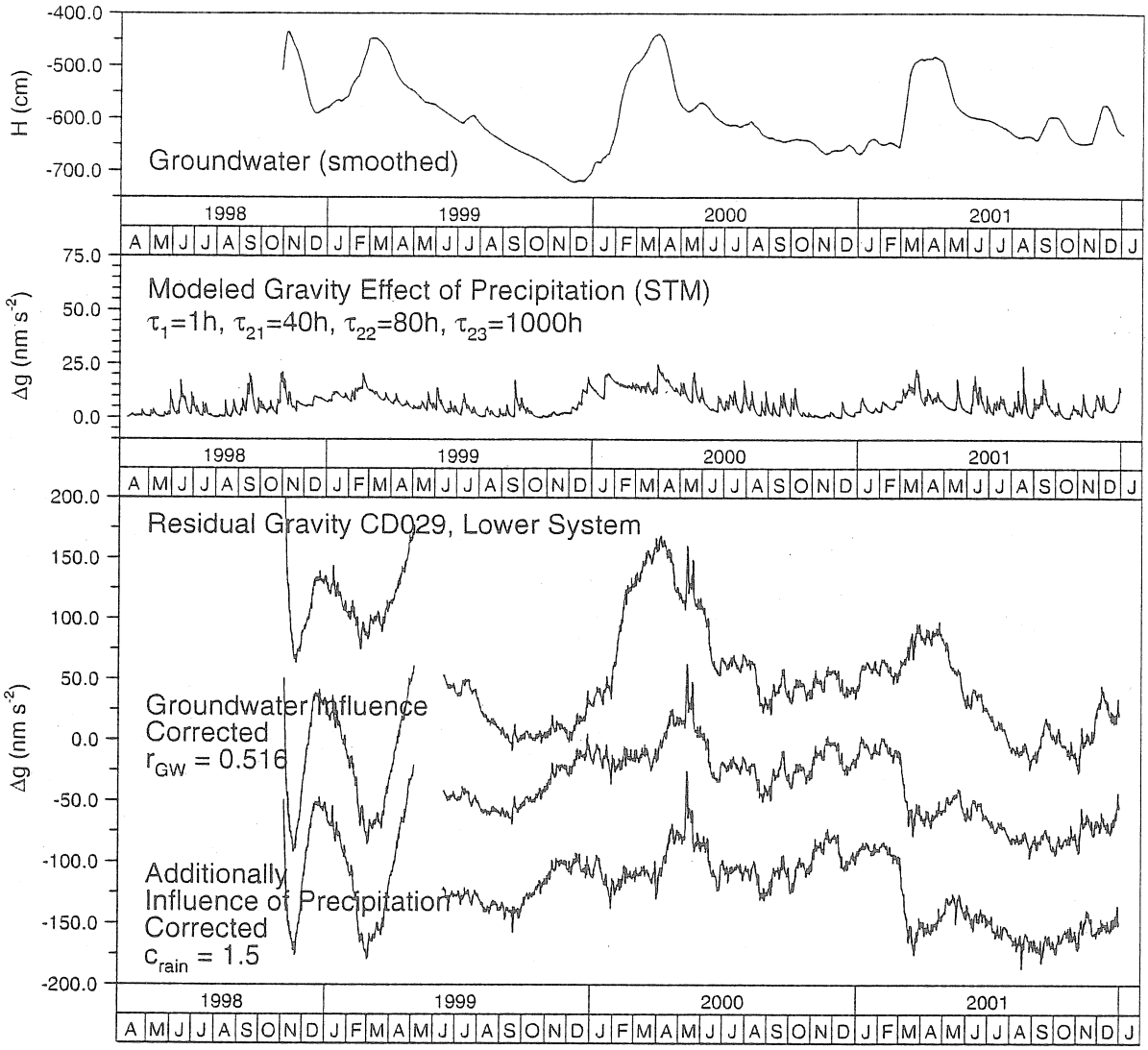

Fig. 13: Hydrological corrections, 1.4.1998 – 30.6.2001. Groundwater smoothed. The modeled gravity effect of precipitation (short-term model STM) is plotted in an enlarged scale (approx. 2:1) compared with the three curves in the lowermost frame.

8. Conclusions

- The investigations presented here generally confirm, that gravity measurements may be affected significantly by hydrological influences.
- At Wettzell an annual wave with a double amplitude of about 70 nm s^{-2} is to be expected, caused by variations of the groundwater level throughout the year. The correction of such influences is of great importance for the investigation of other long-term phenomena (e.g. gravity effect of the polar motion).
- At Wettzell the long-term gravity effects are closely correlated with changes of the groundwater level, while the modeled gravity effect of precipitation better corresponds to the short-term gravity variations.
- At Wettzell the influence of groundwater variations may be described by a linear regression model with a mean regression coefficient in the order of 0.52 nm s^{-2}/cm. However, between mid-May and mid-September the influence seems to be stronger (0.93 nm s^{-2}/cm) than in the remaining part of the year (0.25 nm s^{-2}/cm).
- If the seasonal variations of the groundwater regression coefficient are neglected, errors may arise by over- or under-compensation of the disturbing hydrological influences.

Acknowledgement

The authors express their thanks to

- the BKG, which permitted the use of the data and supported our investigations.
- Thomas Klügel (FS Wettzell), who reliably made available the groundwater data and initiated the installation of the soil moisture sensor. He always was ready for discussions and gave many hints with concern to the local hydrogeologic situation at Wettzell.

References

1. Harnisch, M., Harnisch, G.:
   Processing of the data from two superconducting gravimeters, recorded in 1990 - 1991 at Richmond (Miami, Florida). Some problems and results.
   Marées Terrestres, Bull. Inf., Bruxelles (1995) 122, pp. 9141 - 9147
2. Crossley, D. J., S. Xu and T. van Dam (1998):
   Comprehensive Analysis of 2 years of SG Data from Table Mountain, Colorado.
   Proc. 13th Int. Symp. Earth Tides, Brussels, July 1997. Obs. Royal Belgique, Brussels 1998, 659 – 668.
3. Harnisch, M., Harnisch, G.:
   Hydrological Influences in the Registrations of Superconducting Gravimeters and Ways to their Elimination.
   Marées Terrestres, Bull. Inf., Bruxelles 131 (1999), pp. 10161 - 10170
4. Harnisch, M., Harnisch, G., Nowak, I., Richter, B., Wolf, P.:
   The Dual Sphere Superconducting Gravimeter C029 at Frankfurt a.M. and Wettzell. First Results and Calibration.
   Cahiers du Centre Européen de Géodynamique et de Séismologie, Luxembourg 17(2000), pp. 39 - 56
5. Harnisch, M., Harnisch, G., Jurczyk, H., Wilmes, H.:
   889 Days of Registrations with the Superconducting Gravimeter SG103 at Wettzell (Germany).
   Cahiers du Centre Européen de Géodynamique et de Séismologie, Luxembourg 17(2000), pp. 25 - 38
6. Harnisch, M., Harnisch, G., Nowak, I., Richter, B., Wolf, P.:
   The Dual Sphere Superconducting Gravimeter GWR CD029 at Frankfurt a.M. and Wettzell. First Results and Calibration.
   IAG Symposia, Vol. 121, Springer-Verlag Berlin Heidelberg 2000, pp. 155 - 160
7. Falk, R.:
   Deutsches Schwerereferenzsystem (DSRS). Deutsches Schweregrundnetz (DSGN)
   Poster. INTERGEO, Berlin 2000

EFFECTS OF ENVIRONMENTAL PARAMETERS ON HEIGHT AND GRAVITY VARIATIONS.

S. Zerbini[1], B. Richter[2], C. Romagnoli[3], L. Lago[1], F. Domenichini[1], D. Simon[2]
[1]Dipartimento di Fisica, Università di Bologna, Viale Berti Pichat 8, 40127 Bologna, Italy, e-mail zerbini@df.unibo.it;
[2]Bundesamt fuer Kartographie und Geodaesie, Frankfurt am Main, Germany,
[3] Dipartimento di Scienze della Terra e Geologico Ambientali, Università di Bologna.

Continuous GPS and gravity measurements by means of a cryogenic gravimeter started in mid 1996 at Medicina, in Italy. The time variability of gravity and GPS heights in relation to variations of several environmental parameters has been investigated. A marked seasonal signal, of comparable amplitude and phase, has been identified in both data series. It has been interpreted as the sum of different loading and Newtonian attraction effects. Seasonal loading effects induced by air pressure, the ocean and surficial water table were estimated and modeled for both data sets. Mass effects due to the surficial water table and the ocean were also estimated and accounted for. For the gravity series, 12-hour data of balloon radio sounding launches have been used to estimate the attraction effect of the seasonal vertical density distribution of the air pressure column above the station. It is demonstrated the importance of collecting continuous, high-accuracy, multi-parameter data series for an appropriate interpretation of signals related to environmental variability.

Influence of sea level variations in seismic normal mode band on superconducting gravimeter observation at Syowa Station

Kazunari Nawa* (Geological Survey of Japan, AIST)
Naoki Suda (Graduate School of Science, Hiroshima University)
Shigeru Aoki (National Institute of Polar Research)
Kazuo Shibuya (National Institute of Polar Research)
Tadahiro Sato (National Astronomical Observatory)
Yoshio Fukao (Earthquake Research Institute, University of Tokyo)

Abstract

The Earth's background free oscillations were detected from an analysis of SG records at Syowa Station, Antarctica for the first time (Nawa et al., 1998), and then the phenomenon was confirmed by analyses of global broadband seismometer network records. However, as pointed out by Suda et al.(1998), there exist some differences in spectrum features between Syowa Station and other sites. On the Syowa Station spectrum, their intensity is seasonally varying larger than shown by Nishida et al.(2000), they have high intensity at frequencies between 3 and 4 mHz, and in particular, they are visible even at frequencies down to 0.3 mHz and there are peaks that do not correspond to seismic normal modes. In order to investigate the possible atmospheric effect on the observed seasonal variation, we have made the correction for its effect with the similar method by Zurn and Widmer (1995). Although we confirmed some reduction of the noise level by this correction, peaks not corresponding to seismic normal modes were still observed. Therefore, it was thought that the oceanic effect is a possible candidate making these anomalous features in Syowa spectrum because of close to coastal line (Nawa et al., 1998b, 2000), but we could not discuss the possible excitation source on the observational evidence due to a lack of available data to used.

In 1998, Aoki et al.(2000) conducted differential GPS observations on the fast ice at the Syowa Station and detected the vertical displacement which were oceanic tidal variation and high frequency (3-6 minutes) variations in time domain. After his observation made, sea level variation records have been acquired at a sampling rate of 30 seconds with pressure gauge installed by Japan Coast Guard in January 1999. We analyze these data for investigating sea level variation spectrum in seismic normal mode band. As an analysis result, we have obtained very similar feature of temporal variations in spectrum as that observed from the SG data. This strongly suggests that a cause of anomalous features of Syowa SG spectrum is due to the influence of seiches in Lutzow-Holm Bay around the station.

* E-mail address: k.nawa@aist.go.jp

Simplistic models of vertical seismic noise above 0.1 mHz derived from local barometric pressure

by

Walter Zürn

Black Forest Observatory (Schiltach), Universities Karlsruhe/Stuttgart
Heubach 206, D-77709 Wolfach, Germany

1 Introduction

It has long been known that long-period seismic noise in all components has at least some of its sources in the local atmosphere. At periods much higher than the gravest free oscillations of the earth a vast amount of literature exists demonstrating clearly the influence of gravitational attraction of the sensor mass by the local atmospheric mass and of the free air effect due to pressure loading of the local crust (e. g. Warburton and Goodkind 1977). Müller and Zürn (1983) noticed the effects of passing coldfronts on a gravimeter and could explain these observations also mainly by Newtonian attraction. Zürn and Widmer (1995) showed for the first time that free mode observations can be appreciably improved by applying a simple correction for the local air pressure effect as well understood at much longer periods. With this correction one can reach noise power spectral densities (at least for the best gravimeters at the best stations) lower than predicted by the New Low Noise Model of Peterson (1993) for frequencies less than 1 mHz. However, the same authors also noticed that the correction does not work for frequencies higher than 1 - 2 mHz, actually there it reduces signal-to-noise ratios (SNR). This is not a serious problem since barometric pressure could be low-pass filtered before using it for the correction. Still the question arises, why this is the case although the physical mechanisms must be similar. Since much more seismological information can be obtained above than below 1 mHz improved SNRs above 1 mHz would be highly welcome.

2 Simplistic models for higher frequencies

As one tries to understand the seismic noise at higher and higher frequencies and wavenumbers a series of complications arises: the physical processes in the atmosphere

get more and more complicated , the barometric pressure fluctuations get smaller and smaller, quasistatic treatment of the elastic earth will be insufficient and so on.

The cold front model used by Müller and Zürn (1983) already took dynamics and lateral variation of the atmosphere into account to some extent, by incorporation of a typical shape and ground speed of a front and by estimating the density jump across the front from the observed jumps in pressure and temperature. The magnitudes of the observed gravity changes could be rather well explained by this model (see table 1 in Müller and Zürn 1983). However, one major shortcoming of the model was the fact, that the only physical effect taken into account was the gravitational attraction of the gravimeter mass.

A vertical accelerometer senses several forces on its mass. Some sources of deformation have a changing direct gravitational attraction on the sensor mass like the sun, moon (tides) and the atmosphere, mass redistribution in the earth leads to secondary changes in gravitation, local vertical displacements cause a free air effect and inertial effects. Table 1 shows for different phenomena the relative contributions of these effects to the total recorded signal. Note that additional contributions are possible, one exotic example being Coriolis forces from toroidal modes (Zürn et al., 2000). In the frequency range just above 1 mHz the inertial effect plays already a very strong role and must be considered. So naturally our next step must be the inclusion of this effect.

Table 1: Relative contributions to signals sensed by a vertical accelerometer. The third example corresponds to a simple vertical motion like on a shake table or calibration platform.

Signal	Frequency	Inertial effect	Free air effect	Mass redistr. effect	Gravitation
M_2-tide	22.4 μHz	0.0042	0.6	-0.45	1.00
${}_oS_2$	0.30 mHz	0.815	0.67	-0.48	0.0
—	0.28 mHz	0.500	0.500	0.0	0.0
${}_oS_{10}$	1.725 mHz	0.98	0.025	-0.008	0.0
Rayleigh-Wave	0.05 Hz	1.00	0.0	0.0	0.0
P-wave	1.0 Hz	1.00	0.0	0.0	0.0

The first new model just adds the inertial effect to the model so successful below 1 mHz. It consists of an elastic layer with thickness D and Lamé constants μ and λ over a rigid halfspace and under a laterally homogeneous atmosphere. The density in this atmosphere is either exponentially decreasing with altitude z and a scale height H (isothermal model $\rho(z) = \rho_o \cdot exp(-z/H)$) or constant with height ($\rho(z) = \rho_o$) up to H and zero above. When pressure varies harmonically with angular frequency ω the admittance between pressure Δp and vertical acceleration Δg for both atmospheric models is:

$$\frac{\Delta g}{\Delta p}_B = -\frac{2 \cdot \pi \cdot G}{g} + \frac{(\lambda + \mu) \cdot D}{\mu \cdot (3\lambda + 2\mu)} \cdot (\omega^2 + |\frac{\delta g}{\delta z}|) \tag{1}$$

where G is the gravitational constant and g is the gravitational acceleration at the surface. The first term is very simple and results in -4.27 nm/s^2. The second and third term depend on the elastic layer and represent the inertial and free air effects, respectively, due to the vertical displacement induced by the pressure load. This model does not take into account, that the spatial scale of atmospheric density variations decreases with increasing frequency, so eventually at some higher frequency it must fail for this reason.

The second model is the one already described by Neumann and Zürn (1999): a pressure wave propagates horizontally with phase velocity c_h, angular frequency ω and horizontal wavenumber k_h over an elastic halfspace with Lamé constants as above. Density in the air decays exponentially with height z and with a scale height H as in an isothermal atmosphere.

$$\Delta p = p_o \cdot exp(i \cdot (k_h \cdot x - \omega \cdot t)) \tag{2}$$

$$\Delta \rho = \frac{p_o}{c^2} \cdot exp(i \cdot (k_h \cdot x - \omega \cdot t)) \cdot exp(-z/H) \tag{3}$$

This is a perfect model for Lamb waves. For acoustic-gravity waves with real vertical wavenumbers (Lamb waves have imaginary vertical wave number $k_v = i \cdot 1/H$) the loading effects will be well modeled, but not the direct gravitation (e. g. Gossard and Hooke 1975). For a vertical accelerometer on the surface of the halfspace we have the pressure admittance:

$$\frac{\Delta g}{\Delta p}_W = -\frac{2 \cdot \pi \cdot G \cdot H}{c^2 \cdot (1 + k_h \cdot H)} + \frac{\lambda + 2 \cdot \mu}{2 \cdot \mu \cdot (\lambda + \mu) \cdot k_h} \cdot (\omega^2 + |\frac{\delta g}{\delta z}|) \tag{4}$$

with c the velocity of sound, $k_h = \omega / c_h$ and $H = c^2/g$. For infinite horizontal wavelength $k_h = 0$ and the first term reduces to $-2 \cdot \pi \cdot G/g$ as for the first model. Note that c_h can assume values from 10 m/s up to the sound velocity c (330 m/s).

These two admittances are now frequency dependent and they can be used to compute (in the frequency domain) from an observed time series of local atmospheric pressure p(t) the pressure induced "signal" (noise) deterministically as a time series (pressure seismogram) or statistically in the form of noise power spectra. The spectrum of the "pressure seismogram" is:

$$w_z(\omega) = \frac{1}{i \cdot \omega} \cdot H_v(\omega) \cdot \frac{\Delta g}{\Delta p}(\omega) \cdot \Delta p(\omega) \tag{5}$$

where H_v is the transfer function of the accelerometer for output w_z (in volts or counts) w. r. t. ground velocity, as normally used in seismology for broadband seismometers.

Inspection of the equations for the admittances in both models shows that an angular frequency ω_o can be found for which the admittance vanishes, because the effects compensate each other. This is certainly a property of the simplistic models, in reality this will not be true and in any case this "hole" will be filled by noise from other sources (eventually the instrumental noise). and the background free oscillations of the earth, e. g. Ekström, 2001). The Bouguer plate model has only one such conditions while the wave model has a second one at very long periods, where the inertial effect is negligible, but the free air effect gets so big that it compensates the gravitational effect. This is an unrealistic feature, because of the halfspace approximation.

3 Examples

Two 10-day pressure time series and seismograms from an STS-1 vertical seismometer from BFO (Richter et al. 1995) were selected in order to check these models, one from July 2000 with strong pressure disturbances, the other from May 2002 with less strong pressure variations. The tides were removed from the seismograms by subtracting a few tidal lines. Power spectral densities in acceleration were computed, for the seismic data these were corrected for the instrument response, for the pressure data they were multiplied by the acceleration-pressure admittances given by eqns. (1) and (4) in order to make them comparable. In all cases $\lambda = \mu = 75GPa$ for the basement rocks of the area around BFO was assumed, corresponding to S- and P-velocities of 5.0 and 8.6 km/s for a density of 3000 kg/m^3. These are certainly on the high side. For the Bouguer model D = 20 km was adopted. Figs. 1 to 3 present these power spectral densities for acceleration (PSD) as functions of frequency. For comparison the New Low Noise Model (NLNM) of Peterson (1993) is also shown. It is clear that any seismically produced power in the PSDs of the seismic data can never be modeled by air pressure variations. The quieter the station, the more seismic signals one will detect in a time series and days without them cannot really be found.

Fig. 1 shows the results for the time series from July 1, 12:00 to July 9, 12:00, Fig. 2 for May 1, 12:00 to May 9, 12:00, Fig. 3 for May 3, 0:00 to May 6, 12:00; all times are UTC. For the July seismogram the PSD is more than a factor of ten above the NLNM for most frequencies, reflecting strong pressure variations at long periods and seimic activity at the high frequencies. It is The Bouger and Wave models explain the PSD well up to frequencies of 2 and 0.7 mHz, respectively. This part is dominated by the gravitation effect which cannot be modified by the elastic part of the models. Both models have deep "holes" where the admittances go through zero as discussed above. The wave model starts dropping off at the low frequency end because of the second zero also mentioned above. The Bouguer model clearly overpredicts the observed noise at frequencies above a few mHz, not unexpectedly, because the atmosphere is assumed to stretch from infinity to infinity horizontally in two dimensions. This result, of course, depends on the thickness of the elastic layer and the shear modulus assumed. The horizontal phase velocity c_h for the wave model was chosen such (200 m/s), that the

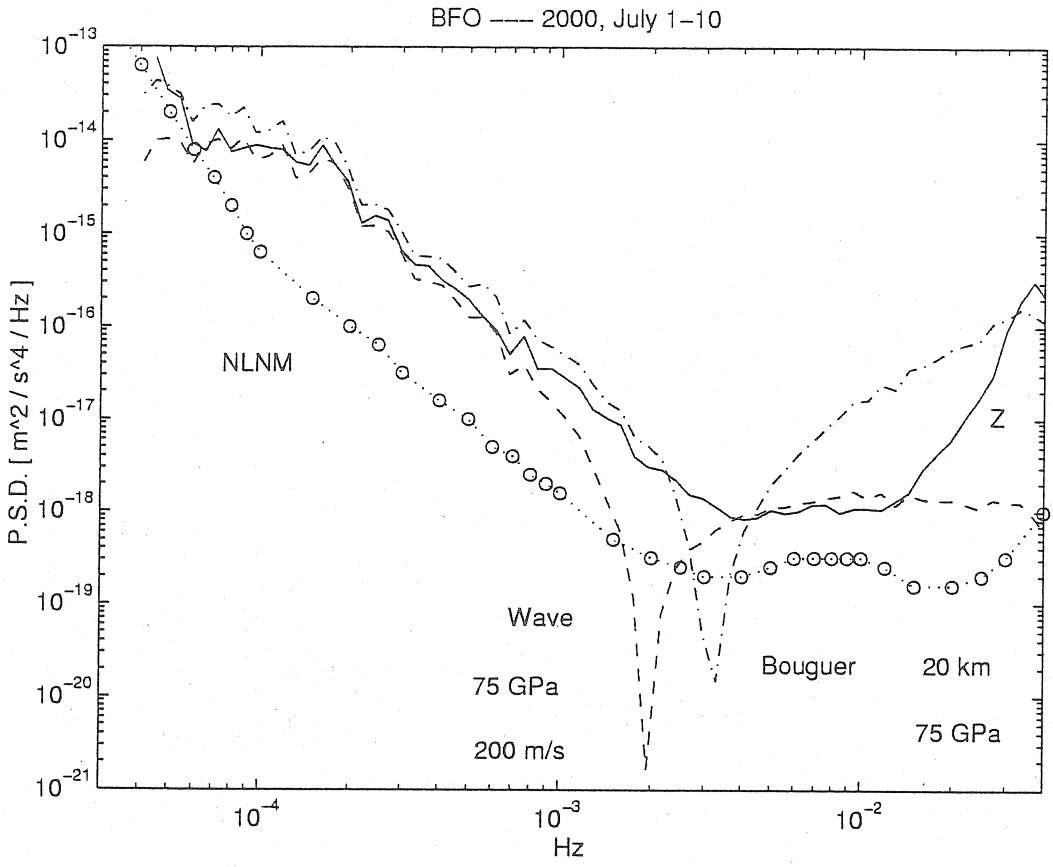

Figure 1: Acceleration power spectral densities against frequency for a 9-day (July 1, 12:00 to July 9, 12:00, 2000) vertical seismogram (data, solid line) from the STS-1 seismometer at BFO. The New Low Noise Model of Peterson (1993) is given for comparison (NLNM, dotted line with open circles). The Bouguer plate and horizontal wave models for vertical noise computed from local barometric pressure variations can be compared to the simultaneously observed noise. Model parameters are given in the figure and text.

predicted noise nearly equals the observed noise between 3 and 10 mHz. This plateau can easily be moved up and down by raising and lowering this value at constant μ, the "hole" then moves to lower and higher frequency.

For the 9 days in May 2002 the observed PSD is closer to the NLNM. The only model parameter different from Fig. 1 is $c_h = 300$ m/s, close to the speed of sound, because only by raising this value the PSD for the wave model at least in a small frequency range gets close to the observed. At low frequencies the wave model underpredicts the observed noise (because the "holes" approached each other) and it also underpredicts by far the high frequency noise, but there real seismic noise comes in to raise the observed level as demonstrated below. The Bouguer model predicts the observed noise over a very wide range of frequencies, with the exception of th vicinity of the "hole". Again we show below that this is only a fortuitous result.

For Fig. 3 the 3.5 days of the May 2002 time series was selected which had the

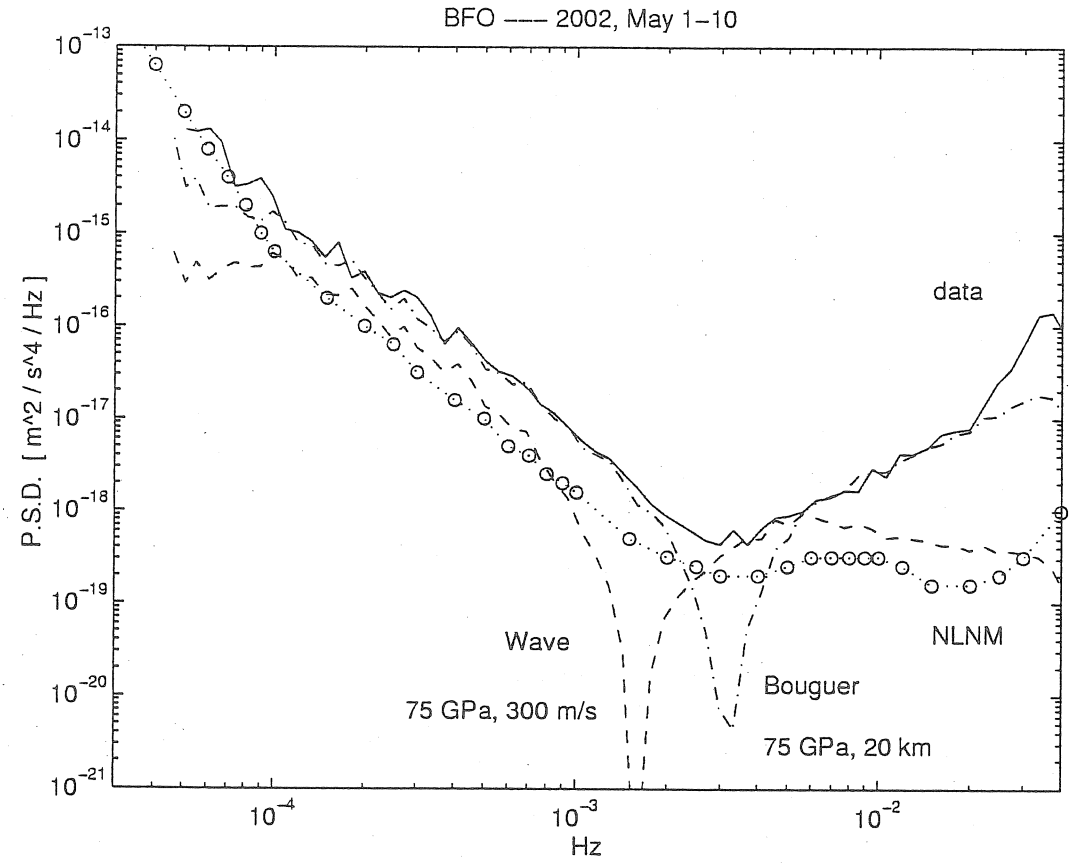

Figure 2: Same as figure 1 for the 9 days from May 1, 12:00 to May 9, 12:00, 2002.

least seismic activity in it. The models are both identical to the ones used for Fig. 2. The results clearly show firstly that the observed noise level is much lower above 5 mHz, and secondly that the same Bouguer model now overpredicts the observed noise as for July 2000. The wave model performs similarly poorly as for the full series.

The following conclusions can safely be drawn. Both (purely physical) models are predicting the general noise levels fairly well. This is not surprising below 1 mHz, because they are not significant modifications to the classical modal used by the tidal gravity community. According to Zürn and Widmer (1995) the NLNM can clearly be improved on by simple correction for local atmospheric pressure with factors very close to the first term in eq. (1). The Bouguer model tends to overpredict the higher frequency PSDs because it does not take decreasing scale of atmospheric cells for higher frequencies into account. Both (and any other) models have deep minima at frequencies depending on the chosen parameters, but generally in the range of frequencies, where the NLNM has its flat minimum. This property of the atmospheric effects has with high probability an effect on the shape of the NLNM, because it makes the contribution of the atmosphere to the noise even smaller than the dropping barometer PSD alone. Since 1998 (Nawa et al., 1998, see Ekström 2001 for more references) it is clear that in the minimum of the NLNM between 2 and 7 mHz one can see the incessantly excited free oscillations of the earth with the global atmosphere as

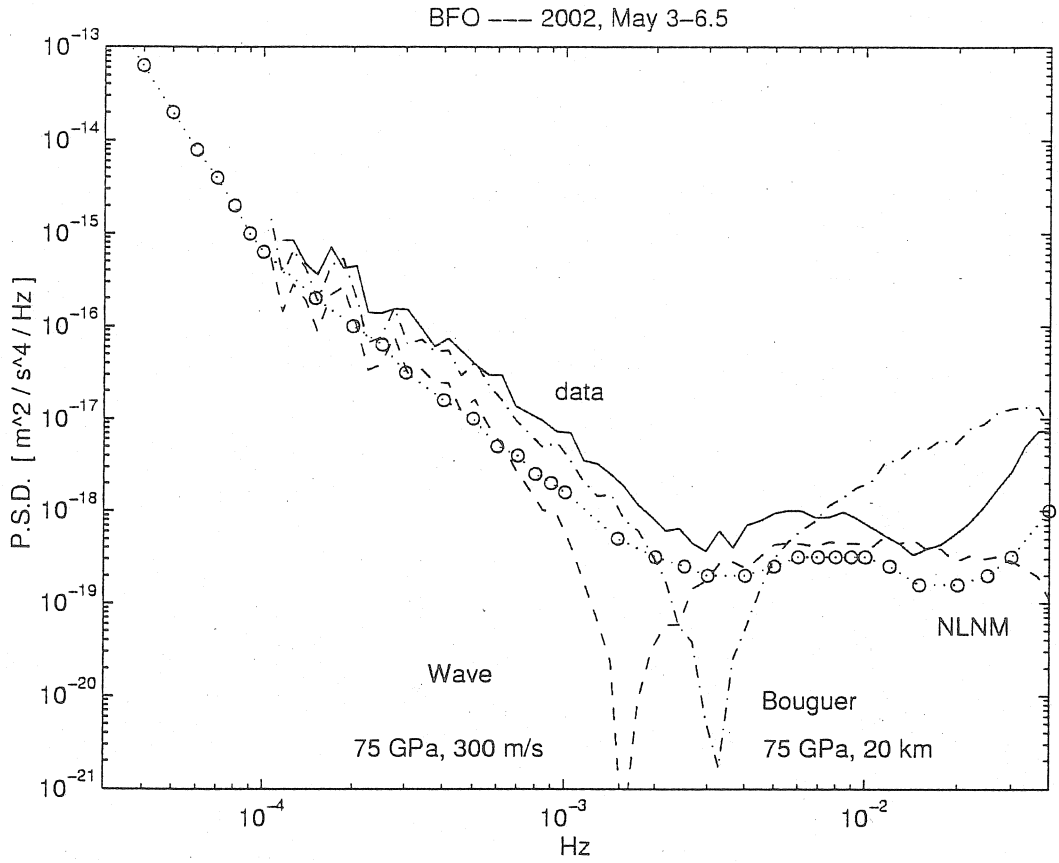

Figure 3: Same as Figure 2 but for only the part of the time series with reduced seismic activity from May 3, 0:00 to May 6, 12:00, 2002

the favored source. Since these modes cannot be seen in a single 24 hr-window, another noise source is competing strongly in this range (see Widmer-Schnidrig, this volume) which is probably of instrumental origin. Since not every station reaches values near the NLNM outside of earthquakes, some station noise could also contribute at the very good stations (Agnew and Berger, 1978). At frequencies much higher than the ones discussed here Sorrells (1971) considered propagating elastic waves as the important physical effect for producing noise, this has completely be neglected in the simplistic models tested in the work here.

References

Agnew, D. C., Berger, J. (1978). Vertical Seismic Noise at Very Low Frequencies. *J. geophys. Res.*, **83**: 5420 - 5424.

Ekström, G. (2001). Time domain analysis of Earth's long-period background seismic radiation. *J. geophys. Res.*, **106**: 26,483 - 26493.

Gossard, E. E., Hooke, W. H. (1975). *Waves in the Atmosphere.* Elsevier, Amsterdam, 456 pp.

Müller, T. and W. Zürn (1983). Observation of gravity changes during the passage of cold fronts. *J. Geophys.*, **53**: 155 - 162.

Nawa, K., Suda, N., Fukao, Y., Sato, T., Aoyama, Y., Shibuya, K. (1998). Incessant excitation of the Earth's free oscillations. *Earth Planets Space*, **50**: 3 - 8.

Neumann, U., Zürn, W. (1999). Gravity signals from atmospheric waves and their modeling. *Bull. Inf. Marées Terrestres* **131**: 10139 - 10152.

Peterson, J. (1993). Observations and Modeling of Seismic Background Noise. U. S. Geol. Surv., Open-File Rep. 93-322, 1 - 45.

Richter, B., H.-G. Wenzel, W. Zürn and F. Klopping (1995). From Chandler wobble to free oscillations: comparison of cryogenic gravimeters and other instruments in a wide period range. *Phys. Earth planet. Inter.*, **91**, 131 - 148.

Sorrells, G. G. (1971). A preliminary investigation into the relationship between long-period seismic noise and local fluctuations in the atmospheric pressure field. *Geophys. J. R. astr. Soc.*, **26**: 71 - 82.

Warburton, R. J., Goodkind, J. M. (1977). The influence of barometric pressure variations on gravity. *Geophys. J. R. astr. Soc.*, **48**: 281 - 292.

Zürn, W., Laske, G., Widmer-Schnidrig, R., Gilbert, F. (2000) Observation of Coriolis coupled modes below 1 mHz. *Geophys. J. Int.* **143**: 113 - 118.

Zürn, W. and R. Widmer (1995). On noise reduction in vertical seismic records below 2 mHz using local barometric pressure. *Geophys. Res. Lett.* **22**: 3537 - 3540.

Simplistic models of atmospheric effects in horizontal seismograms

by

Walter Zürn

Black Forest Observatory (Schiltach), Universities Karlsruhe/Stuttgart
Heubach 206, D-77709 Wolfach, Germany
e-mail: walter.zuern@gpi.uni-karlsruhe.de

and

Udo Neumann

Max Planck - Institute for Astronomy, Heidelberg, Germany

1 Introduction

It is common knowledge, that horizontal seismic noise at a given station is larger by factors between five and fifteen than the vertical noise at essentially all frequencies. A typical example is presented by Müller and Zürn (1983) in their Fig. 6. This fact definitely contributes to the large difference in use of horizontal and vertical seismographs and seismograms. It is also well known that at low frequencies tilts are an important mechanism for production of noise signals on the horizontal components. Tilts associated with changes in atmospheric pressure have been effectively removed from signals by Beauduin et al. (1996) and Neumann and Zürn (1999) in order to improve the quality of the seismograms. It is very desirable to understand the physics of the horizontal noise in order to possibly take measures against it or devise correction algorithms to remove noise from the already recorded seismograms. This and the companion paper by Exss and Zürn (2002, this volume) take steps to identify the physical mechanisms leading to horizontal noise.

A horizontal accelerometer senses several forces on its mass. Some sources of deformation have a changing direct gravitational attraction on the sensor mass like the sun, moon (tides) and the atmosphere, mass redistribution in the earth leads to secondary changes in gravitation, the local displacement field causes tilts and inertial effects. There are other effects which are usually of minor importance. Table 1 shows for different phenomena the relative contributions of these effects to the total recorded signal. An enlightening discussion of sensor sensitivity for horizontal seismographs can be found in Rodgers (1968). He took special design features into account, which are to some part avoided in modern broadband feedback seismometers (e. g. Wielandt and Streckeisen, 1982).

Note that the tilt effect is the largest contribution to ${}_oS_2$, while for the fundamental toroidal mode ${}_oT_2$ on a laterally homogeneous earth tilt does not exist. In the following

Table 1: Relative contributions to signals sensed by a horizontal accelerometer.

Signal	Frequency	Inertial effect	Tilt effect	Mass redistr. effect	Gravitation
M_2-tide	22.4 μHz	0.0042	-0.6	0.30	1.00
${}_oS_2$	0.30 mHz	-0.118	2.13	-1.015	0.0
${}_oT_2$	0.38 mHz	1.000	0.0	0.0	0.0
${}_oS_{10}$	1.725 mHz	0.87	0.14	-0.008	0.0
P-wave	1.0 Hz	1.00	0.0	0.0	0.0

we are not concerned with purely instrumental effects and we only consider effects of local atmospheric pressure.

2 Two simplistic models for horizontal noise

Both of our models are quasistatic in the sense, that we assume that there are no elastic waves excited by the changing pressure field. At higher frequencies this will not be the case, of course (e. g. Sorrells, 1968; Kanamori and Mori, 1992; Widmer and Zürn, 1992).

The first model is extremely simple. It assumes that the surface near the station is loaded by a laterally homogeneous pressure field changing with time. The station underground is assumed to be elastic, so clearly there are displacements, tilts and strains which have the same time dependence as the barometric pressure without phase leads or lags. The amplitudes of these signals will depend strongly on the local geology, topography and geometry of the station and the pier on which the instrument sits. In tidal tilt and strain measurements such local effects from stressing the locality with tidal stresses were clearly observed and they hamper the interpretation of tidal signals in terms of Love numbers (e. g. King et al. 1976). The pressure admittance for this case can be written as follows:

$$\left(\frac{\Delta a_h}{\Delta p}\right)_L = C_p \qquad (1)$$

where Δa_h is the change in acceleration in the horizontal direction indicated by h, Δp is the change in atmospheric pressure and C_p is a positive or negative constant strongly dependent on the position and sensitive direction of the sensor but not on frequency

or on the propagation direction of atmospheric masses or waves. We believe that the results by Beauduin et al. (1996) were due to such effects, because they obtained results strongly dependent on the position of the sensor within one observatory and independent of time.

Our second model was described by Neumann and Zürn (1999) and by Zürn (2002) and consists of a horizontally propagating plane wave with horizontal phase velocity c_h, horizontal wave number k_h and angular frequency ω in the atmosphere over an elastic halfspace with Lamé constants λ and μ. We assume $\lambda = \mu$ in the following:

$$\Delta p(x,t) = p_o \cdot exp(i \cdot (k_h \cdot x - \omega \cdot t)) \tag{2}$$

p_o is the peak pressure of the sinusoidal variation. The density decreases exponentially with height z and with scale height H from the surface value:

$$\Delta \rho(x,z,t) = \frac{p_o}{c^2} \cdot exp(i \cdot (k_h \cdot x - \omega \cdot t)) \cdot exp(-z/H) \tag{3}$$

where c is the speed of sound. These equations describe the properties of a Lamb wave with imaginary vertical wavenumber $k_z = i/H$, while they only approximate the behavior at the surface of an acoustic-gravity wave with real vertical wave number k_z (Gossard and Hooke 1975). For a horizontal accelerometer on the surface (x = 0, z = 0) of the halfspace we have the pressure admittance:

$$\left(\frac{\Delta a_h}{\Delta p}\right)_W = i \cdot \frac{2 \cdot \pi \cdot G}{g} \cdot \frac{1}{(1 + \frac{\omega \cdot c^2}{c_h \cdot g})} + i \cdot \frac{3}{4} \cdot \frac{g}{\mu} + i \cdot \frac{1}{4 \cdot \mu} \cdot c_h \cdot \omega \tag{4}$$

with $k_h = \omega / c_h$ and $H = c^2/g$ and $i = \sqrt{-1}$. c_h can assume values from 10 m/s up to the sound velocity c (330 m/s). The three terms represent the gravitational attraction, the tilt and the inertial effect, respectively. Note that all three contributions are in phase with each other, but in quadrature with the pressure signal. All three have a different dependence on frequency. The tilt term surprisingly does not depend on the wavelength for this model, so the amplitude of the sinusoidal surface deformation must be proportional to the wavelength (then tilt = amplitude/wavelength is constant). Thus the tilt term does not correspond to the pressure gradient but to the Hilbert transform of the pressure variation, a result noticed by Möckli (1988).

The relative importance of the effects can be obtained from the terms in eqn. (4):

$$\frac{tilt}{inertia} = \frac{3 \cdot g}{c_h \cdot \omega} \tag{5}$$

This ratio increases with ω^{-1} for constant c_h and equals one for frequencies of 0.468 and 0.014 Hz for horizontal phase velocities of 10 and 330 m/s, respectively.

$$\frac{tilt}{gravitation} = \frac{3}{8 \cdot \pi} \cdot \frac{g^2}{\mu \cdot G} \cdot \left(1 + \frac{\omega \cdot c^2}{c_h \cdot g}\right) \tag{6}$$

The second term in the parentheses is always larger than 1 and only increases as frequency increases. To underestimate the ratio we use μ = 100 GPa and the factor

in front of the parentheses results in the value 1.7, so the tilt is for all frequencies and model parameters larger than the gravitational effect, except when the halfspace is unrealistically stiff.

We compute (in the frequency domain) from an observed time series of local atmospheric pressure p(t) the pressure induced "signal" (noise) deterministically as a time series (pressure seismogram). The spectrum of the "pressure seismogram" is:

$$A_h(\omega) = \frac{1}{i \cdot \omega} \cdot H_v(\omega) \cdot \frac{\Delta g}{\Delta p}(\omega) \cdot \Delta p(\omega) \tag{7}$$

where H_v is the transfer function of the accelerometer for output a_h (in volts or counts) w. r. t. ground velocity, as normally used in seismology for broadband seismometers. After application of inverse Fourier transformation the "pressure seismograms" can be compared to real ones (between earthquake signals). The model seismograms can be fit by least squares to the data for different time windows and/or atmospheric phenomena or situations and the regression factors found may be interpreted in terms of the parameters in eqns. (1) and (4). First results will be reported by Exss and Zürn (2002, this volume).

Acknowledgments: We thank Erhard Wielandt, Rudolf Widmer-Schnidrig, Axel Roehm, Corinna Kroner, Thomas Jahr, Klaus Klinge, Kasper Fischer und Malte Westerhaus for discussions and cooperation. Financial support by the "Deutsche Forschungsgemeinschaft" under grants number KR 1906/3-1 and WE 2628/1-1 is gratefully acknowledged.

References

Beauduin, R., P. Lognonné, J. P. Montagner, S. Cacho, J. F. Karczewski and M. Morand (1996). The Effects of Atmospheric Pressure Changes on Seismic Signals or How to Improve the Quality of a Station. *Bull. seism. Soc. Am.*, **86**: 1760 - 1769.

Exss, J., Zürn, W. (2002). Reduction of noise in horizontal long period seismograms using local atmospheric pressure. This volume.

Gossard, E. E., Hooke, W. H. (1975). *Waves in the Atmosphere.* Elsevier, Amsterdam, 456 pp.

Kanamori, H., Mori, J. (1992). Harmonic excitation of mantle Rayleigh waves by the 1991 eruption of Mount Pinatubo, Philippines. *Geophys. Res. Lett.*, **19**: 721 - 724.

King, G.C.P., Zürn, W., Evans, R., Emter, D. (1976). Site Corrections for Long Periodic Seismometers, Tiltmeters and Strainmeters. *Geophys. J. R. astr. Soc.*, **44**: 405 - 411.

Möckli, A. (1988). Versuche zur Luftdruckabschirmung langperiodischer Seismometer. Diploma thesis, Institute of Geophysics, ETH Zürich, 93 p.

Müller, T. and W. Zürn (1983). Observation of gravity changes during the passage of cold fronts. *J. Geophys.*, **53**: 155 - 162.

Neumann, U., Zürn, W. (1999). Gravity signals from atmospheric waves and their modeling. *Bull. Inf. Marées Terrestres* **131**: 10139 - 10152.

Rodgers, P. W. (1968). The response of the horizontal pendulum seismometer to Rayleigh and Love waves, tilt, and free oscillations of the earth. *Bull. seismol. Soc. Am.*, **58**: 1384 - 1406.

Sorrells, G. G. (1971). A preliminary investigation into the relationship between long-period seismic noise and local fluctuations in the atmospheric pressure field. *Geophys. J. R. astr. Soc.*, **26**: 71 - 82.

Widmer, R., Zürn, W. (1992). Bichromatic excitation of long-period Rayleigh and air waves by the Mount Pinatubo and El Chichón volcanic eruptions. *Geophys. Res. Lett.*, **19**: 765 - 768.

Wielandt, E., Streckeisen, G. (1982). The Leaf-Spring Seismometer: Design and Performance. *Bull. seism. Soc. Am.*, **72**: 2349 - 2368.

Zürn, W. (2002). Simplistic models of vertical seismic noise above 1 mHz derived from local barometric pressure. This volume.

Sources and transfer mechanism of seismic noise: Preliminary results from FEM models

Kasper D. Fischer *
Institut für Geowissenschaften
Friedrich-Schiller-Universität
D-07740 Jena / Germany

Abstract

The influence of barometric pressure changes and dynamic pressure load on seismic records is investigated with numerical models for the Geodynamic Observatory Moxa (MOX). The numerical model is based on the finite-element-method (FEM). The geometry of the model is derived from the topography in the vicinity of the observatory. It can be shown that barometric pressure, dynamic pressure and the geometry of the station vicinity have a large influence on the noise level of seismological data. The tilt produced by dynamic pressure loads caused by wind can significantly influence the quality of seismic records. The results obtained from the model are in good agreement with observed data.

1 Introduction

Interpretation of long period seismograms (and gravity records) are mainly limited by noise due to barometric pressure (BEAUDUIN et al., 1996; ZÜRN & WIDMER, 1995). Enhancements of the signal to noise ratio can be achieved i. e. by regression methods (EXSS & ZÜRN, 2002; ZÜRN & NEUMANN, 2002) or numerical models of the involved physical processes. Significant enhancements can be expected for the horizontal components of seismometers. This can be very useful in the frequency range 0.01 mHz to 10 mHz where changes in atmospheric pressure are a major source of the noise. This frequency range is also the range of the earth's free oscillation. Changes in barometric pressure and dynamic pressure (wind) lead to strain at the earth's surface. This strain can cause significant tilts (strain-tilt-coupling) at the locations of seismometers or other geodynamical observation instruments (ZÜRN & NEUMANN, 2002), thus adding signals (noise) to the records. The process of strain-tilt-coupling is understood

*E-Mail: kfischer@geo.uni-jena.de, Phone +49 3641 948664, Fax +49 3641 948662

in principle but the real coupling in a non-uniform environment can be very complex. In additon numerical models are the only way to quantify the physical processes of strain-tilt-coupling in realistic environments.

This paper focuses on the numerical modeling of such processes at the location of the Geodynamic Observatory Moxa (MOX), Germany. The observatory is equipped (besides other instruments) with two horizontal strainmeters (north-south and east-west, each 25 m long), a laser strainmeter (forming a triangle with the two other strainmeters), a STS-1 and a STS-2 seismometer, and a superconducting gravimeter (SG CD-034). The strainmeters and seismometers are located in a 94 m long gallery. The numerical model concentrates on quantifying the tilt at the location of these instruments caused by barometric pressure and wind.

Knowledge of the physical processes and relations improves our understanding of observable phenomena related to barometric pressure in geodynamical recordings. Empirical relations between the modeled changes in pressure and calculated tilts can yield standard procedures to correct for barometric noise in the relevant frequency band.

2 The FEM-Model

The nature of the observed noise in seismological data is investigated with a numerical model of the vicinity of the Geodynamic Observatory Moxa with the finite-element-method (FEM). The model (Fig. 1) has an overall dimension of 1600 m $\times$ 1600 m in the horizontal directions and extends to a depth of 250 m below the top surface. The geometry of the model reflects the local topography around the station, which is located in a narrow valley. The entrance of the gallery is marked with a circle in figure 1. The gallery extends 60 m perpendicular to the valley axis in an east-west direction into a mountain. Then the gallery turns southwards and extends another 34 m further into the mountain. The flank of the valley rises 30 m in height with a slope of 20.8°. The gallery is included as void space in the model. The finest mesh size of the model is about 0.5 m at the gallery and the coarsest mesh size about 50 m at large distances from the observatory. The modeled elastic material has a Young's modulus of 76.53 GPa, a Poisson's ration of 0.25 and a density of 2710 kg/m^3. The boundary conditions of the FEM-model restrict the motions of element nodes at the edges of the model:

- No motion perpendicular to the edge at the northern, southern and eastern edge.
- No motion in the vertical direction at the bottom surface of the model.
- Elastic forces restrict the motion of the nodes at the western edge of the model. These forces simulate the crustal material of the western half of the valley which is not included in the model.

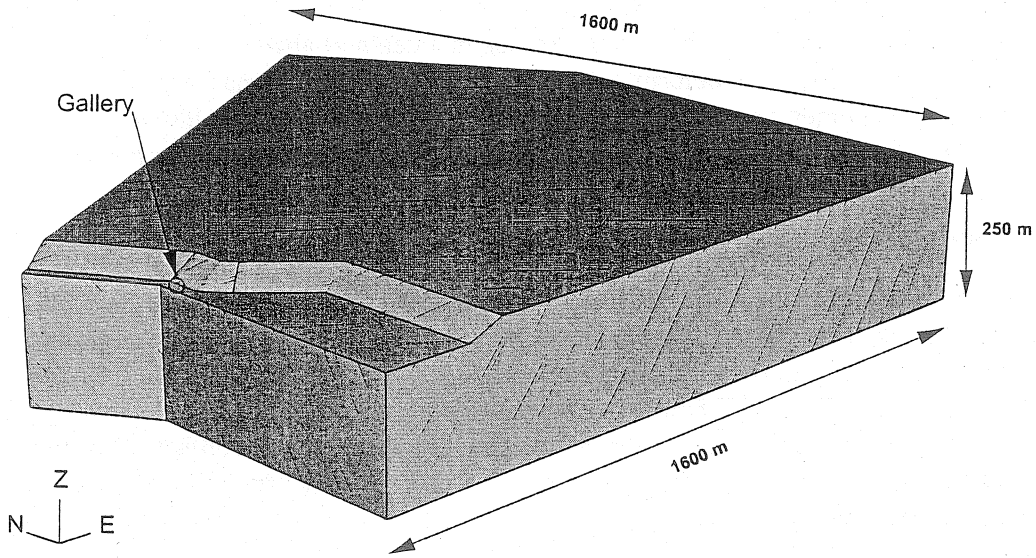

Figure 1: The FEM-model of the Geodynamic Station Moxa and its vicinity. The location of the gallery entrance is marked with a circle. Only the eastern part of the valley is included in the model.

To investigate the influence of changes in barometric pressure the model is loaded with three load cases:

1. A homogeneous pressure of 100 hPa on the top surfaces of the model.
2. A pressure of 10 hPa on the flanks of the hill simulating the dynamic pressure of the wind.
3. Case 1 and 2 simultaneously.

The obtained results for the deformation are directly proportional to the magnitude of the applied pressure. This is the result of the pure elastic rheology which satisfies the principle of superposition.

3 Results

The obtained strain and tilt at the surface of the model are shown in figures 2 and 3 respectively. It is clearly seen that the geometry of the north-south extending valley

influences the direction and magnitude of the deformation significantly. The deformation decreases rapidly with depth: Strain and tilt are largest on the surface of the model and especially at the flanks of the hill and vanish in a depth of about 50 m.

More important than the deformation at the surface is the deformation at the locations of the seismometer and strainmeters within the gallery. Table 1 summarizes the strain at the location of the strainmeters and the tilt at the location of the seismometer.

3.1 Strain

The strain varies from $1.0\,10^{-9}$ to $5.7\,10^{-9}$ depending on direction and load case. The strain is about a factor of 4 higher in the north-south direction than in the east-west direction for the load case of homogeneous pressure. The dynamic pressure of the wind load leads to the same amount of strain in both components. The calculated strains are smaller than the resolution of the strainmeters. This is confirmed by the observed strain records which show no obviously correlation of the noise level with changes in barometric pressure.

3.2 Tilt

The tilt at the location of the seismometer shows a more complex pattern than the results for the strain at the strainmeter position. The highest values occur in the east-west direction in contrast to the results for the strain. These values are 2 – 3 times higher than the ones for the north-south direction. The largest difference shows up in the load-case with dynamic pressure loading only. The records of the horizontal components of the STS-1 seismometer in Moxa also show high noise level in the frequency range of 0.01 – 10 mHz on windy days (EXSS & ZÜRN, 2002). The results of EXSS & ZÜRN (2002) yield that the noise level of the north-south component correlates better with atmospheric pressure than the east-west component. This supports the modeled difference in tilt. The strong dependence of the noise level on wind speed is also seen in records of a borehole tiltmeter in front of the observatory (located in a depth of 50 m), which measures the tilt directly and not the displacement induced by the tilt. This supports the modeled difference of the load cases with and without wind.

Table 1: Calculated strain ε and tilt ϕ at the location of the strainmeter and seismometer in the gallery of the Geodynamic Observatory Moxa.

	$\varepsilon_{NS}[10^{-9}]$	$\varepsilon_{EW}[10^{-9}]$	$\phi_{NS}[10^{-9}]$	$\phi_{EW}[10^{-9}]$
barometric pressure	−4.2	−1.0	17.3	34.8
dynamic wind load	−1.5	−1.4	3.7	10.1
pressure + wind	−5.7	−2.3	21.0	44.9

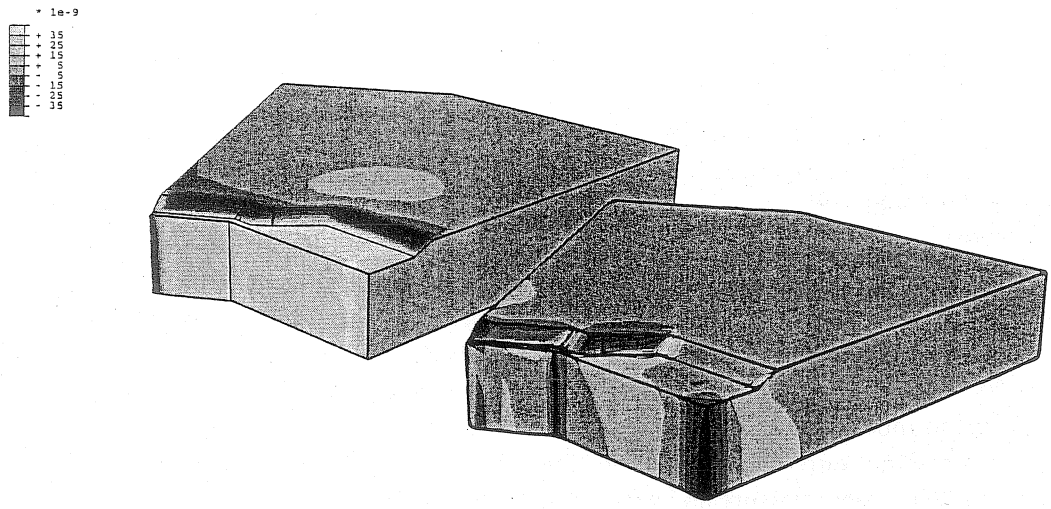

Figure 2: Strain at the model surface for the east-west (left) and north-south component (right).

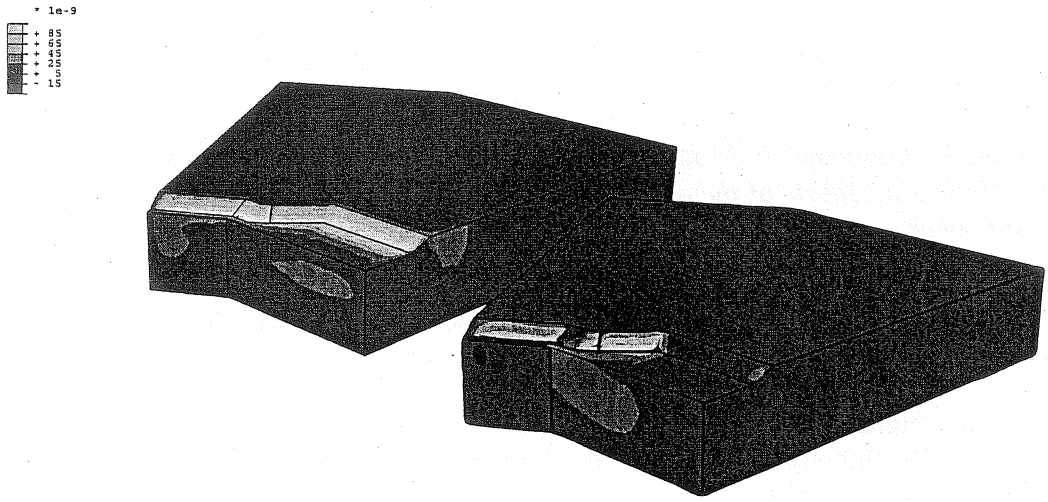

Figure 3: Tilt at the model surface for the east-west (left) and north-south component (right).

4 Conclusions

The results obtained from the preliminary numerical model are qualitatively in good agreement with the observed tilt and strain at the Geodynamic Observatory Moxa. Especially the higher values in the east-west direction of the tilt fit very good to the observed differences of the correlation of noise level and atmospheric pressure by EXSS & ZÜRN (2002). The high influence of the dynamic pressure load (wind) is clearly seen in the model and in the records of the seismometers, strainmeters, and borehole tiltmeter. The quantitative relationship between barometric and dynamic pressure and the induced tilts and strains has not been explicitly evaluated yet. This will be done for an enhanced model, which is in preparation. It can be expected that a revised model can reproduce not only the observations qualitatively but also provides a quantitative relationship between pressure and wind variations and observed noise in seismological and in other geodynamical records. The expected quantitative results will give physical explanations for the coupling between barometric and dynamic pressure and the induced deformations.

Acknowledgment

The author wants to thank C. Kroner, W. Zürn and J. Exß for helpful discussions within the common project. The financial support of the Deutsche Forschungsgemeinschaft (DFG, Germany) is greatfully acknowledged.

References

Beauduin, R., Lognonne, P., Montagner, J. P., Cacho, S., Karczewski, J. F. & Morand, M., 1996: *The effects of the atmospheric pressure changes on seismic signals or how to improve the quality of a station*, BSSA 86 (6): 1760–1769.

Exß, J. & Zürn, W., 2002: *Reduction of noise in horizontal long period seismograms using local atmospheric pressure*, Bulletin d'Information des Marées Terrestres **this issue**.

Zürn, W. & Neumann, U., 2002: *Simplistic models of atmospheric effects in horizontal seismograms*, Bulletin d'Information des Marées Terestres **this issue**.

Zürn, W. & Widmer, R., 1995: *On noise reduction in vertical seismic records below 2 mHz using local barometric pressure*, Geophysical Research Letters 22 (24): 3537–3540.

Reduction of Noise in Horizontal Long Period Seismograms Using Local Atmospheric Pressure

Jan Exß *
Geophysical Institute
University Karlsruhe
D-76187 Karlsruhe / Germany

Walter Zürn †
Black Forest Observatory Schiltach
Universities of Karlsruhe / Stuttgart
Heubach 206
D-77709 Wolfach / Germany

1 Introduction

It is well known that the noise level of the horizontal components of seismic sensors is much higher than the level of the vertical ones. It is often assumed that the tilt of the seismometer's monument due to local pressure variation – besides other meteorological effects – is responsible for that effect, mainly in the frequency range below 10 mHz.

To improve the signal-to-noise ratio we try to find correlations between the seismic noise and pressure seismograms by using regressions that are based on simplistic physical models (ZÜRN & NEUMANN, 2002) and calculated by application of the seismometer's transfer function. The resulting pressure seismogram can be used to reduce the noise by substraction from the observed seismogram. The general plausibility of the models is demonstrated by numerical computation using the finite element method (FISCHER, 2002). Models will be modified according to results. We test our models for the geodynamic observatories BFO and MOX.

*E-Mail: jan.exss@gpi.uni-karlsruhe.de, Phone +49 721 608 4679
†E-Mail: walter.zuern@gpi.uni-karlsruhe.de, Phone +49 7836 2151

2 Physical Models

Two different physical models (ZÜRN & NEUMANN, 2002) are used which describe the response of the horizontal seismometer to local pressure variations.

1) **Local Deformation Tilt (LDT).** Tilt caused by quasistatic pressure changes.

2) **Travelling Wave Tilt (TWT).** Horizontal wave in atmosphere above elastic half space with attraction, tilt and inertial effect. See ZÜRN & NEUMANN (2002) for details.

3 Examples

3.1 Example 1: MOX

The first example is taken from a Moxa record in July of 2001, with a length of only 24 hours. Figure 1-a shows the original seimic data of the EW STS-1 seismograph of station MOX. There is an unusual signal which doesn't seem to be caused by seismic motion of the ground. Additionally, the pressure signal is shown in Figure 1-b. To

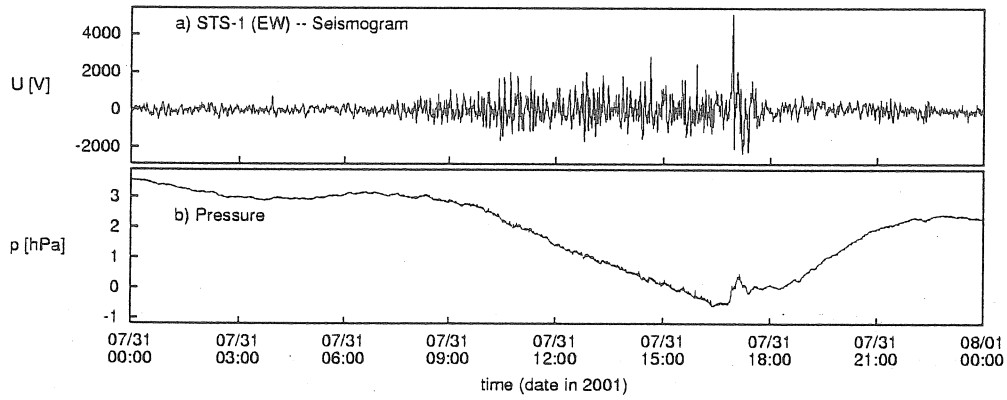

Figure 1: Example 1 – MOX. Original seismic and pressure data (EW)

reduce the noise of the seismic record, both models LDT and TWT are used to calculate pressure seimograms, which represent the motion of the seismometer's monument according to local pressure changes, correctness of the theoretical models assumed. These are then fit simultaneously to the data using least squares. The resulting model seismogram is shown in Figure 2-a. Figure 2-b shows the residual seismogram after subtraction of the model from the observed data. This method clearly reduces the noise of the seismic record.

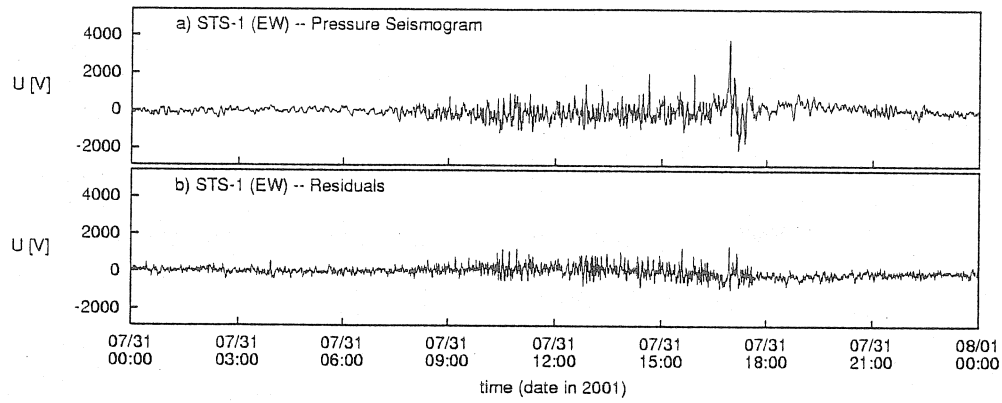

Figure 2: Example 1 – MOX. Calculated pressure seimogram and residuals (EW)

3.2 Example 2: BFO

As an example for more typical seismic signals, Figure 3 is showing a ten days record from BFO (Schiltach). Earthquake activity was very low in that period of time. Therefore, a lot of the energy forming the seismogram is produced by local air pressure rather than by earthquakes or other seismic signals, such as microseismic noise. There

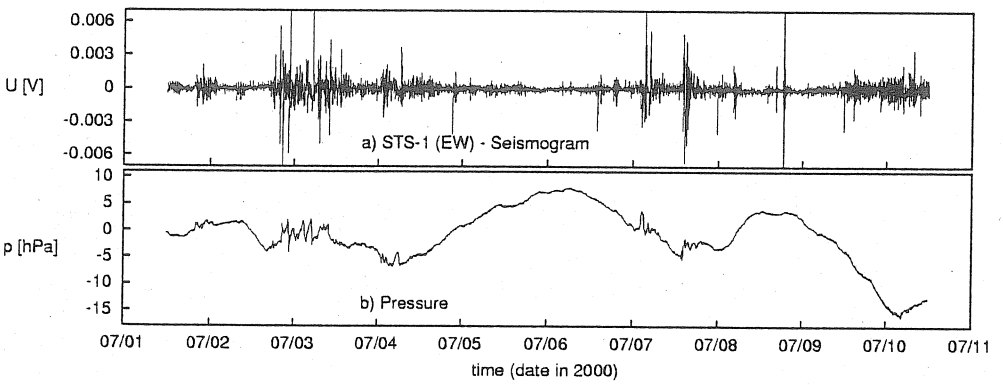

Figure 3: Example 2 – BFO. Original seismic and pressure data (EW)

are several obvious disturbances by pressure changes to the seismic sensor's output, especially on the 3rd and 7th of July. On the other hand there are signals that are most likely caused by real seismic motion, for example the earthquake in the second half of the 8th of July. We applied the same method as above to find the optimal pressure seimogram (Figure 4-a) and subtracted this from the observed data (Figure 4-b). Whereas the earthquake signals are taken over with no change, the signals that had been evoked by local tilts of the monument are clearly reduced.

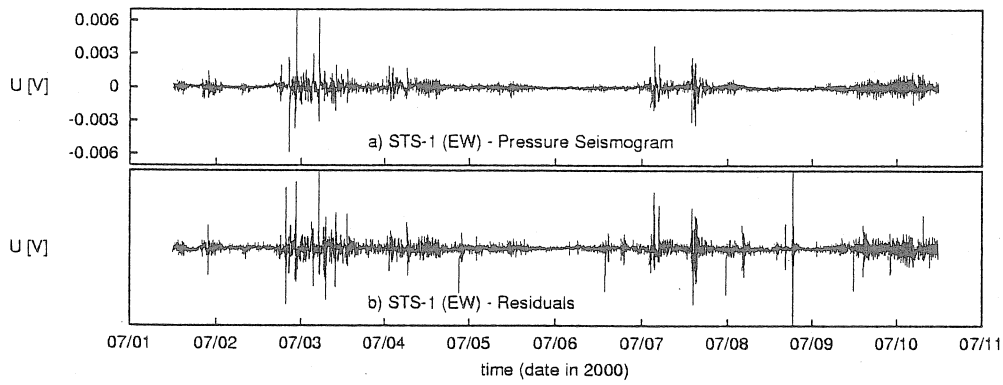

Figure 4: Example 2 – BFO. Pressure seismogram and residuals (EW)

4 Variance Reduction

Processing seismic records using our simplified models results in a considerable noise reduction. Figure 5 depicts the acceleration power spectral density of STS-1 EW-component at BFO for the same period of time as used in Section 3.2. The dotted line is the spectral density of the original record, the solid line the residuals. For comparison, Peterson's New Low Noise Model (PETERSON, 1993) for vertical seismic noise is also shown (labeled NLNM). The variance reduction is more than 50 percent, half of an order of magnitude.

The present focus of our interests is on testing the procedure's stability. Dependent on the length of the analyzed record and on the presence of small teleseismic signals the average variance reduction is about 40 percent for the NS-component and more than 50 percent for EW. For the station MOX we get variance reductions of more than 20 percent for the EW-component, whereas the NS-sensor appears to be insensitive to pressure. That might be due to a lower dependency of that component on local pressue changes or it could mean that there is a need to measure the air pressure in a different location than we did in the past.

When the second data example (the 10 days BFO record of July 2000) is analyzed for different time windows, we get variance reductions as shown in Figure 6. Parts a) and b) give the pressure seismogram and the residuals as a reference, while Figure 6-c) and d) document the regression coefficient's dependence on the window length and on the seismic signal, respectively. For a time window length of 2 days, as in Figure 6-c), the variance reduction is very high for signals induced by local pressure variation only, as on the 3rd of July and on the 7th, respectively. Teleseismic signals like the ones on the 5th and 9th of July 2000 lower the variance reduction to nearly zero, as espected. Usually, time windows of at least 4 days give reasonable results, i. e. the the variance reduction is stable, as shown in Figure 6-d).

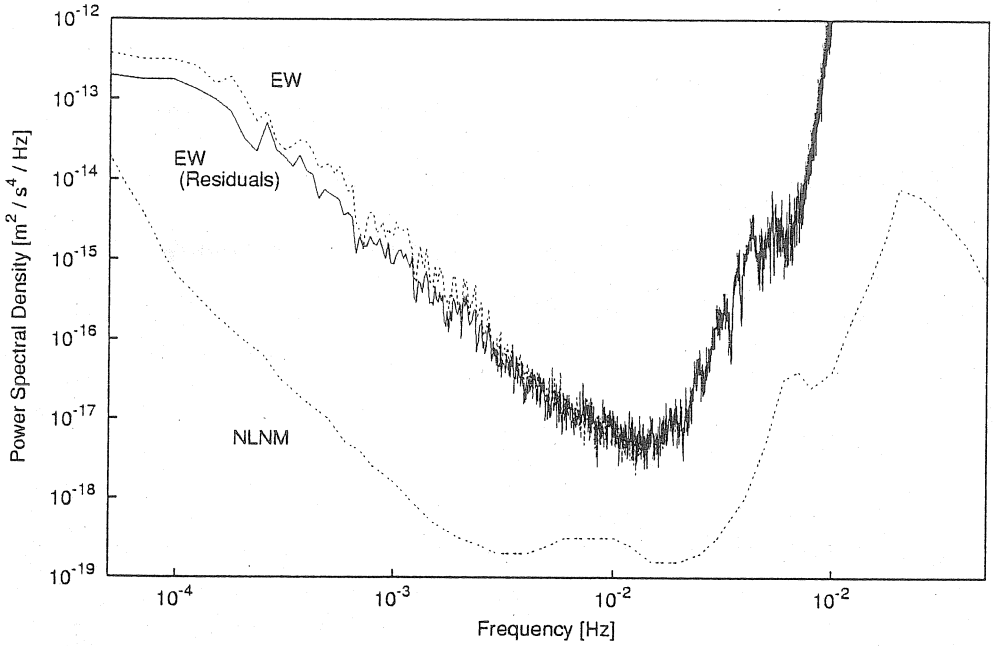

Figure 5: PSD-reduction for one horizontal seismic sensor when using both models LDT and TWT. Computed for 10 day record from BFO (EW-component)

5 Outlook

To improve the reduction of noise in horizontal seismograms we will try to continue with the following items:

- Stability: We need to process more data sets to check the stability of the procedure. Checks with very long time series need to be done as well.
- Models: We need to tune the simple physical models according to the results of the numeric modeling.
- MOX: Concerning the present lack of pressure resistent doors we might have to use pressure sensors inside the station as as well as outside.
- BFO: To learn more about effects of a travelling pressure wave we want to establish a small pressure sensor array around the station.

References

Fischer, K. D., 2002: *Sources and transfer mechanism of seismic noise: Preliminary results from FEM models*, Bulletin d'Information des Marées Terestres **this issue**.

Peterson, J., 1993: *Observations and Modeling of Seismic Background Noise*, U. S. Geol. Survey,Open-File Rep. **93-322**: 1–45.

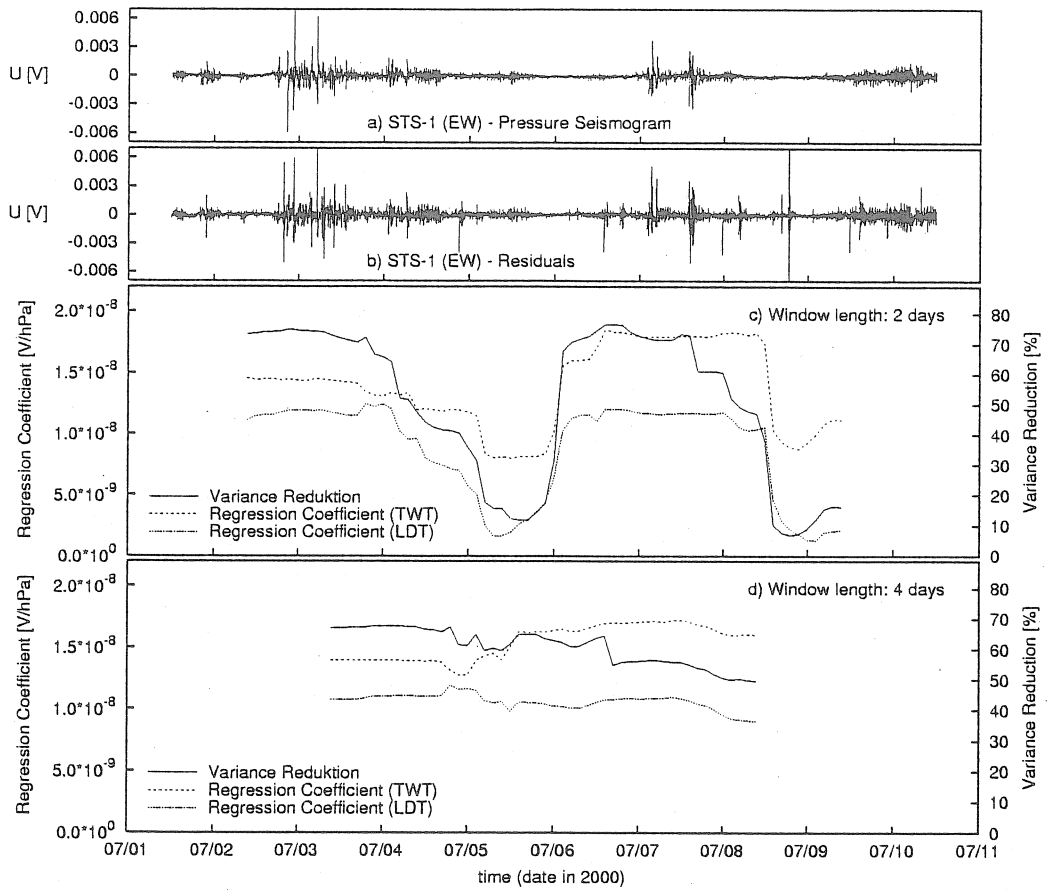

Figure 6: Stability of regression coefficients and variance reduction vs. time and for different window lengths.

Zürn, W. & Neumann, U., 2002: *Simplistic models of atmospheric effects in horizontal seismograms*, Bulletin d'Information des Marées Terestres this issue.

Microbarograph for investigation of geodynamical phenomena caused by atmospheric pressure variations influenced by lunisolar effects

Gyula Mentes

Geodetic and Geophysical Research Institute of the Hungarian Academy of Sciences,
Csatkai E. u. 6-8. H-9400, Sopron, Hungary

Abstract

The air pressure variations due to lunisolar effects cause the deformation of the Earth and therefore directly and indirectly influence several geodynamical phenomena. For a better understanding of these effects a microbarograph of high sensitivity was developed in the Geodetic and Geophysical Research Institute of the Hungarian Academy of Sciences in 1991. In this paper the construction of the instrument and the calibration method are described and the measured data are presented. The microbarograph data can be used to study atmospheric tides, the connection between air pressure variations and relevant geodynamical phenomena, the relationship between barometric pressure and instrumental effects. The results of the first data analyses are also given.

1. Introduction

Earth tide measurements are influenced by several environmental disturbances that must be taken into account before these records are used to obtain information on physical properties or geodynamics of the solid Earth. One of such phenomena is the barometric pressure variation on the surface. The influence of pressure variation on Earth tide measurements - gravitational and other types (extensometric, tilt, etc.) - consists of two main parts:

- direct attraction of the atmospheric mass,

- indirect effect due to elastic deformation of the Earth which causes change in gravity due to vertical displacement of the Earth's crust and due to redistribution inside the Earth.

The dominant part is the direct attraction. According to investigations the total effect of air pressure variations cause a gravity response of 0.3-0.4 μGal/mbar in the case of local pressure fluctuations (responsible for a part of the random fluctuations of gravity records) while the response to the global atmospheric tides is significantly larger (0.66 μGal/mbar for S_1 and 0.47 μGal/mbar for S_2, for the two main pressure tide waves) according to the results published by Warburton and Goodkind [1977]. For these reasons it is very important to correct Earth tide measurements for atmospheric variations. To provide appropriate corrections air tide parameters must be determined for the given location and response effects have to be investigated.

Another reason for monitoring of air pressure variations is that there are a lot of connections between atmospheric tides and different geodynamical phenomena of the solid Earth. To

study these relationships high sensitive barographs are needed. The difficulty of such investigation lies in the fact that the magnitude of the air pressure variations is much higher than the one caused by lunisolar effects. For that reason a very sensitive microbarograph with a broad measuring range was developed at the Geodetic and Geophysical Research Institute of the Hungarian Academy of Sciences (GGRI) in 1991.

2. Construction of the microbarograph

The principle of the microbarograph is shown in Fig.1. The pressure sensor is a very sensitive closed diaphragm applied in conventional mechanically recording barographs used for meteorological measurements. The bottom of the closed diaphragm is firmly fixed to a rigid frame. The displacements of the top of the closed diaphragm due to air-pressure variations are sensed by a differential condenser. The moving plate of the transducer is fastened to the middle point of the top of the diaphragm and the fix plates are fastened to the rigid frame isolated electrically from it. The capacitance changes of the transducer are measured in a bridge circuit developed at the GGRI (Mentes, 1983, 1994).

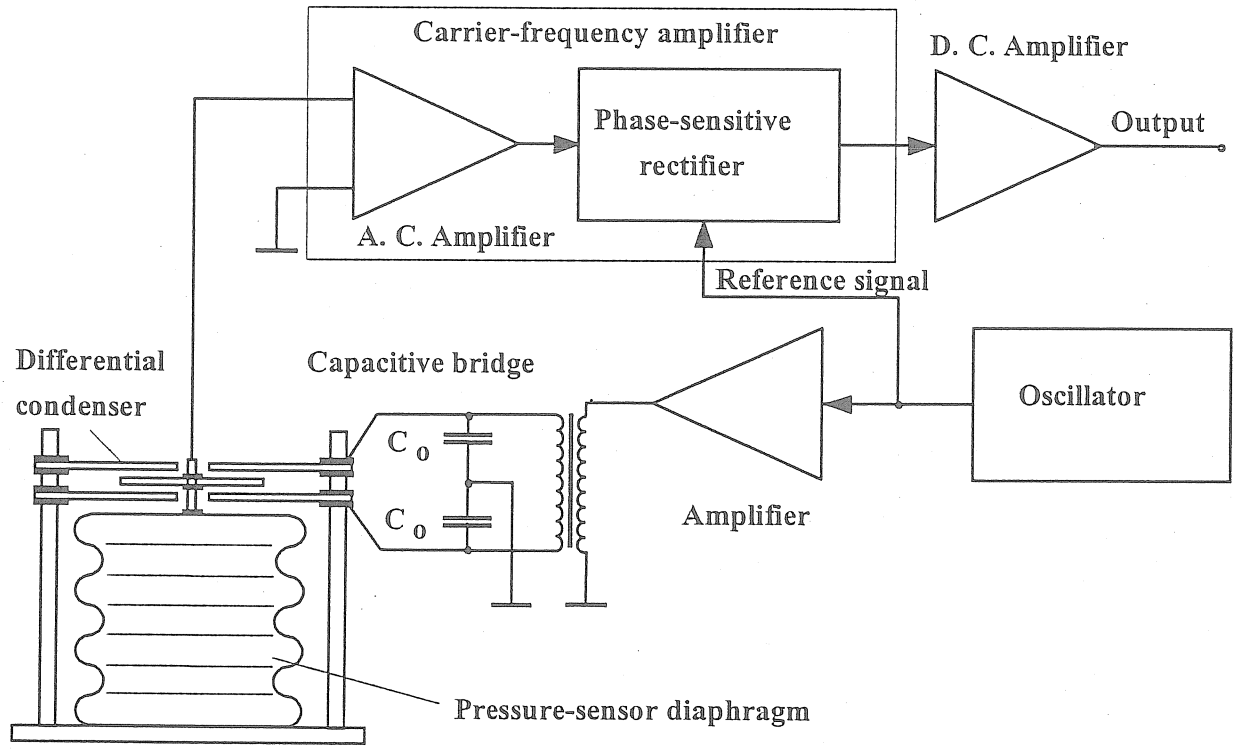

Fig.1. The construction of the high sensitive microbarograph

3. Calibration of the microbarograph

At first the calibration of the microbarograph was made by comparision of its output signal with the air pressure measured by other precision barometers during large barometric pressure changes. This solution had a limited accuracy and was not suitable for the exact determination of the characteristics of the microbarograph. For regular in-situ calibration of the instrument a calibration equipment shown in Fig. 2. was constructed. The microbarograph is placed in a vessel, in which the air pressure can be increased or decreased in relation to the

actual air pressure by means of air pumps. During recording air pressure valve 1 is open and valves 2, 3 are closed. During the calibration valve 1 is closed. In this case an additional pressure can be added to the external air pressure by means of the compressor if valve 3 is open and the compressor is working (valves 1, 2 are closed). The air pressure in the vessel can be decreased in relation to the external air pressure by the vacuum pump when valves 1, 3 are closed and 2 is open. The air pressure differences can be measured manually by means of an U-gauge filled with water. In this case the measurement of the pressure is made on a clear physical principle and therefore the measurements are not affected by the errors of other electrical pressure sensors. Figures 3 and 4 show the inner part of the microbarograph and the calibration equipment respectively.

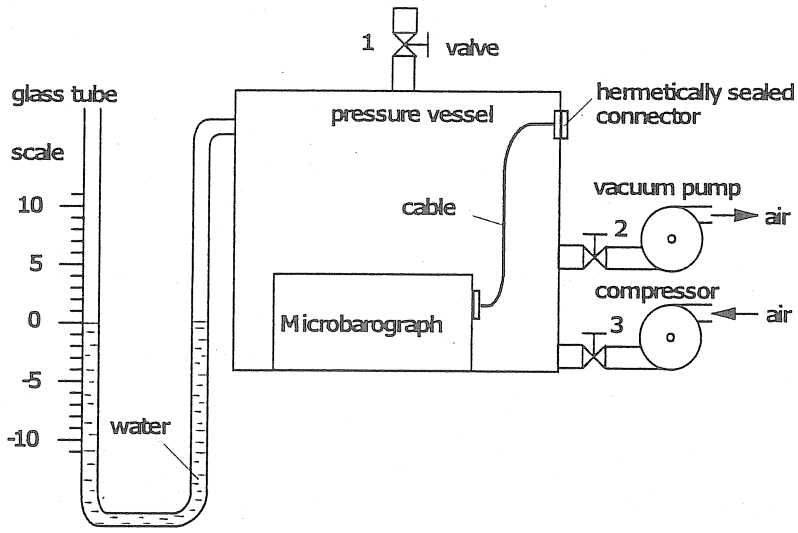

Figure 2. Equipment for the calibration of the microbarograph

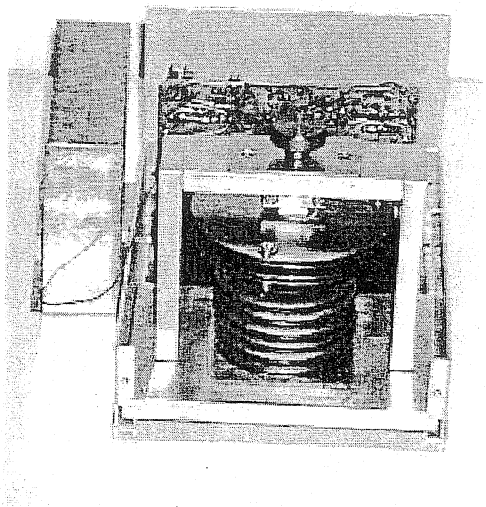

Fig. 5. The inner part of the microbarograph

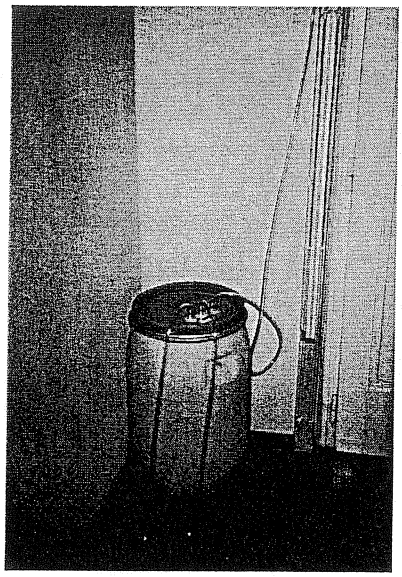

Fig. 6. The calibration equipment of the microbarograph

The scale factor of the microbarograph obtained by several calibrations is 0.3 V/hPa. The characteristics of the instrument and its linearity errors are shown in Fig. 5. The highest linearity error of the instrument in the investigated measurement range (approx. 65 hPa) is less than 1%. The instrument must have a lower linearity error because one part of the errors arises from the calibration method.

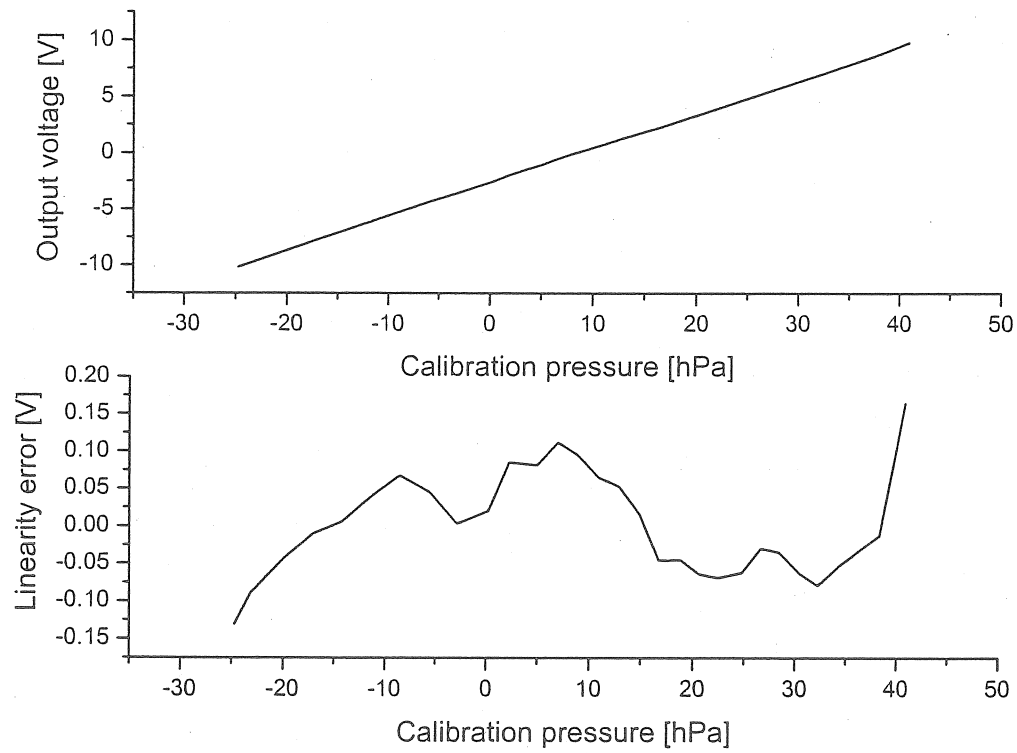

Fig. 5. Characteristics of the microbarograph and its linearity errors

4. Results of the atmospheric tide measurements

The microbarograph was installed at the Geodynamical Observatory of the Geodetic and Geophysical Research Institute of the Hungarian Academy of Sciences in Sopron for recording air pressure variations in the vicinity of the long quartz tube extensometer. The annual temperature variation in the recording room is less than 0.5 °C. The constant temperature is very important because the sensor membrane of the microbarograph is sensitive to temperature variations.

Since 1992 several series of experimental analogous recordings have been made. This time for the calibration of the instrument a conventional high precision pointer barometer was used and its pressure values were regularly compared with the signal of the microbarograph. From the recorded data three continuous data series and their amplitude spectra are shown in Fig. 6. The recorded data show how strongly depends the barometric record on the weather, especially on the daily temperature variations. Regarding the construction of the microbarograph it means that the instrument must have high resolution and a high dynamic range simultaneously because the weather effect is much greater than the tidal one.

The Fourier representation of the raw data series was produced to detect atmospheric tidal variations covered by much larger pressure changes caused by weather system variations. To

enhance the tidal peaks in the spectrum the raw data (sampling rate: 10 min.) were filtered by a moving average filter which replaces raw data by the average calculated of the data being in question and of 12-12 data before and after it.

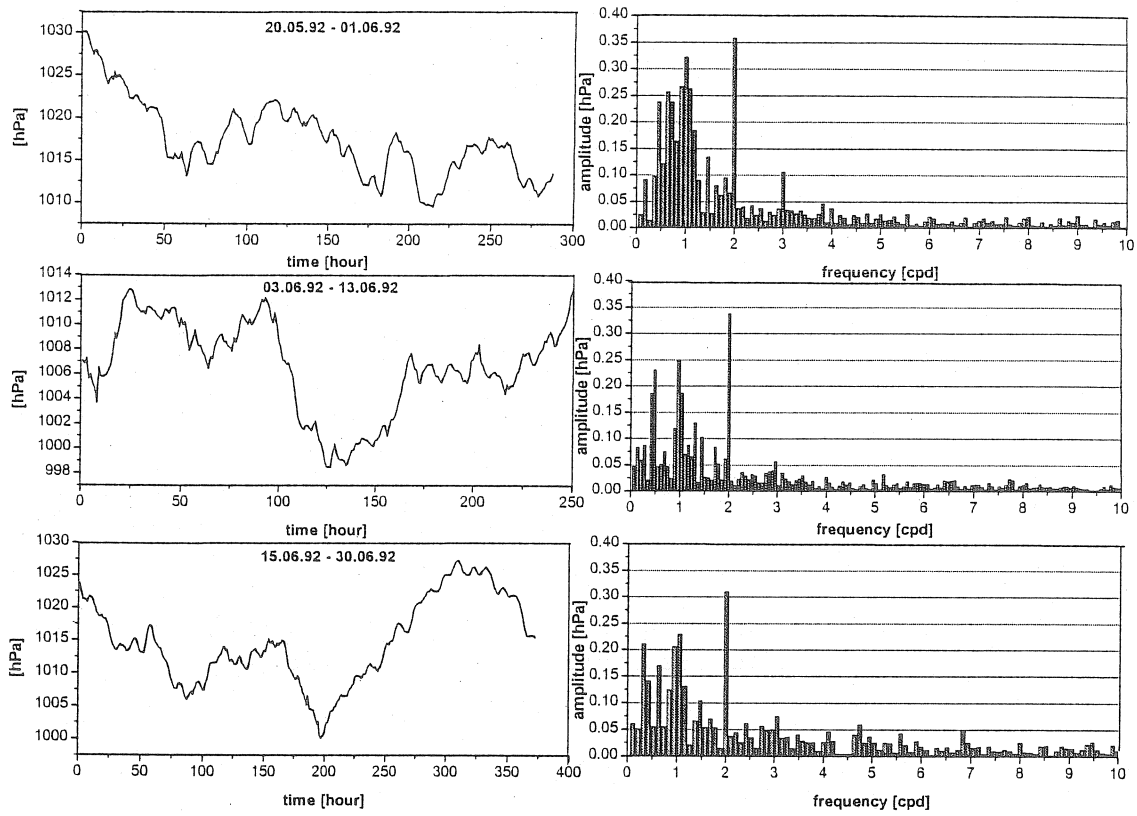

Fig. 6. Air pressure recorded by the microbarograph in the time interval: 20.05.92. - 01.06.92.

To investigate the temperature dependence of the instrument we placed it in the institute in a room where the temperature variation was high. The air pressure and temperature pressure variations were measured simultaneously. Figure 7. shows the raw data measured from 01.01.2001 till 28.08.2001. The large amplitudes are cut by the datalogger at ± 2500 mV. The drift of the microbarograph is very low and has no correlation with the trend of the temperature. It means that the direct temperature effect on the instrument is negligible and the sensitivity of the instrument can be further increased if we apply a datalogger with a greater input range and a higher resolution. This will make possible to detect smaller components of the barometric tides. The correlation between pressure variations and the short periodic temperature variations is obvious. This is due to the dependence of the air pressure on the temperature variations.

Figure 8 shows only the variations of the air pressure and the amplitude spectrum of the data presented in Fig. 7. These data series are longer than the ones shown in Fig. 6. Therefore the amplitude spectrum of the later one is much more disturbed in the long periodic range than the one of the shorter data series. The reason is the seasonal variation of the air pressure.

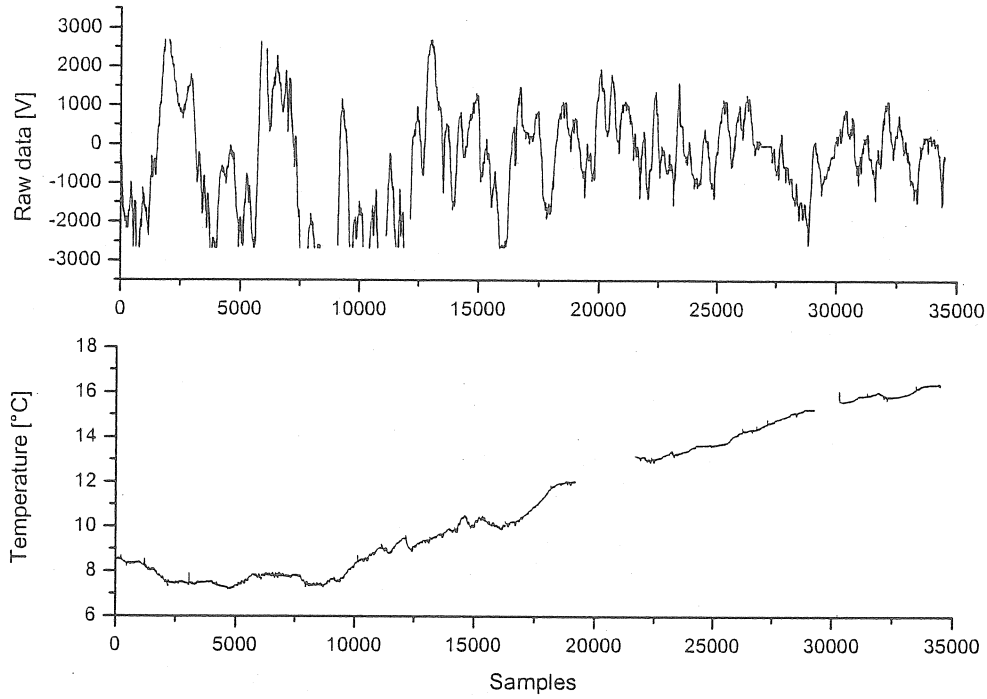

Fig. 7. Air pressure recorded by the microbarograph and simultaneous temperature record in the time interval: 01.01.2001. - 28.08.2001.

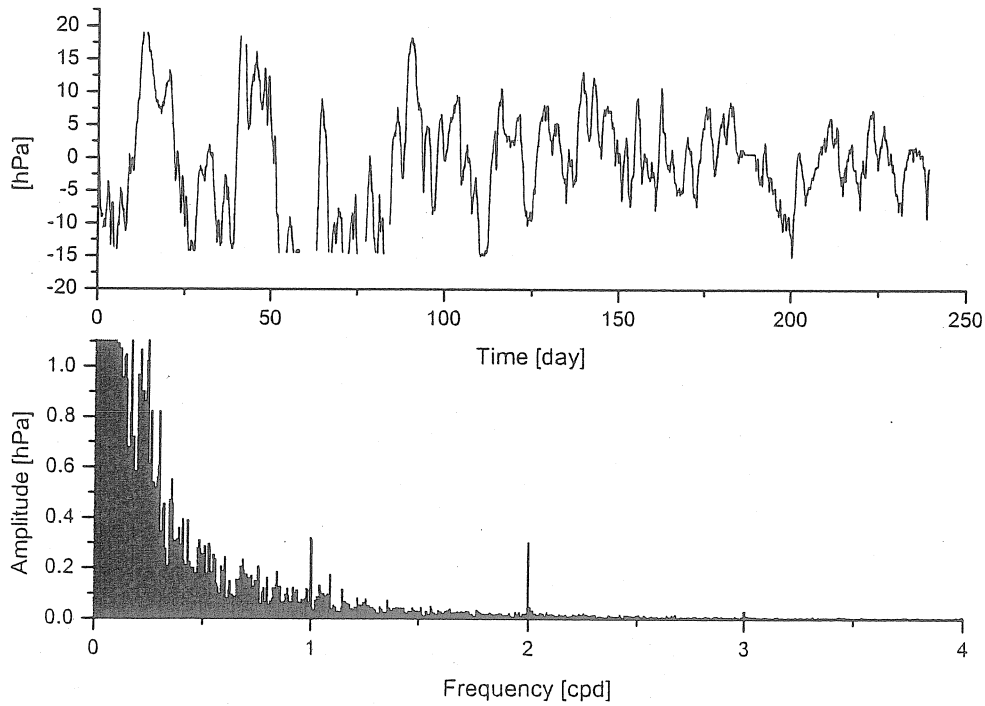

Fig. 8. Variation of the air pressure recorded by the microbarograph from 01.01.2001 till 28.08.2001 and the amplitude spectrum of the pressure variations

There are small periodic oscillations in the Earth's atmospheric pressure variations. These worldwide coherent waves are excited thermally and gravitationally, where the gravitational part is in general much weaker. One type of air tide waves is solar waves driven thermally with frequencies of one solar day and integer multiples ($S_1(p)$, $S_2(p)$, $S_3(p)$, $S_4(p)$). In this case the most important sources of excitation are the insolation and the absorption by ozon and water vapor. The other type is the lunar air tide waves with frequencies of one lunar day having significantly smaller amplitudes. The main components of the measured barometric tidal variations are the solar semidiurnal (dominant) and diurnal waves. The S-type waves are larger at equatorial regions, than at middle latitudes. They reach an amplitude of approx. 0.4 hPa.

The amplitude spectra calculated from the data measured by the microbarograph show the S-type waves very clearly. These are the diurnal, semidiurnal and terdiurnal peaks (Figs 6 and 8). The peaks S_4 apear also but they are very small. Table 1. summarizes the amplitudes of the detected S-type main atmospheric tidal waves. In spite of the analyzed short data series (especially data series 1-3. shown in Fig. 6.) the obtained amplitudes of the diurnal (S_1), semidiurnal (S_2) and terdiurnal (S_3) waves approximate rather well the values published by others (Chapman and Lindzen, 1970). The published annual mean amplitude of S_1 is 0.23 -0.24 mbar and the one of S_2 is 0.41 -0.42 mbar at the latitude of 45°. The air tide has also a seasonal variation. Therefore the mean values of the different type waves are given in special groupings. For example in the group J-season S_1 is 0.33 -0.34 mbar and S_2 is 0.4 mbar.

Table 1. Amplitudes of the different S-type waves measured by the microbarograph

Waves	Amplitudes [hPa]				Mean value [hPa]	RMS error [hPa]
	Data series 1.	Data series 2.	Data series 3.	Data series 4.		
S_1	0.322	0.249	0.229	0.313	0.278	0.026
S_2	0.358	0.337	0.309	0.302	0.327	0.015
S_3	0.106	0.057	0.070	0.031	0.066	0.018
S_4	0.037	0.0086	0.026	0.0046	0.019	0.011

Acknowledgements

This research was supported by grant OTKA T 031713, T038123 and by Deputy Under-Secretariat of Ministry of Education for Research and Development and by its foreign contractual partner, Friedrich Schiller Universität, Institut für Geowissenschaften, Jena (Hungarian project no. D-8/99) in the frame of the Scientific and Technological Cooperation between Germany and Hungary.

References

Chapman S, Lindzen R S 1970: Atmospheric tides. D. Reidel Publlishing Co.

Warburton R J, Goodkind J M 1977: J. Geoph. Res., 48, 281-292.

Mentes Gy.1983. Capacitive transducers for horizontal pendulums and gravimeters, Acta Geod. Geoph. Mont. Hung., 18, 359-368.

Mentes, Gy. 1994. Instruments for Precise Determination of Horizontal Deformations in the Pannonian Basin, Acta Geod. Geoph. Mont. Hung., 29, 161-177.

The effect of atmospheric pressure on strain measurement at the Sopron Observatory, Hungary

Gyula Mentes
Ildikó Eperné-Pápai
Geodetic and Geophysical Research Institute of the Hungarian Academy of Sciences
9400 Sopron, Csatkai E. u. 4-6.
Hungary

Abstract

We have investigated the effect of local atmospheric pressure on deformation measurement in Sopron Geodynamical Observatory, western Hungary. The atmospheric pressure variation is measured by a microbarograph and the strain data are measured by a quartz tube extensometer placed in a rock gallery. We found that in the frequency range above 2 days period the strain data has approximately 4 nstr/hPa extension with increasing pressure for 116° azimuthal location. Further we found a negative time shift regarding the best correlation of the time series of the parameters. One possible reason lies in the topography of the rock mass and the placement of the instrument.

1. Introduction

In the Sopron Geodynamical Observatory which is located about 5 km from the town of Sopron, a quartz tube extensometer has been working since 1990. The observatory is an artificial tunnel driven in gneiss, the coordinates are: latitude 47,7° N, longitude 16,5° W. In Fig. 1. the scheme of the observatory and location of the instruments are shown. The total length of the instrument is 22 m, it is situated about 30 m from the entrance and it is thermally insulated by three doors. The annual temperature variation near the instrument is less then 0,5 °C (Mentes, 1991).

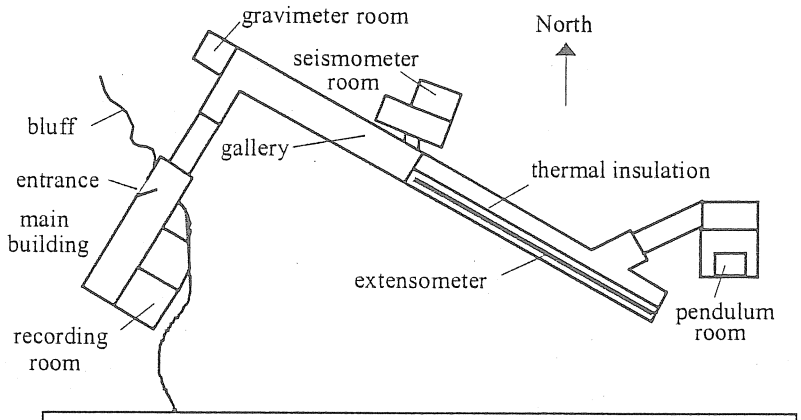

Fig. 1. Scheme of the Geodynamical Observatory of Sopron

A highly sensitive microbarograph was developed in the institute (Mentes, 1994) which is capable of measuring pressure variations and also atmospheric tides with good resolution (Mentes and Eper, 1997). This instrument was installed in the observatory in 1992 and it is working, with breaks for technical reasons, under the same conditions that apply to the extensometer.

When the global deformations of the Earth are measured by means of continuous geodynamical methods it can provide information on periodic deformations (Earth's tides). The long term variations can be related to tectonic forces and these records contain also the exogenic influences such as ocean and atmospheric loading. In the case of deformation measurements the records are influenced by meteorological parameters and by local elastic effects, like cavity, topography and geology depending on the given measurement site. The atmospheric pressure causes the following effects: the gravitational effect which is the direct attraction of the air mass, has no meaning in deformation measurements, and the indirect or deformation effect (vertical displacement of the earth's crust and mass redistribution inside the Earth) causes the deformation of the rock masses around the instrument. In the case of strain measurements the Earth's response to air pressure deviation from the mean pressure is ±10 nstr on the surface (Rabbel and Zschau 1985). In this paper we investigate the influence of local barometric pressure variation on deformation measurements under the conditions of the instrument site.

2. Data analysis

Continuous recording of the extensometric measurement is available since January 1990 and since the end of 1999 we have got digitally recorded data with a sampling interval of 10 minutes. The extensometer is calibrated once a day by a magnetostrictive coil. In the data analysis we have used a four months period: from September to December 2001. Both the extensometric and microbarograph data were filtered to 1 hour sampling interval and calibrated to the proper physical unit of measure.

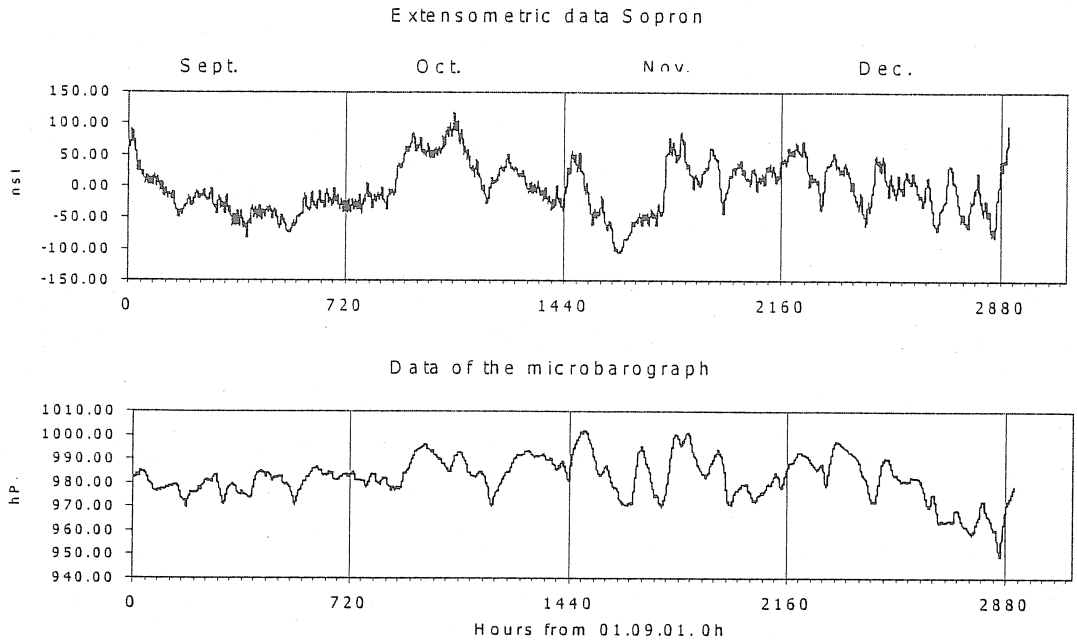

Fig. 2. Data of the extensometer and the microbarograph after preprocessing. Period is Sept.-Dec. 2001

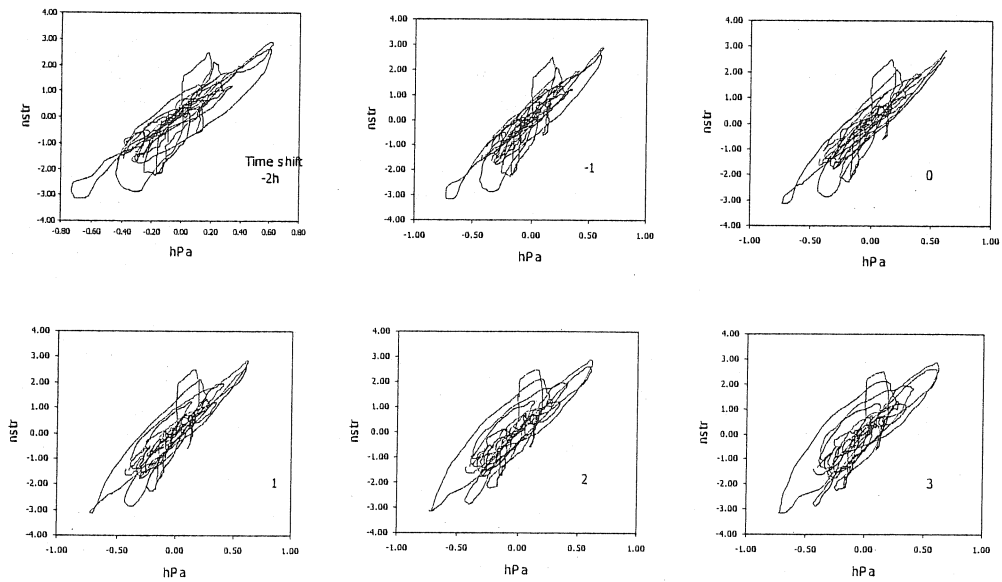

Fig. 3. Relation between strain and atmospheric pressure change data. 0,5 cpd low pass filtering is applied. Time shifts are from –2 to 3 hours

During the preprocessing operations steps in the data series were corrected, and gaps were interpolated by means of a least square fitting method in the vicinity of the gaps, using theoretical data series which were produced by Eterna 3.3 tidal data processing package. Data are shown in Fig. 2. after preprocessing steps. From the strain data the long term trend was removed by fitting a parabola within the measurement period. In this figure the connection between the strain data and the meteorological parameter is clearly visible.

In this data analysis procedure we investigated the relationship between strain and atmospheric pressure in the non-tidal frequency band. Firstly the long term trend was removed from the extensometric data and the short periods were reduced by low pass filtering with a cut off frequency of 2 days period. In Fig. 3. difference data series of the strain and pressure changes are drawn, with different time shifts between the series. It can be seen that when the atmospheric pressure increases the rock deformation shows extension. We evaluated the average strain change per unit pressure and the time shifts were statistically analysed. The best fit for low pass filtered data is one hour when strain change will be ahead of atmospheric pressure change. The same methods were applied to lower frequency bands. In Fig. 4. similar relation diagrams are drawn for the 2-3 days period band pass filtered data series. In this frequency band the best fit can be revealed also at 1 hour time shifting.

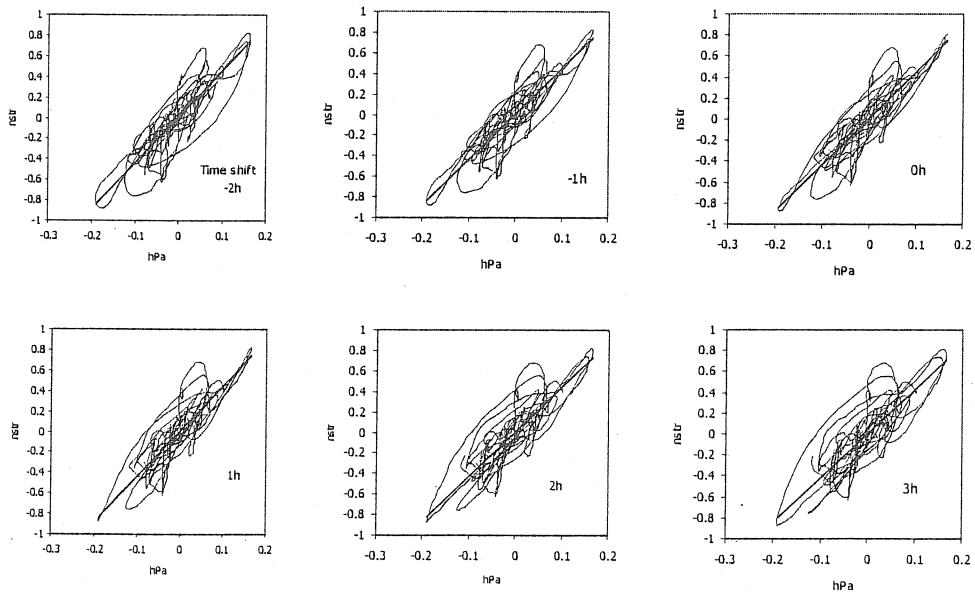

Fig. 4. Relation diagram between strain and atmospheric pressure change data. 0,33-0,5 cpd band pass filtering is applied. Time shifts are from –2 to 3 hours

The same procedure was carried out for lower frequency bands also. The chart in Fig. 5. shows the frequency dependence of the strain change per unit pressure. It can be seen from the values that for these measurement data the relation between strain and atmospheric pressure data depend weakly on frequency, although definite direction can be observed in the frequency function.

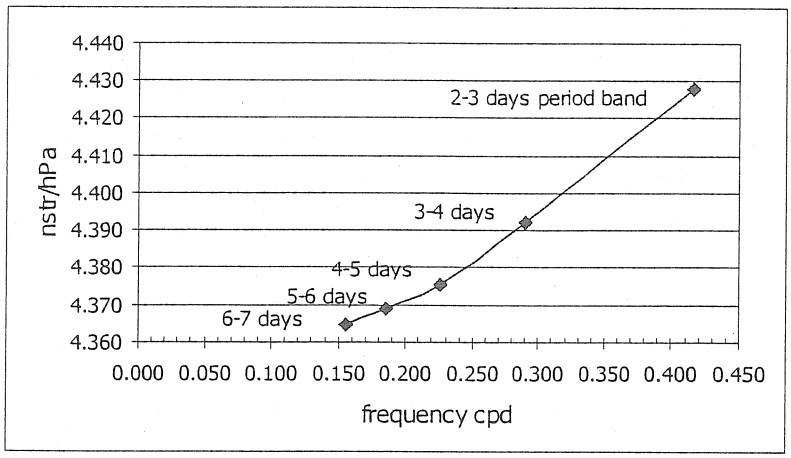

Fig. 5. Strain rate per unit atmospheric pressure change for frequency bands from 0,14-0,17 to 0,33-0,5 cpd

3. Discussion

We investigated the atmospheric pressure effect on extensometric data of Sopron. The relationship between the change of the atmospheric pressure in the gallery where the instruments are placed and the change of the rock deformation is clear. Considerable part of the non-periodic variations of the deformation measurements can be attributed to the pressure changes. It was found that in the frequency range above 0,5 cpd the regression coefficient varies with frequency in a narrow interval of strain per unit pressure, namely the average coefficient is around 4,4 nstr/hPa and the variation is approximately 0,1 nstr/hPa. From other investigations it seems that the influence of the pressure variation on different strain components strongly depends on the topography of the measurement site (Onoue and Takemoto, 1998). In the case of the Sopron Observatory the extensometer is not perpendicular to the high rock wall. Probably it is due to this topographic situation that our results show extension with increasing pressure while the atmospheric loading is dominant in the horizontal direction perpendicular to the wall.

Regarding the time shifts between the data series the strain data can be evaluated 1 hour ahead the local pressure. A possible explanation for this result can be the regional changes of the weather system and the atmospheric pressure, which can cause the outside deformation of the whole rock mass.

Although it was found that the extensometric data have low correlation with regional atmospheric pressure variation (Mentes, 2000). It is known that the atmospheric pressure has seasonal characteristics. We intend to investigate the role of seasonal pressure variations in the long term trend of strain data.

Acknowledgements

This research was supported by grant OTKA T 031713, T038123 and by Deputy Under-Secretariat of Ministry of Education for Research and Development and by its foreign contractual partner, Friedrich Schiller Universität, Institut für Geowissenschaften, Jena (Hungarian project no. D-8/99) in the frame of the Scientific and Technological Cooperation between Germany and Hungary.

References

Mentes Gy., 1991. Installation of a quartz tube extensometer at the Sopron Observatory. Marees Terrestres Bulletin d'Informations, no. 110, pp. 7936-7939

Mentes Gy., 1994. Instruments for precise determination of horizontal deformations in the Pannonian Basin. Acta Geod. Geoph. Hung., vol. 29. no. 1-2., pp. 161-177

Mentes Gy. and Eper I. P., 1997. Atmospheric tide measured by microbarograph. Marees Terrestres Bulletin d'Informations, no. 127., pp. 9826-9833

Mentes Gy., 2000: Influence of temperature and barometric pressure variations on extensometric deformation measurements at the Sopron Station. Acta Geod. Geoph. Hung., vol. 35., no. 3., pp. 277-282

Onoue K. and Takemoto S., 1998. Atmospheric pressure effect on ground strain observation at Donzurubo Observatory, Nara, Japan. in: Proc. of the 13th Int. Symposium on Earth Tides, eds.: Ducarme B. and Pâquet P., pp.157-164

Rabbel W. and Zschau J., 1985. Static deformations and gravity changes at the earth's surface due to atmospheric loading. Journal of Geophysics, vol. 56., pp. 81-99

Environmental effects on strain observation, their applications for geophysical study and necessity of deep borehole observation for noiselessly high quality

H.ISHII
Tono Research Institute of Earthquake Science (TRIES),Japan

We have been doing tilt and strain observation for both crustal movements and earthquake prediction studies by utilizing observation vaults or deep boreholes. Environmental effects sometimes influence observed data. In this presentation we discuss these effects by focusing on strain observation. Also we will demonstrate that environmental effects as considered to be noise can be usefully utilized for geophysical research.
Results obtained by our research are summarized as follows:

1.Strain observations in vaults are occasionally influenced by rainfall and effects depend on thickness of rock from ceiling of a vault to the surface of the mountain. Sometimes their responses can be successfully simulated by tank model or porous elastic theory. Strain observations in boreholes deeper than depth of 500m hardly are influenced by rainfall.

2.Strain response to rainfall reflects occasionally information on tectonic stress and there are some examples that anomalous strain variations caused by rainfall were related to occurrence of nearby earthquakes.

3.We have been doing continuous crustal movements observation in deep boreholes like 350m, 800m and so on. We have performed some active experiments like water injection and pump up water by means of different boreholes near these boreholes. Behavior of under water and constants related to response of the medium could be determined by these experiments. It is found that active experiments are important for crustal movements study.

4. On processes of studying environmental effects on crustal movements observations, it is clarified that deep borehole observation is necessity for obtaining noiselessly high quality data. By taking into account this, we have developed multi-component borehole instruments that can observe three components of horizontal strain, two components of inclined strain, a vertical strain, two components of tilt, 4 components of geomagnetism, three components of seismic waves and temperature. The multi-component borehole instrument has a size with 6cm to 10 cm of diameter and 150 cm to 500 cm of length depending on how many observation sensors are incorporated in the instrument. The instruments of about 50 were set up in areas with active crustal activities in Japan by some universities and governmental institutes up to now. Most of the instruments were installed in boreholes with depths from 150m to 800m for earthquake prediction observation and have recorded well data.

Environmental effects in tide strain observations near the Mt. Elbrus, Central Caucasus

A.Kopaev and V.Milyukov

Sternberg Astronomical Institute of Moscow State University,
Universitetsky prosp. 13, V-234, Moscow, 119899, Russia;
e-mail: **kopaev@sai.msu.ru**

Abstract

Results of tide strain observations with laser interferometric strain meter located near the sleeping volcano Mt. Elbrus during the 1998-2000 are presented. Sophisticated procedure of data processing using TSOFT, Preterna and Eterna programs helped to get reliable signal/noise ratio for M2 wave (up to 100) in spite of extremely high environmental perturbations. Simplified correction for topographic effect gave rather low value of amplitude coefficient of about 0.7 that could be caused by the influence of shallow hot magma chamber.

1. Introduction

Northern part of the Main Caucasian Ridge (*Fig. 1*) represents one of the most tectonically active regions of Russia and is characterized with intensive crustal movements reaching 1.5 cm/year. So-called Elbrus block is of particular interest as it houses the highest top of Europe – famous sleeping volcano Mt. Elbrus, see *Fig. 2*.

Elbrus is classified as an active volcano according to UNESCO, as its last eruption took place some 1700 years ago and there exist a lot of geophysical implications about the possibility of its awakening *(Bogatikov et al., 1998, Kopaev et al., 1995)*.

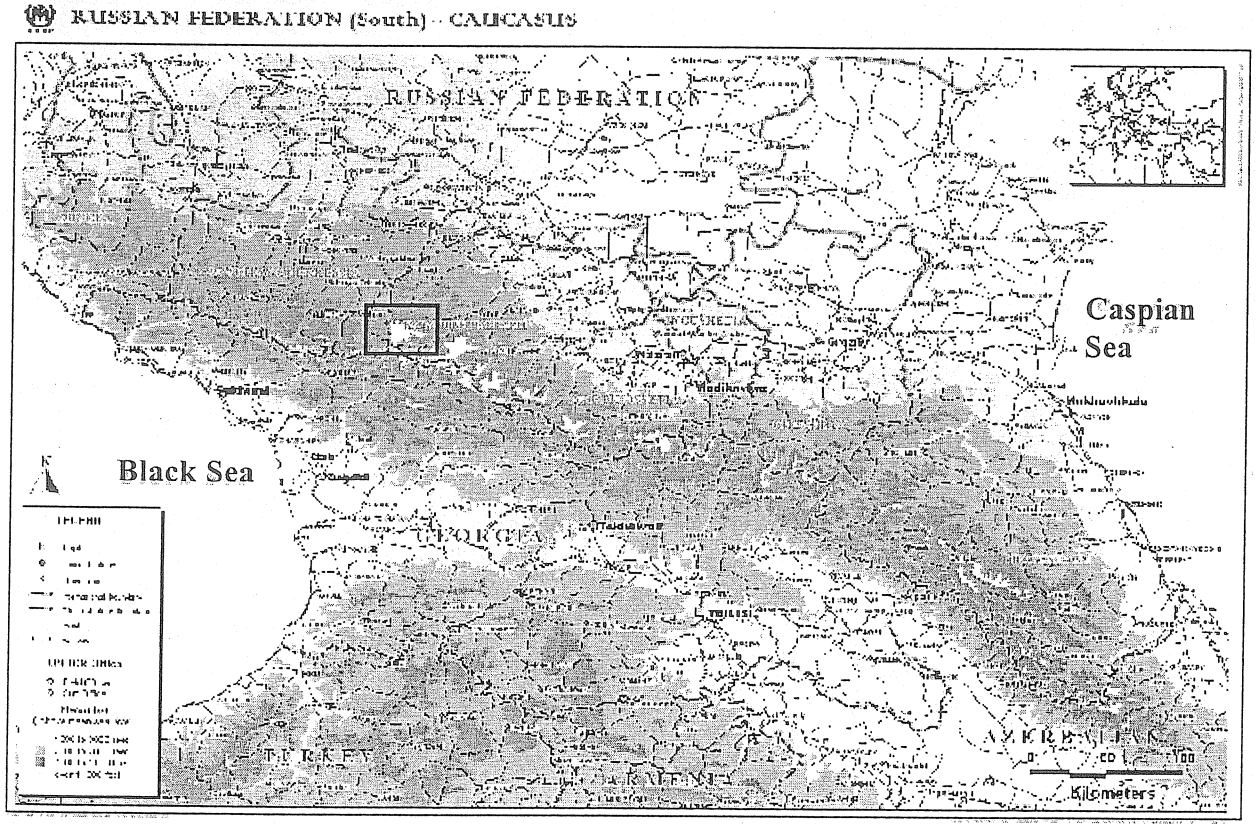

Fig 1. Southern Russia and Caucasus. Black box represents the Mt. Elbrus area, see *Fig. 2*.

The only habitated area near the Mt. Elbrus is Baksan Valley, where a lot of small towns with hotels for climbers and tourists exist. Up to 100 000 people visit this area each year, 10 % of which come from Western Europe, USA and Japan.

The Baksan geodynamical observatory of Sternberg Astronomical Institute of Moscow State University is located in this valley, 15 km apart from Elbrus in rock massive on the depth of 600 m in 4.2 km long technological tonnel of Baksan Neutrino Observatory of ... Institute of Nuclear Research of Russian Academy of Sciences (*Fig. 2, 3*). This tonnel houses two unique scientific installations – Underground Scintillation Neutrino Telescope and Gallium-Germanium Neutrino Telescope located at the depths respectively of 500 and 3500 m from the entrance.

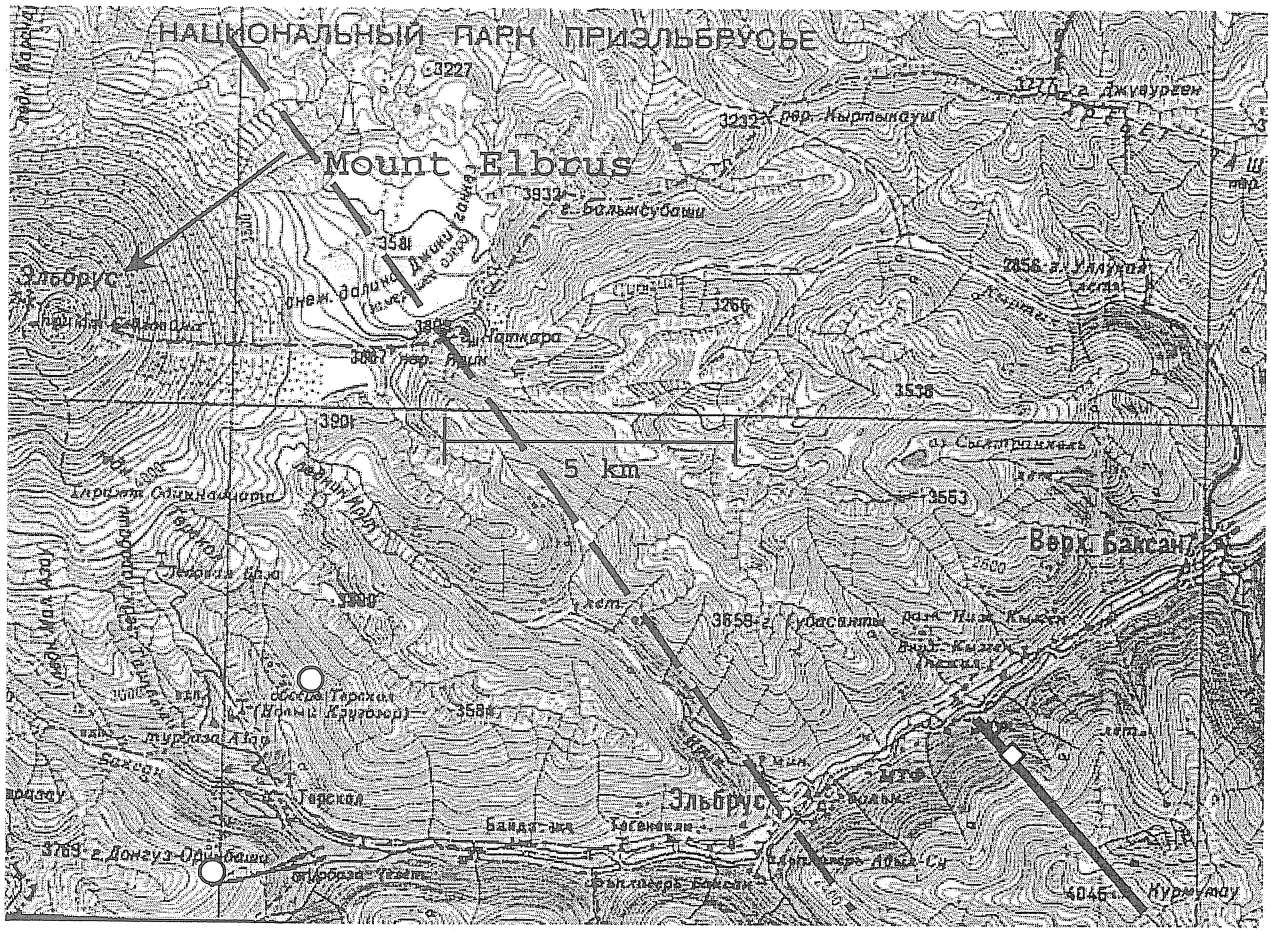

Fig. 2. Location of Baksan geodynamical observatory. Thick black line denotes the tonnel, small open box - location of laser strain meter. Small open circles represent locations of GPS points, observed in 1993 and 1994 by IfAG. The nearest fault is denoted by thick dashed line.

The observatory is equipped with a laser interferometric strain meter of Michelson type with non-equal arms ($L_{observational}$ = 75 m, $L_{reference}$ = 0.5 m) located in the main non-thermostatized tonnel and oriented along its axis (latitude = 43°12', longitude = 42°43', azimuth = 150°37'). Thermostatized room of observatory is isolated from tonnel and houses two pillars, larger one has been used for absolute gravity observations by FG'5-101 of IfAG in 1994 *(Wilmes et, 1994).* Smaller pillar has been used for tide gravity observations with modernized Sodin-gravimeter in 1998-1999 *(Kopaev and Yushkin, 2000).* A gravity calibration baseline with range of 127 mGal is installed along a 4.2 km long tonnel. Observations have been carried out in 1992-2002 using 6 Sodin gravimeters (S208, S209, S210, S212, S311and S312) that have been calibrated using Moscow calibration baseline and tilt calibration platforms, the accuracy of gravity values ranges from 12 to 21 μGal. Two additional common outdoor calibration baselines exist in this area, one with range of 650 mGal, and second with range of 85 mGal. They are equipped with excellent pillars, but as the uplift in this area is of the order of 1.5-2 cm/year, its stability is at the moment

under our checking. Two GPS-stations exist in this area, they are located very close to the Elbrus itself (see *Fig. 2,* third one is located 30 km to the East) and have been observed twice with IfAG team in 1993 and 1994 *(Wilson et al, 1994).*

The laser strain meter has been in use starting from 1993 with irregular observations for evaluation of its performance and numerous improvements, so the early data are of limited quality and are used only for seismic studies, mainly for investigation of eigenvibrations of the Earth.

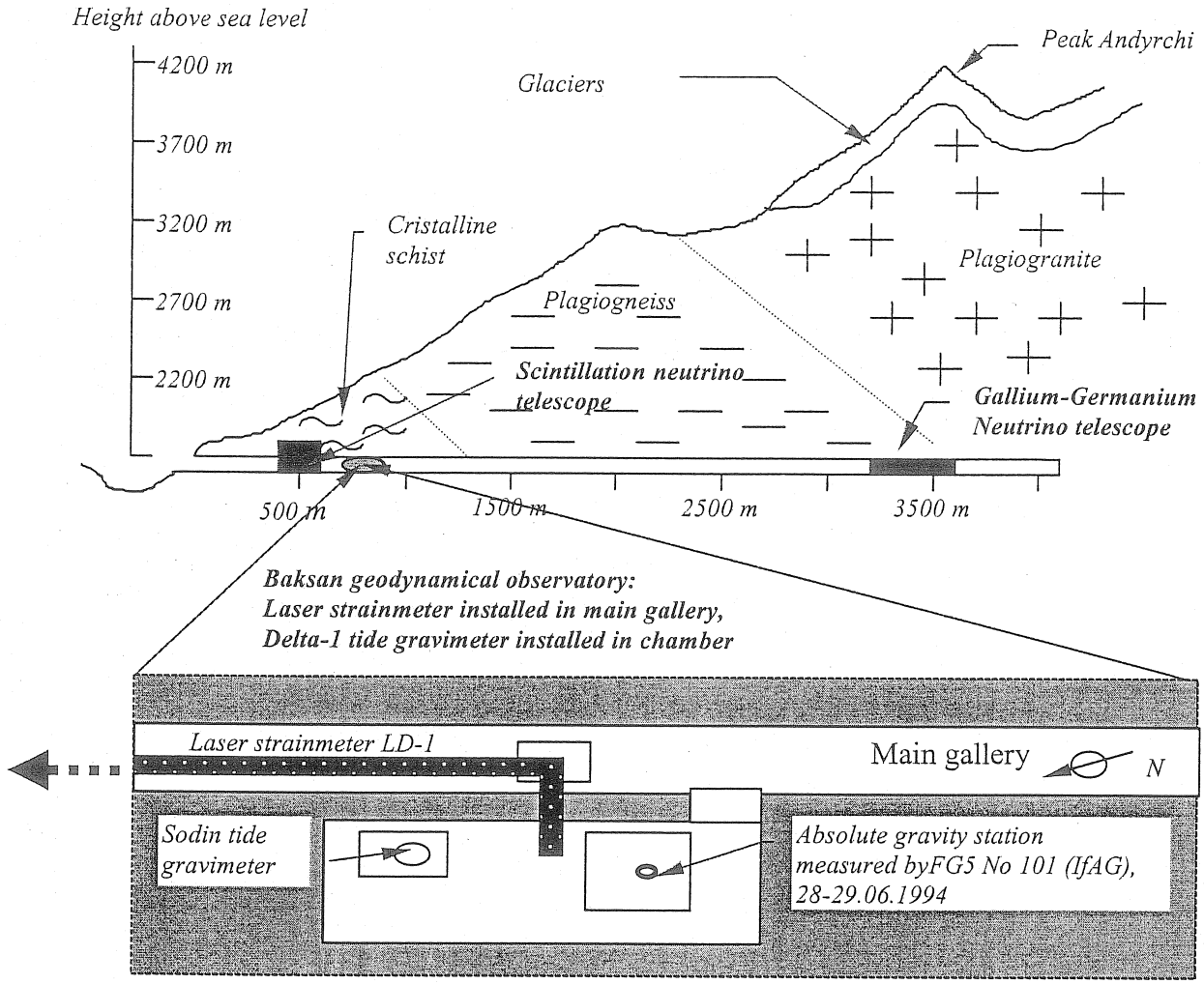

Fig. 3. Geological cross-section and situation of Baksan Geodynamical Observatory.

2. Description of Baksan laser strain meter

Laser interferometers represent perfect (but rather expensive) devices for strain measurements as they have infinite dynamic range, high precision and "build-in" usually perfectly stable permanent calibration possibility.

Optical system and path of the Baksan laser interferometer are located in specially constructed tanks and pipes under the vacuum of 10^{-5} mm Hg, which is supported by 2-stage system of vacuum pumps. Parameters of frequency stabilized He-Ne laser are the following: wavelength $\lambda = 0.63$ μm; power = 2 mWt; relative instability of $\lambda < 10^{-9}$/day.

Laser radiation is modulated on the frequency of 60 Hz by means of electro-mechanical modulation of laser resonant cell.

A very sophisticated feedback system for strain recording is used that includes electro-mechanical galvanometer, rotating mirror and photodetector. If the displacement exceeds the value of one interferometric fringe ($\lambda/2$, of 0.3 μm), feedback systems turns the mirror and returns to the

center of interferometric pattern by introducing the step of $\lambda/2$ into the signal. This steps offer an ideal permanent calibration and are removed automatically during the preprocessing procedure.

All the parts of strain meter (laser, beam-splitters, reflecting mirrors, vacuum chambers) are located on special pillars deepened into the bedrock that are isolated from tonnel floor. Vacuum pumps are installed on special sand "pillows" to reduce microseismic noise caused by its permanent operation.

Temperature and atmospheric pressure variations are recorded simultaneously with deformation signal using respectively SKIBA microbarograph with resolution of 1 μBar and self-made thermistors with resolution of 0.001 K.

3. Tide strain observations and data processing

Long term observations suitable for tide strain investigations started in spring of 1998 (with many gaps caused by numerous problems due to the vacuum pump malfunction, power supply interruptions and different logistic problems), so the data coverage is of about of 50 % only. As the device itself is located in the open ventilation tonnel for neutrino installations, no thermal insulation exists at all and all the outdoor temperature changes cause thermal deformations of the rock and different parts of instrument. It is obvious from the excellent correlation of long-term strain signal with temperature variations (*Fig. 4*).

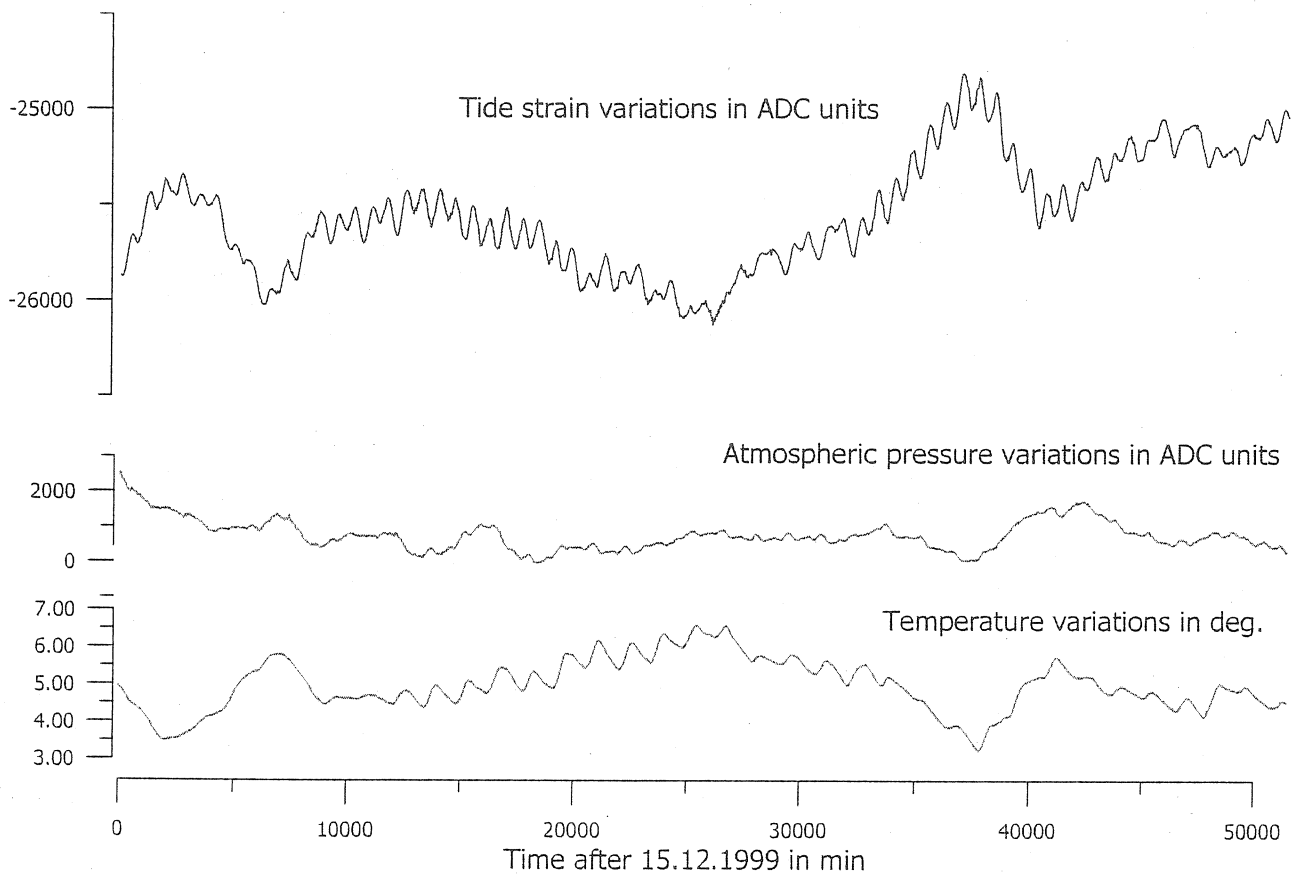

Fig. 4. Example of tide strain record obtained with Baksan laser strainmeter

That is why we started our tidal data processing with a lot of doubts. But after some experiencing the appropriate techniques has been developed that includes: 1) common PRETERNA data processing; 2) using TSOFT for consecutive band-pass filtering of hourly strain, temperature and pressure data in semi-diurnal (between 11 and 13 hours) and diurnal (from 22 to

26 hours), following search for best correlation between the different channels by means of its mutual shifting; 3) application of ETERNA to strain data together with shifted pressure and temperature data and 4) return to PRETERNA with known strain/pressure and strain/temperature admittances, and so on. Two or three iterations are usually enough to get best possible (in our case) signal to noise ratios of 10-20 for O1 wave and 50-100 for M2 wave and standard deviation of hourly values of 2-3 nstrain. In the beginning of the process this ratios are usually 2-5 times worse. The data occasionally represent a set of blocks, separated by gaps of different duration varying form several days to several months, so these blocks were processed first separately and all the results are represented in *Table 1* and *Fig. 5*. Than a common processing has been carried out for the whole data set of almost 400 days. The results are represented in *Table 2* as a standard ETERNA listing.

Table 1. Summary of Baksan laser strainmeter data tidal analysis during 03.1998 – 07.2000

Wave	O_1			M_2			σ,	Pressure	Temperature
Time interval (N_{days})	S/N	Amplitude factor	Phase, deg.	S/N	Amplitude factor	Phase, deg.	nstr	admittance, nstr/mBar	admittance, nstr/°C
1998									
04.03–25.04 (52)	14	1.02 ± 0.07	-5 ± 4	85	1.01 ± 0.01	$+1 \pm 1$	2	$+0.7 \pm 0.2$	2.1 ± 0.1
24.07–18.08 (26)	*4*	0.7 ± 0.2	-13 ± 17	*61*	1.09 ± 0.02	$+1 \pm 1$	*6*	$+3 \pm 1$	0.4 ± 0.6
1999									
20.02–27.03 (35)	*4*	0.5 ± 0.1	$+23 \pm 14$	*33*	0.93 ± 0.03	-21 ± 2	*4*	$+3.7 \pm 0.4$	0.4 ± 0.2
28.03–24.04 (27)	18	0.97 ± 0.05	-5 ± 3	51	1.01 ± 0.02	-3 ± 1	2	-0.1 ± 0.3	23 ± 1
14.05–09.06 (27)	18	1.28 ± 0.06	$+7 \pm 3$	50	1.04 ± 0.02	-3 ± 1	2	-0.6 ± 0.3	0.8 ± 0.2
11.06–29.07 (43)	14	1.3 ± 0.1	-8 ± 4	66	1.05 ± 0.02	$+2 \pm 1$	2	$+0.2 \pm 0.1$	0.2 ± 0.1
24.09-19.10 (26)	12	0.77 ± 0.07	-4 ± 4	43	0.74 ± 0.02	$+2 \pm 1$	2	-0.7 ± 0.4	1.0 ± 0.1
25.11-31.12 (37)	10	1.1 ± 0.1	-8 ± 6	95	0.79 ± 0.01	$+1 \pm 1$	2	$+0.5 \pm 0.2$	0.03 ± 0.07
2000									
03.01–08.02 (36)	8	1.2 ± 0.1	-8 ± 7	47	1.03 ± 0.02	$+1 \pm 1$	3	-1.7 ± 0.3	6 ± 1
23.02–15.04 (51)	7	1.0 ± 0.2	$+4 \pm 9$	45	1.02 ± 0.02	-3 ± 1	3	-0.3 ± 0.2	3.5 ± 0.3
15.04–17.05 (31)	13	1.0 ± 0.1	-14 ± 4	65	1.03 ± 0.02	$+8 \pm 1$	3	-0.1 ± 0.3	1.3 ± 0.1
18.05–18.07 (61)	9	0.9 ± 0.1	$+1 \pm 6$	45	1.03 ± 0.02	0 ± 1	4	-0.1 ± 0.3	1.2 ± 0.1
Mean	11	0.98 ± 0.17	-1 ± 3	57	0.98 ± 0.03	-1 ± 2	3	0.4 ± 0.5	1.5 ± 0.5
Common adjustment	15	0.98 ± 0.07	-3 ± 3	65	0.98 ± 0.01	-1 ± 1	4	0.4 ± 0.1	0.56 ± 0.03
Common adjustment with series 2,3 excluded	20	1.07 ± 0.05	-4 ± 3	76	0.98 ± 0.01	1 ± 1	3	0.2 ± 0.1	0.86 ± 0.03

4. Discussion

We are not very satisfied with results, however this tonnel represents the only possible place to put interferometer and it cannot be isolated due to the clear technical reasons, so our aim was to do all the best. Nevertheless, the application of optimized combination of ETERNA, TSOFT and PRETERNA helps to reduce the huge influence of environmental disturbances up to appropriate

level, at least for M2 wave. Signal/noise ratios for M2 ranging between 50 and 100 are rather common for usual non-laser strain meters. The same values for O1 range between 10 and 20 only, obviously due to the residual thermal influence and could hardly be reduced. They are not represented on *Fig. 4*. Nevertheless the common processing of all the data reveals clearly the K1 wave, however K1/O1 amplitude ratio (0.85) is considerably larger than its theoretical value 0.6). Temperature and pressure admittances as well as corresponding time lags (not shown in Table 2, ranging from 2 to 6 hours for atmospheric pressure and from 4 to 8 hours for temperature) show chaotic variations in amplitude and even in sign (for pressure admittance). The latter one is however mostly statistically insignificant that is confirmed with common adjustment of best data (last row in *Table 1*). Temperature admittance is on the contrary mostly statistically significant and its value is close to 1 nstr/°C. All the error bars on the *Fig. 5* correspond to 2σ, whereas simple 1σ standard deviations are listed in Table 1.

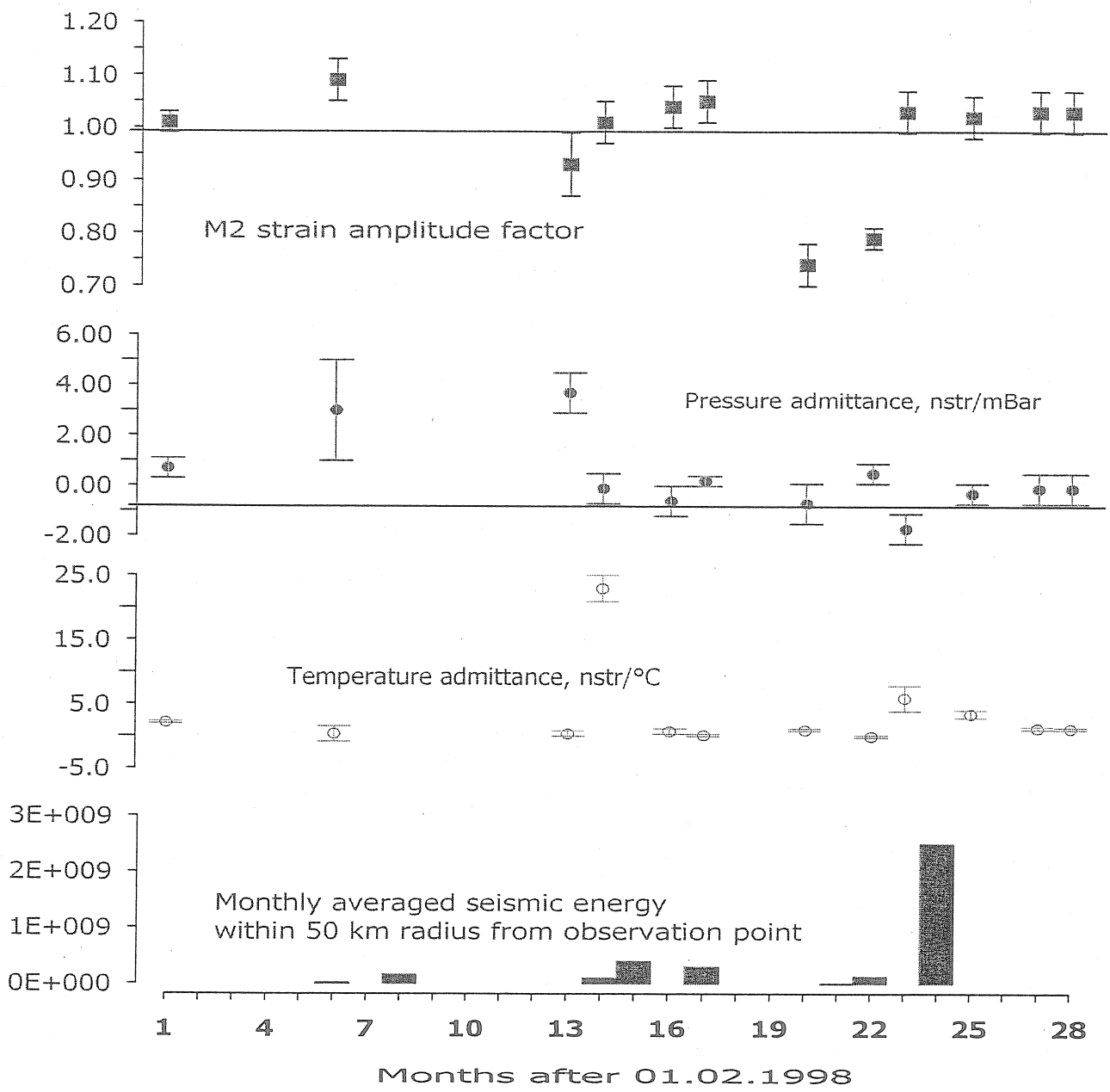

Fig. 5. Summary of Baksan laser strain meter data tidal analysis during 03.1998 - 07.2000.

As for time variations of the amplitude of M2, it is obvious that only two blocks reveal statistically significant decrease to value of 0.7-0.8 from the mean value close to 1.0, covering the time period approximately from September to December of 1998. This anomaly is not associated

in time with any large disturbances in pressure and temperature admittances, like first blocks, so it could be of natural origin. We show on *Fig. 5* also the time evolution of monthly averaged seismic energy in area with radius of 50 km around the observatory. A series of small seismic events (M < 2.5) occurred some 20 km to the North-East from observatory. The fact that our anomalous decrease in M2 amplitude preceded this events looks too encouraging and speculative (even in terms of *(Beamont and Berger, 1974)*) at the moment especially because of bad data coverage.

Table 2. Results of common data processing for tide strains for the whole observation period

```
#########################################################################
# Earth tide station Baksan, N.Caucasus, Russia                         #
# Sternberg Astronomical Institute of Moscow State University           #
# 43.200N  42.736E H1700 A150.61 Linear deformations                    #
# Long-base laser interferometric strainmeter                           #
# Installation: V.Milyukov                                              #
# Maintenance:  A.Myasnikov, B.Klyachko                                 #
# Processing:   A.Kopaev                                                #
#########################################################################

Summary of observation data :
19980304110000...19980424220000  19980724150000...19980817230000
19990220110000...19990327 90000  19990328140000...19990423150000
19990514 90000...19990608140000  19990611200000...19990621150000
19990622140000...19990629210000  19990701130000...19990713110000
19990714150000...19990729100000  19990924 30000...19991018210000
19991125150000...20000101 10000  20000111 40000...20000207230000
20000415230000...20000516130000  20000518220000...20000718 50000

Number of recorded days in total :   386.17
TAMURA 1987   tidal potential used.
UNITY window used for least squares adjustment.
Numerical filter is PERTZEV 1959 with  51 coefficients.

Estimation of noise by FOURIER-spectrum of residuals
0.1 cpd band 9999.9999  nstr          1.0 cpd band    0.3271  nstr
2.0 cpd band    0.1579  nstr          3.0 cpd band    0.0569  nstr

adjusted tidal parameters :

from   to  wave  ampl. signal/ ampl.fac.    stdv. phase lead    stdv.
nstr      noise                           [deg]     [deg]

286  428 Q1     1.039     3.2   1.04147  0.32803  -12.9764   18.0464
429  488 O1     5.111    15.6   0.98118  0.06281   -4.4051    3.6675
489  537 M1     0.466     1.4   1.13789  0.79859   36.8885   40.2111
538  554 P1     2.669     8.2   1.10136  0.13498  -37.9598    7.0220
555  558 S1     2.708     8.3  47.25116  5.70705   59.0224    6.9202
559  576 K1     6.232    19.1   0.85075  0.04466  -11.3583    3.0076
577  580 PSI1   0.798     2.4  13.92123  5.70731   25.8546   23.4897
581  592 PHI1   1.336     4.1  12.80541  3.13593 -144.1437   14.0312
593  634 J1     0.288     0.9   0.70302  0.79862    9.8499   65.0869
635  736 OO1    0.629     1.9   2.80828  1.45943   22.8996   29.7760
737  839 2N2    0.459     2.9   1.42508  0.48981   -2.8411   19.6928
840  890 N2     1.969    12.5   0.97505  0.07822   -1.2472    4.5963
891  947 M2    10.291    65.2   0.97590  0.01498   -1.1244    0.8793
948  987 L2     0.333     2.1   1.11579  0.52984  -18.3949   27.2071
988 1008 S2     4.485    28.4   0.91419  0.03219   -5.8984    2.0174
1009 1121 K2    1.311     8.3   0.98300  0.11840   -1.0384    6.9012

Standard deviation of weight unit:      0.207
degree of freedom:                      8534
Standard deviation                :     4.136   nstr

Adjusted meteorological or hydrological parameters:

no. regr.coeff.       stdv.  parameter   unit

1     0.42222     0.09337  Airpr.      nstr   /hPascal
2     0.59853     0.03422  Temp        nstr   /deg. C
```

As for the mean undisturbed value of amplitude for M2 wave, the configuration of 2D topography *(Fig. 3)* with slope of more than 30 degrees should increase the actual value by about 20-30 % according to the maps of Harrison and Blair (*Harrison, 1976; Blair, 1976*) and simplified

estimations based on S.Molodenski analytical techniques for 2D relief approximated by linear spline *(Molodenski, 1985, 1986).* So the actual value is of the order of 0.7-0.8 and this anomaly could be attributed (rather speculatively at the moment, before the finite element modeling) to the presence of hot and shallow magma chamber revealed from analysis of Bouguer gravity and seismic data *(Bogatikov et al, 1998),* that could result in decrease of elasticity and therefore of tidal strain amplitudes. As the nearest fault is parallel to the strain meter axes *(Fig. 2)* and the latter one is located sufficiently far from the extremities of the tonnel *(Fig. 3),* we don't expect any serious influence of the fault or cavity on the obtained result.

The value of phase lag for M2 equals however to $-1.1^{o} \pm 0.9^{o}$ and is therefore statistically insignificant.

5. Conclusion

Application of sophisticated data processing techniques resulted in successful determination of amplitude of main tidal semidiurnal M2 wave from the highly thermally disturbed data from Baksan laser strain meter installed in Baksan valley, 15 km apart from sleeping volcano Mt. Elbrus, including statistically significant decrease of M2 amplitude before the sequence of small seismic events in the vicinity of strain meter.

Amplitudes of tidal strains observed in Mt. Elbrus area are low (70 % of model values for M_2) and could be explained by rough topography influence as well as by the presence of magma chamber.

Observations with laser strain meter in such an area are unique, so a way to improve the data coverage should be pursued.

6. Acknowledgements

This work has been partly supported by Russian Foundation for Basic Research (RFBR), grants 98-05-64941 and 00-05-64882.

Authors are very indebted to Profs. B.Ducarme, L.Latynina and S.Molodenski for many helpful duscussions.

7. References

Beamont, C. and Berger, J. Earthquake prediction: Modification of the earth tide tilts and strains by dilatancy. *Geophys. J. R. Astron. Soc., 39, 111-121,* **1974.**

Bogatikov, O., Gurbanov, A., Melekeszev, I., Sulerzhizkiy, V., Sobisevich, L., Katov, D., Kopaev, A., Lyashenko, O., Puriga, A. Problem of possible activisation of Mt.Elbrus volcano and its possible consequences. *In monograph: Global changes of environment, Siberian Branch of RAS Publishing House, 153-165 (In Russian*), **1998.**

Blair, D. Topographic effects on the tidal strain tensor. *Geophys. J. R. Astron. Soc. 46, 127-140,* **1976.**

Harrison, J. Cavity and topographic effects in tilt and strain measurements. *Journ. Geophys. Res., Vol. 81, No. 2, 319-327,* **1976.**

Kopaev, A., Milyukov, V. and Yushkin, V. Geodynamical investigations program in Baksan canyon area. *Proc. of 112th Symp. of IAG "Geodesy and Physics of the Earth", Potsdam, August 2-6, 1992, Springer-Verlag,* 50-52, **1993.**

Kopaev, A., Gurbanov, A., Kumkova, I., Geophysical data on increasing activity of Mt.Elbrus and beginning of its geodetical monitoring. *Abstr. IUGG XXI Gen. Ass., Boulder, July 2-14, GA51B-08,* **1995.**

Kopaev, A., Milyukov, V., Yushkin, V. Tide gravity and strain measurements near the Mt. Elbrus, Central Caucasus. *Abstr. 14th Intern. Symp. On Earth Tides (ETS'2000), Aug.28th-Sept.01st, Mizusawa, 99,* **2000.**

Kopaev, A. and Yushkin, V. Tide gravity observations near Mt. Elbrus, Central Caucasus. *Comptes-Rendus of Journees Luxembourgeoises de Geodynamique, 87th session, 9-11,* **2000.**

Molodenski, S. Evaluation of the tidal strain disturbances in flat relief areas. *Fizika Zemli, No. 7, 80-96,* **1985.**

Molodenski S. Influence of relief in flat areas on tidal tilts and strains – second order effects. *Fizika Zemli, No. 8, 3-14,* **1986.**

Wilmes, H., Schaefer, U., Kopaev, A., Richter, B., Becker, M., Kumkova, I., Miluykov. V. First absolute gravity campaign in the Caucasus region and its relation to the detection of height variations. *Abstr. IGC/ICG Joint Meeting, Sept. 11-17th, Graz, 37,* **1994.**

Wilson, P., Seeger, H., Reinhart, H., Becker, M., Marjanovich, M., Neumayer, P., Habrich, H., Mueller, W., Finkelstein, A., Kumkova, I., Olifirov, V., Yatskiv, Ya. Gaiovich, I., Taradij, V., Reva, Yu., Kopaev, A., Velikhov, V., Chempelev. A.. Experiences with GPS measurements from the Black Sea to the Northern Caucasus in the framework of SELF and WEGENER. *Abstr. 6th Gen Ass. of WEGENER, St.Petersburg, June 20-24, 301-317,* **1994.**

Environmental effects on tilt measurements at Merapi volcano

Malte Westerhaus[1] & Wolfgang Welle[2]

[1]Geodetic Institute, Karlsruhe University, Englerstr. 7, D-76128 Karlsruhe

[2]GeoForschungsZentrum Potsdam, Telegrafenberg, D- 14473 Potsdam

1 Introduction

Deformations of the volcano's edifice due to pressure changes within the internal system of magma chambers and conduits are among the most important volcanic activity parameters. A wide spectrum of instruments and techniques is applied, including spaceborne as well as ground based measurements. Electronic tiltmeters, belonging to the latter group, are widely used if deformations are to be observed continuously. This type of instruments is robust, cheap and capable to monitor local deformations with a resolution of $\sim 10^{-8}$ rad. As was shown by Rebscher at al. (2000) this resolution is high enough to clearly resolve earth tidal peaks. Due to the short base length of less than one meter, tiltmeter records are usually dominated by signals with a short wavelength, generated by nearby cracks and the local topography. Also, the response functions of tiltmeters to environmental disturbances (rain, temperature) may vary considerably from place to place. Effects of local geology may be recognized by combining several instruments in clusters with a side length of ~100 m, and meteorological disturbances are reduced by installing the sensors in bore holes or underground cavities. Insulating measures, however, cannot suppress tilt disturbances if the environmental noise source induces poro-elastic or thermo-elastic deformations of the ground. These signals that must be recorded by a sensitive tiltmeter coupled to the ground may fake or mask signals of volcanic origin. At Merapi Volcano, the situation is aggravated since heavy rain falls occasionally may be able to trigger pyroclastic flows (Purbawinata et al., 1997) that are expected to be accompanied by short term pressure fluctuations within the conduit. Any attempt to relate anomalous tilts to these eruptions (fig. 1) can only be successful if the possible influence of environmentally induced local/regional poro-elastic deformations is accounted for and if suspicious signals are removed from the individual records (as long as deformations of volcanic origin are of the same order of magnitude as the rain induced signals which is the case here). In the following, we will present some simplistic models of rain induced noise in tilt time series recorded at the flanks of Merapi Volcano.

2 The Indonesian-German deformation experiment

Merapi Volcano (2961 m) is located in Central Java, Indonesia (7.45° S, 110.44° E) at the subduction zone between the Eurasian and the Indo-Australian plate. Being one of the most active volcanoes in the world, Merapi has been elected into the list of the 16 so-called Decade Volcanoes. In 1995, the interdisciplinary research project MERAPI (Mechanism

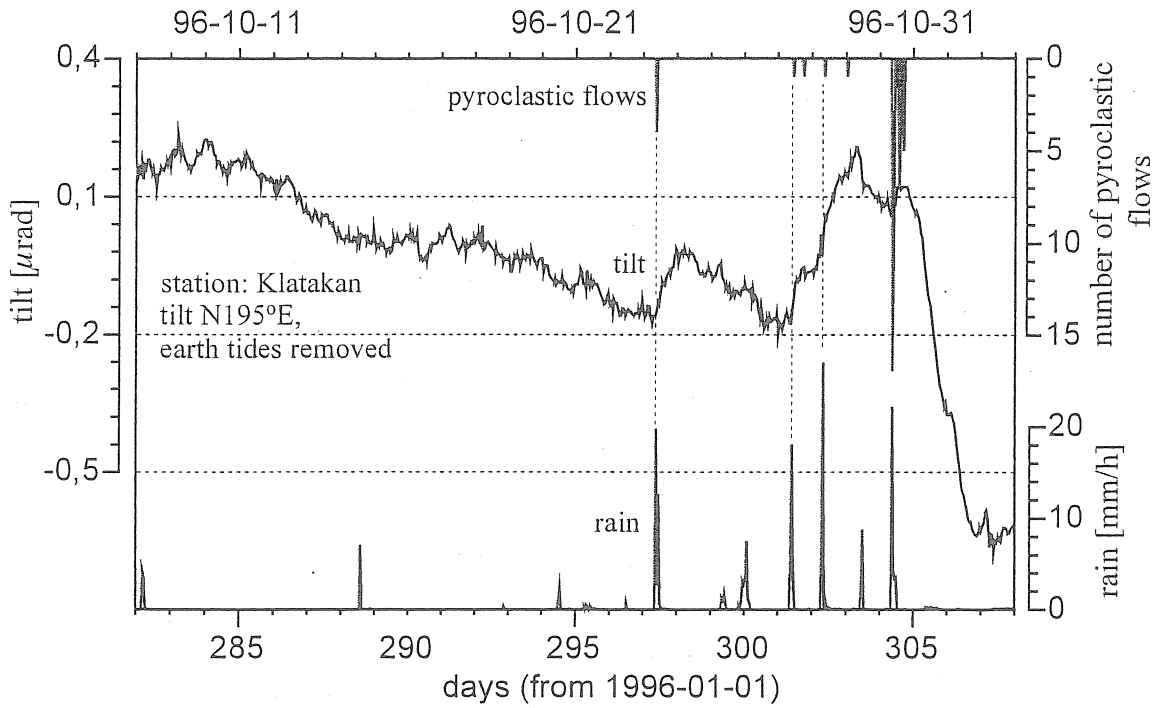

Figure 1: Rain water intruding into fractures of Merapi's active lava dome is apparently capable to trigger explosive eruptions, if the dome is in an unstable condition. Tilt anomalies accompanying the volcanic crisis have to be carefully checked with respect to rain-induced disturbances due to local poro-elastic ground deformation.

Evaluation, Risk Assessment, Prediction Improvement), a cooperation between the Volcanological Survey of Indonesia, the GeoForschungsZentrum Potsdam, and several institutes in Indonesia and Germany, started to investigate Merapi Volcano under different kinds of geophysical, geological and geochemical aspects (Zschau et al., 1998). The Indonesian-German deformation experiment carried out in the frame of MERAPI runs four continuously operating monitoring stations located at the flanks of the volcano at altitudes between 1280 m and 2020 m. Each station consists of one GPS receiver and an array of 3 electronic tiltmeters. Parallel to the deformation components, local environmental parameters (incl. rain, air- and soil temperature) are being recorded (Westerhaus et al., 1998). In contrast to other international groups monitoring tilt at Merapi Volcano, tiltmeters observing inclinations of a vertical ground element are used. They are based on electrolytical sensors in 2 orthogonal directions, with a specified accuracy of 0.1 μrad [Applied Geomechanics, 1991] and an effective accuracy of ~ 0.01 μrad. The vertical design of the tiltmeters allows an installation in boreholes at depths of 3 m to 4 m in order to minimize meteorological noise, especially the influence of temperature variations.

Most tiltmeters operated by other international research groups are installed at the summit of Merapi Volcano, close to the active lava dome. At those places strong tilt anomalies of the order of several hundreds of μrad are observed during phases of volcanic activity. Mostly, these signals result from finite block rotations caused by the growing lava dome and can hardly be inverted with respect to internal pressure changes. To our opinion, this is possible only from locations at the hillsides, far away from the secondary dome growing effects. On the other side, this opportunity has to be paid by much smaller signals. Up to now, tilt anomalies that are supposed to be of volcanic origin are as small as 1 μrad;

the accompanying horizontal displacements are expected to be significantly less than 1 mm (Körner, 2000). Rain induced disturbances are up to 5 μrad on a time scale of days (fig. 4) and up to 25 μrad for the annual alternation of dry and wet seasons. Variations of similar size are observed elsewhere indicating that this magnitude of the rain induced disturbances is not unusual for shallow borehole installations (Kümpel, priv. comm.).

3 Ground deformation induced by rain

The total effect of rain on the tiltmeter installations is a combination of ground loading, i.e. normal compression and shearing of the ground down to the valley due to the added mass of water, and deformations of the soil matrix by movements of water through the pore space. Whereas the tilt reaction on the first effect is instantaneous, the diffusional character of the latter leads to a delayed response of the tiltmeters.

3.1 The loading effect

Fig. 2 shows a three month tilt record from a site (KEN, 1450 m, SE-flank) that is dominated by the loading effect. Negative radial tilt occurs as an instantaneous response to precipitation. The negative sign indicates a down-slope tilting of the top of the tiltmeter, compatible with a shearing of the ground down to the valley. Every negative tilt change is followed by an asymptotic movement in the direction back to the level before, giving a less rapid, positive tilt signal. Under conditions of uniaxial strain the instantaneous response of a tiltmeter to elastic loading of a half-space with a uniformly sloping surface is:

$$\Delta\varphi_l = \rho_w g\, \Delta h \sin\alpha \cos^2\alpha \frac{1}{\rho}\left(\frac{1}{v_s^2} - \frac{1}{v_p^2}\right) \qquad (1)$$

with $\Delta\varphi_l$ = instantaneous tilt effect, ρ_w = density of water, g = gravitational acceleration, Δh = height of the water column, α = slope, ρ = density of the soil, v_s and v_p = velocity of shear- and longitudinal waves in the upper soil layers, respectively. Inserting observed values of $\alpha = 20^\circ$, v_p=850 m/s (Maercklin et al., 2000) and reasonable values of $\rho = 1600$ kg/m^3 and $v_s = 300$ m/s (equivalent to a Poisson's ratio $\nu = 0.43$), an instantaneous rain-tilt coupling coefficient of 0.018 μrad/mm is calculated.

The added water mass is removed from the surface due to overland flow, evapo-transpiration and diffusion to deeper soil layers, resulting in a gradual recovery of the tilt signal. The total loading effect is qualitatively described by a convolution of the rain data by an exponential function (e.g. Langbein, 1990):

$$f_i = \sum_{k=1}^{i} r_k e^{-(t_i - t_k)/\tau} \qquad (2)$$

where r_k is the amount of rain recorded at time t_k, τ is a time constant and f_i is the cumulative effect of all the rain previous to t_k.

The resulting rain function (fig. 2) shows an instantaneous response to every rain event followed by an exponential decay which corresponds to the removal of water from the ground surface. A linear fit of the rain function to the data gives a local rain-tilt coupling coefficient of 0.023 μrad/mm (fig. 3b). This value is 28% larger than the theoretical rain-tilt admittance as calculated above. However, the variability of the soil parameters, especially if direct determinations are missing (ρ and v_s), may be at least as large as this difference. We, thus, conclude that the loading model is reasonable.

By subtracting the rain function f, the rain induced tilts are almost completely removed from the tilt series, with two exceptions on Aug.10, and Oct. 31 (figs. 2, 3). In both cases of apparently failed corrections heavy rainfalls coincided with pyroclastic flows, implying that a volcanic effect might be responsible for the residual tilt anomaly. However, the strong and unusual drift in the corrected tilt data, as observed after Oct. 31 (fig. 2), occurs again during the wet season one year later. Thus, the influence of rain on tilt at Kendil may not be explained completely by ground loading. As for other stations, poro-elastic deformations due to rain water infiltrating into the soil may be present, at least on an annual time scale.

3.2 The infiltration effect

The infiltration effect consists of two parts: (i) expansion of the upper soil layers due to increased pore pressure if water fills up formerly unsaturated pore space, and (ii)

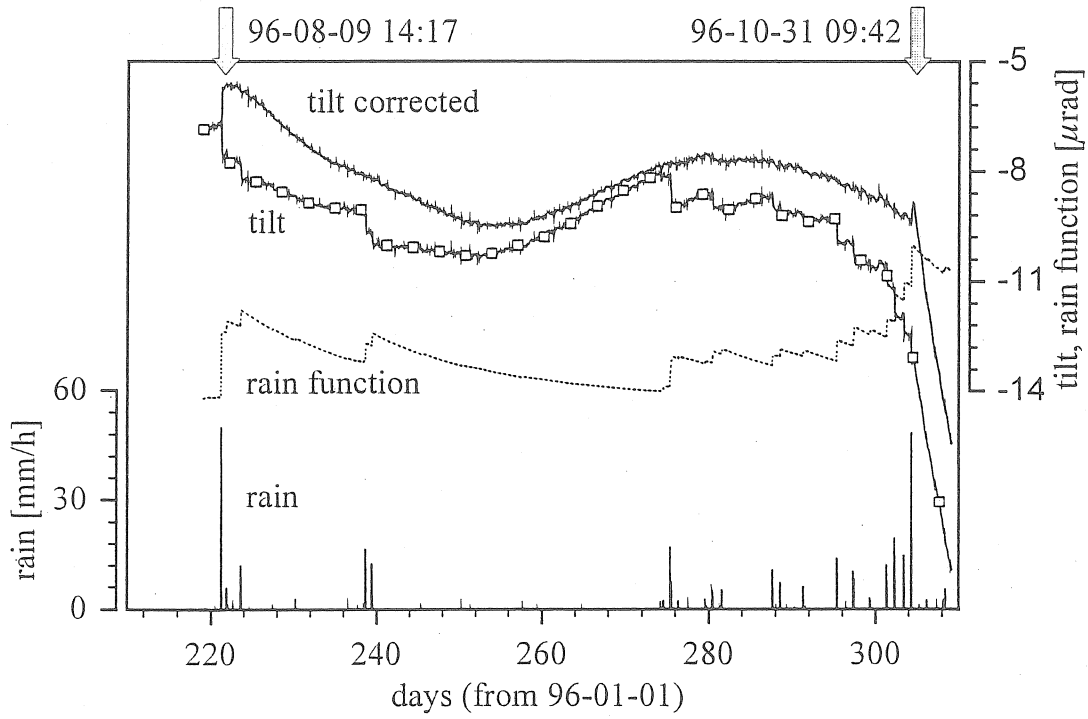

Figure 2: Illustration of the loading effect. The rain function has been calculated according to eq. (2) with τ= 15 days. The tilt component is oriented parallel to the local slope; negative tilts indicate a down-slope tilting of the top of the tiltmeter. Arrows mark volcanic events.

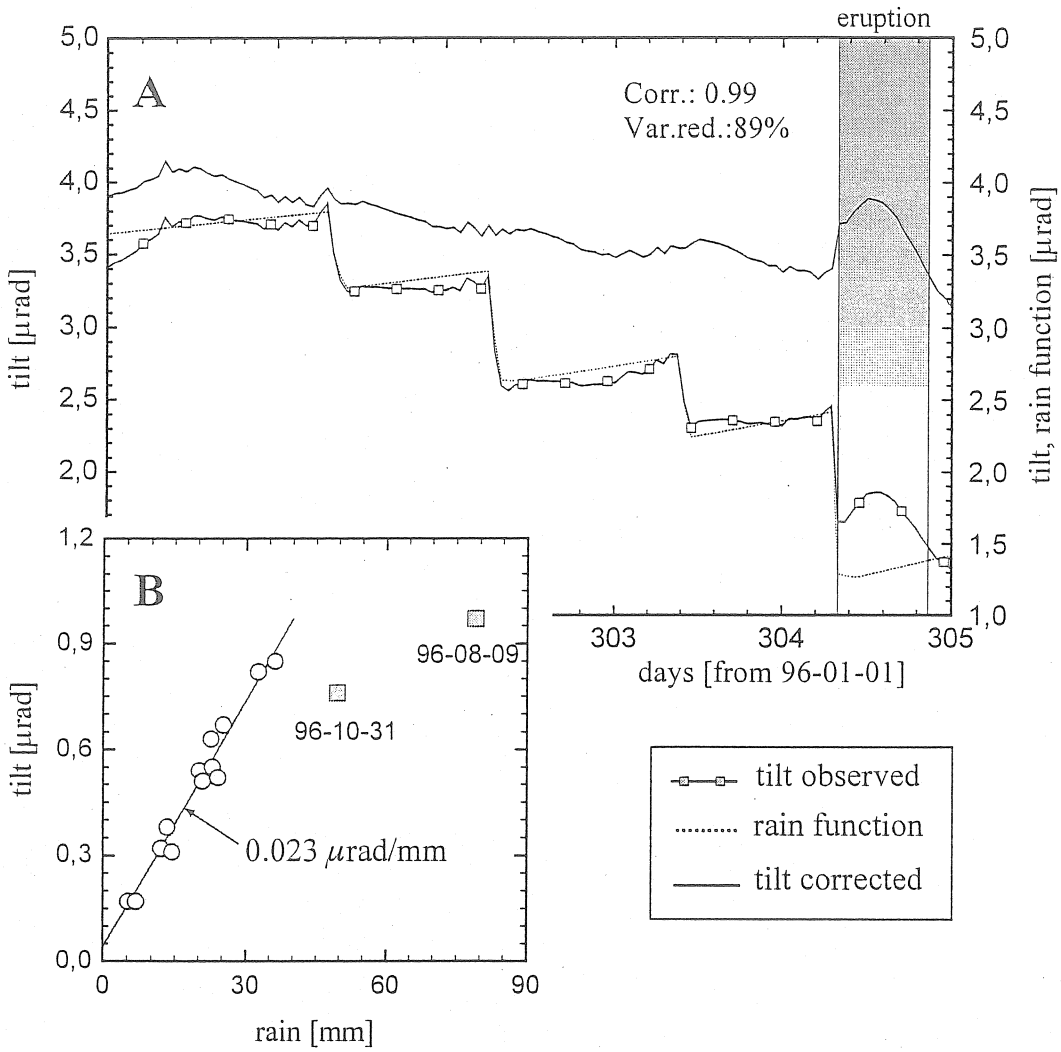

Figure 3: (A) days 300-305 of the timeseries shown in fig. 2; (B) linear regression between instantaneous tilt and rain (i.e. the steps in the tilt and in the rain function *f*). Values during phases of volcanic activity (rectangles) deviate considerably from the straight regression line. (A) shows the residual anomaly on Oct. 31, 1996, after subtracting the rain function from tilt according to the coupling coefficient 0.023 µrad/mm.

deformation of the soil matrix due to frictional resistance to flow of water. Expansion of the soil layers generates a tilt of a vertical element:

$$\Delta\varphi_p = \frac{1}{6}\frac{1+\nu}{1-\nu}(c - c_s)\sin 2\alpha\ \Delta p(z,t) \qquad (3)$$

with $\Delta\varphi_p$ = delayed tilt anomaly due to pore pressure increase; ν = Poisson's ratio; c = compressibility of the soil matrix; c_s = compressibility of the grains; Δp = pore pressure variation. Δp now is a function of depth z and time t, since the fluid needs time to diffuse through the pore space. Eq. (3) follows from the stress-strain relation under conditions of uniaxial strain analogous to the thermo-elastic tilt effect (e.g. Harrison and Herbst, 1977). With $c = 1*10^{-9}$ Pa, $\nu = 0.43$ and a soil porosity $\Phi = 0.5$ the admittance between pore

pressure and surface tilt amounts to $\Delta\varphi_p$ = 0.006 mrad/mm. As with the instantaneous effect, the sign is negative; i.e. increased pore pressure causes a down-slope tilting of the top of the tiltmeter. It should be mentioned that this model assumes 100% saturation. It can be shown that the high compressibility of gas bubbles would reduce the pore pressure immediately as soon as the volume fraction of gas in the pore space reaches approximately 1 part in 10^3 (Westerhaus, 1996). It seems well conceivable that such a small fraction of gas could be trapped in the pores during infiltration of rain water from above; in such a case expansion of the ground remains small and will contribute only marginally to the tilt disturbance.

The second effect is the result of pore fluid movements, driven by negative pressure gradients existing between the recharge and discharge areas. Friction between the mobile and immobile components of the soil leads to a deformation of the soil matrix. Kümpel et al. (1996) gave a comprehensive discussion of this mechanism for tiltmeters installed in the vicinity of pumped water wells. They showed that the resulting tilt anomaly:

$$\Delta\varphi_f = F(Ge, B, D, Q, z, t) \tag{4}$$

is a function of the geometry, *Ge*, Skempton's parameter *B*, diffusivity *D*, discharge *Q* as well as space and time.

Since most of the parameters entering eq. (4) are unknown, a quantitative calculation of the tilt disturbances is currently not possible. However, focusing on the diffusional character of the process we may be able to compute a rain function that qualitatively displays the time dependence of the deformations induced by the moving pore fluid. Neglecting the real geometry and assuming that a rain event generates a pore pressure disturbance at the surface of a semi-infinite half-space, pore pressure at depth z is governed by the complementary error function (see for example Turcotte & Schubert , 1982, pp 158, for the equivalent problem of heating or cooling of a semi-infinite half-space). The tilt effect may be described qualitatively by convolving the rain data by the complementary error function:

$$f_i = \sum_{k=1}^{i} (r_k - r_{k-1})\, erfc\left(\frac{z}{2\sqrt{D(t_i - t_k)}}\right) \tag{5}$$

with erfc = complementary error function; z = depth (i.e. distance to the surface pressure disturbance; D = diffusivity. The approach assumes that the pore pressure disturbance at the surface consists of a series of Heavyside functions with the amplitudes (positive or negative) determined by the difference of two consecutive rain values. Each pressure step at the surface is continuated downwards by diffusion; pressure at depth z and time t is the cumulative effect of each previous step. In contrast to the exponential function the value of erfc at time $t_i = t_k$ is zero. Therefore, the response of the rain function to a rain event is not instantaneous but delayed; the maximum being reached after several days. Note, that no information about z and D is available; f_i is fitted to the observed tilt data by changing the ratio z/(2*sqrt(D)). The approach was successfully tested for the annual variations of soil temperature which is continuously monitored at each tilt station (in that case, depth z is known, and a reasonable guess of D is available from literature). Using air temperature as

surface input in eq. (5), variations of the soil temperature are quantitatively predicted. Thermo-elastic effects in the tilt records are not obvious.

The infiltration effect is nicely illustrated for site GEM (1380m) at the western flank of Merapi (fig. 4). The tilt record mirrors the rain function in almost any detail. As expected from eq. (5) the response of the tiltmeter to a rain event is delayed. An increase in the rain function causes a tilting of the top of the tiltmeter in the direction of the negative pore pressure gradient (the tilt curve in fig. 4 is rotated by 180° for comparison). Although the comparison done in fig. 4 strongly suggests that the tilt record is dominated by the rain influence, the correlation is not perfect. The tilt residuals still exhibit short term variations of up to 5 μrad. The problem is that most hydraulic parameters like diffusivity, D, are a function of the saturation of the soil (e.g. Raudkivi & Callander, 1976, p. 25) resulting in a variable time shift between the tilt and rain function. To take this effect into account, diffusivity in eq. (4) was allowed to vary as a linear function of pore pressure (fig. 5a). Additionally, the limited capability of the soil to absorb water was accounted for by

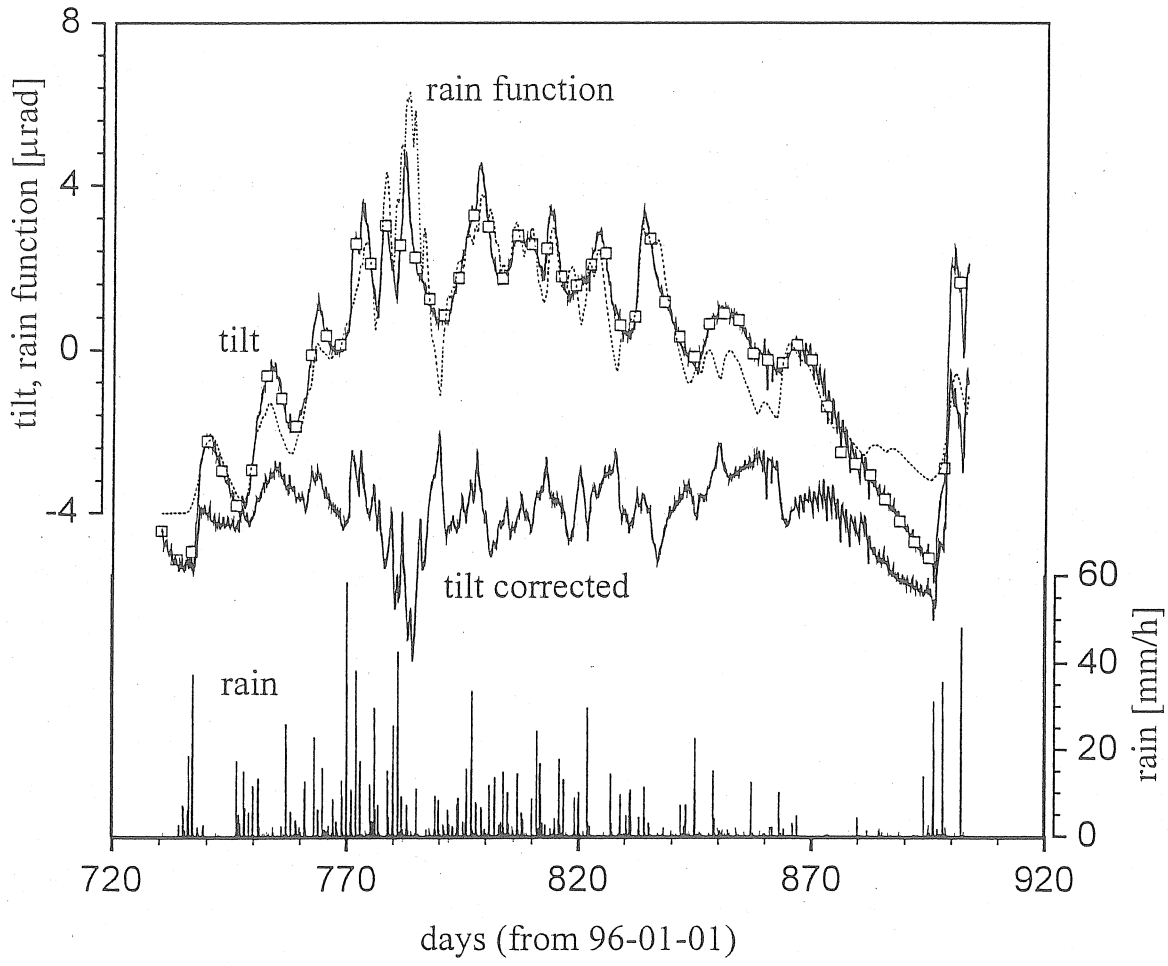

Figure 4: Illustration of the infiltration effect. The rain function has been calculated according to eq. (5) with z = 100 m, D varying linearly with pressure (fig. 5a) and soil retention (fig. 5b). The tilt component has been rotated in the direction of maximum rain influence (approx. parallel to the local slope).

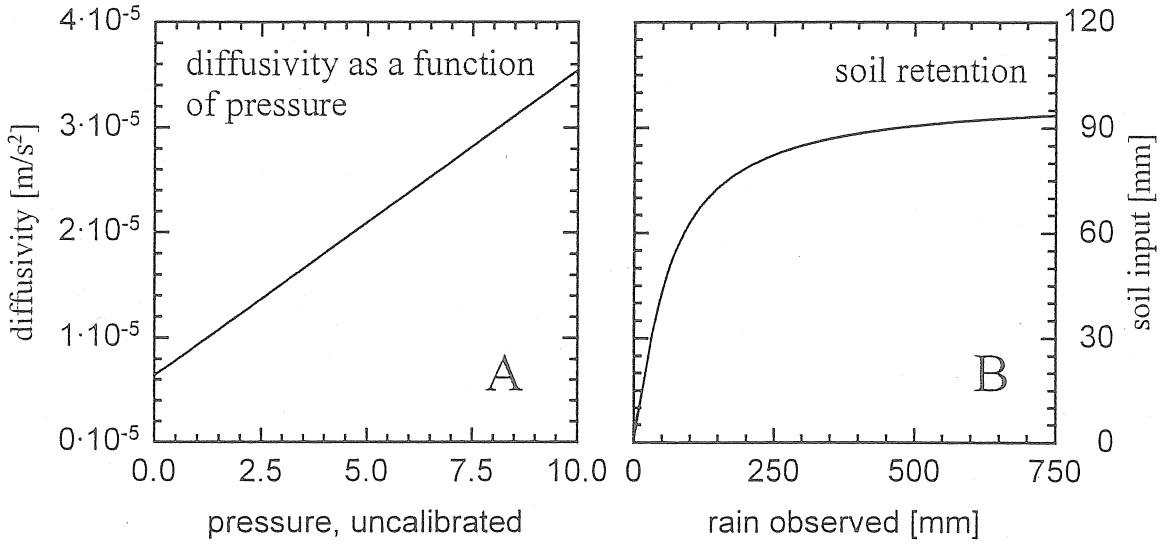

Figure 5: (A) assumed variation of diffusivity with fluid pressure; (B) model of soil retention. Note that the D-values in (A) are arbitrarily since the real geometry of the problem is not known (z=100 m chosen in eq. (5)).

assuming an exponential model of soil retention (fig. 5b, see also Peters et al., 1991). These two assumptions improved the fit of the rain function to the tilt record fairly well. The variance reduction amounts to 83% with variable D and soil retention model, compared to 72% with constant D and no soil retention model.

The insufficient knowledge of the geometry of the problem and the time/saturation dependence of hydraulic soil parameters impedes an optimal fit of the rain function to the tilt data for time series longer than several weeks. This holds especially for the annual alternation of wet and dry seasons since the influence of soil retention becomes increasingly important with longer time periods. For short time segments, however, correction of the tilt records by subtracting an individually fitted rain function is capable to unravel 'interesting' signals by leaving only those tilt anomalies that are not induced by rain. These anomalies may then be investigated with respect to volcanic activity (fig. 6).

Conclusion

It is generally not possible to protect tiltmeters installed in shallow bore holes against real ground deformations that are induced by meteorological parameters like air pressure, air temperature and rain. It was shown that there are at least three ways for the rain to enter tilt observations: (1) compression of the ground by the added water mass, (2) expansion of the ground due to rising pore pressure with water infiltrating the soil, and (3) deformation of the soil matrix due to water flowing through the pore space. Mechanisms (1) and (2) are present in case of a sloping ground surface; mechanism (3) is invoked by horizontal pore pressure gradients. While (1) induces an instantaneous response of the tiltmeter that decays exponentially, (2) and (3) are governed by diffusion leading to a delayed response. The general response of a tiltmeter will be a combination of all three effects with their relative

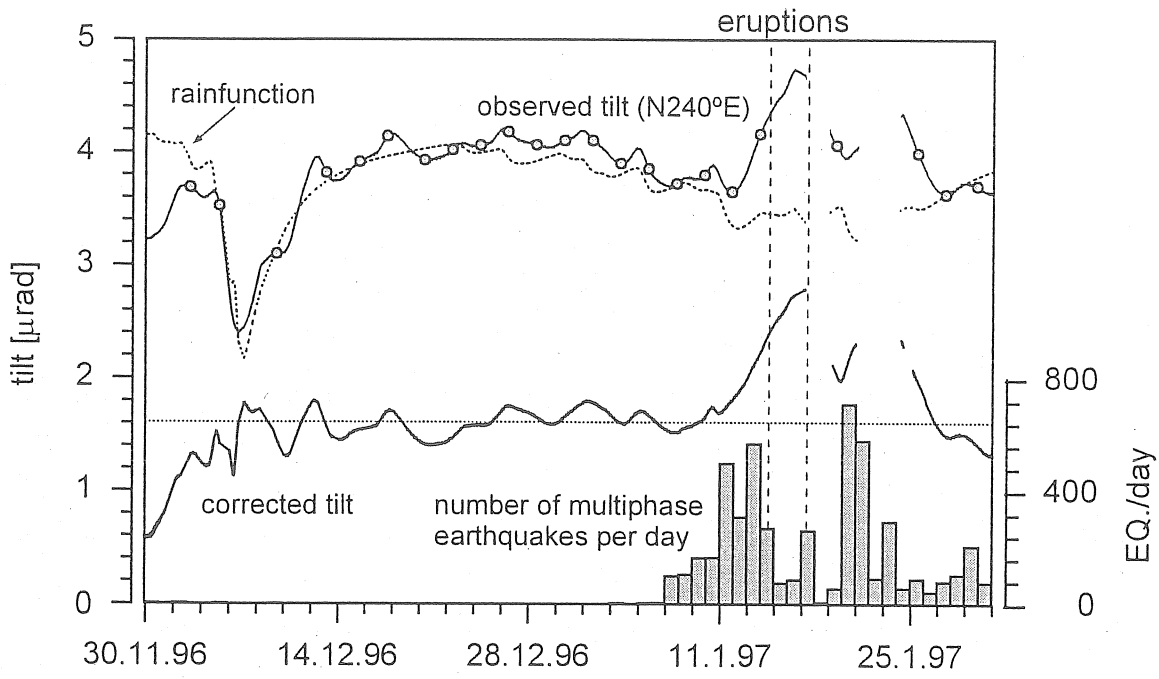

Figure 6: Fit of a rain function (eq. (5), constant *D*) to a 2-months tilt series at site KLT (1800m, W). After correction of rain induced disturbances a tilt anomaly during the volcanic crisis in January 1997 becomes clearly visible.

weights depending on the local conditions. The experience with the tiltmeter installations at the flanks of Merapi shows that usually infiltration of rain water into the ground is the predominant tilt generating process. The discussion of this process showed that it is not sufficient to just record precipitation. The amount of meteoric water observed at a location does give only the potential water input; it does not give sufficient information about the real changes in the soil water content. Thus, it is recommended to monitor the soil moisture directly. Replacing potential with the real soil water content in eq. (5) and considering effects of incomplete saturation will facilitate a more realistic modeling of the rain induced tilt disturbances.

References

Applied Geomechanics, *Users's Manual*: Model 722 Borehole Tiltmeter, High Performance Option, Santa Cruz, USA, 20 pp, 1991.

Harrison, J. C. and Herbst, K. (1977). Thermoelastic strains and tilts revisited, *Geophys. Res. Lett.*, 4, 535-537.

Körner, A. (2000). *Deformationsmodelle nach Auswertung von Tilmeter- und GPS-Daten für den Vulkan Merapi (Indonesien),* PhD-thesis, Universität Potsdam, 108 pp.

Kümpel, H.-J., Varga, P., Lehmann, K., and Mentes, Gy., (1996). Ground tilt induced by pumping - Preliminary results from the Nagycenk test site, Hungary, *Acta Geod. Geoph. Hung.*, 31, 67-79.

Langbein, J. O., Burford, R. O. and Slater, L. E. (1990). Variations in Fault Slip and Strain Accumulation at Parkfield, California: Initial Results Using Two-color Geodimeter Measurements, 1984-1988, *J. Geophys. Res.*, **95**: 2533-2552, 1990.

Peters, G., Klopping, F. J. and Berstis, K. A. (1995). Observing and modelling gravity changes caused by soil moisture and groundwater table variations with superconducting gravimeters in Richmond, Florida, U.S.A., *Cahiers du Centre Europeen de Geodynamique et de Seismologie*, **11**, 147-159.

Purbawinata, M. A., Ratdomopurbo, A., Sinulingga, I. K., Sumarti, S. and Suharno (Ed.) (1997). *Merapi Volcano - A Guide Book,* Volcanological Survey of Indonesia, Bandung, Indonesia, 64 pp.

Raudkivi, A. J. and Callander, R. A. (1976). *Analysis of Groundwater Flow*, Arnold, London, 214 pp.

Rebscher, D., Westerhaus, M., Welle, W. and Nandaka, I. M. A. (2000). Monitoring ground deformation at the Decade Volcano Gunung Merapi, Indonesia, *Phys. Chem. Earth*, **25**, 755-757.

Turcotte, D. L. and Schubert, G. (1982). *Geodynamics*, John Wiley, New York, 450 pp.

Maercklin, N., Riedel, C., Rabbel, W., Wegler, U., Lühr, B.-G. and Zschau, J. (2000). Structural Investigation of Mt. Merapi by an Active Seismic Experiment, In: *Deutsche Geophys. Gesellschaft - Mitteilungen*, Sonderband IV/2000, 13-16.

Westerhaus, M. (1996). *Tilt- and well level tides along an active fault*, Scientific Technical Report STR96/05, GFZ-Potsdam, 265 pp.

Westerhaus, M., Rebscher, D., Welle, W., Pfaff, A., Körner, A. and Nandaka, I.G.M. (1998): Deformation measurements at the Flanks of Merapi Volcano, *Deutsche Geophysikalische Gesellschaft, Mitteilungen,* Sonderband III/1998, 3-8.

Zschau, J., Sukhyar, R., Purbawinata, M. A., Lühr, B. and Westerhaus, M. (1998) Project *MERAPI* - Interdisciplinary Research at a High-Risk Volcano, *Deutsche Geophysikalische Gesellschaft, Mitteilungen,* Sonderband III/1998, 3-8.

TILT VARIATIONS AT SHALLOW DEPTH: IMPLICATIONS FOR THE INSTALLATION OF A LASER GYROSCOPE AT THE GEODETIC OBSERVATORY WETTZELL

Klügel, T.

FESG, TU Munich, Fundamentalstation Wettzell
Sackenrieder Str. 25, 93444 Kötzting, Germany
(e-mail: kluegel@wettzell.ifag.de)

Introduction

Observation pillars near the earth's surface are always subject to local ground deformations which mainly result from thermoelastic and hydrologic induced stresses. The importance of such effects rises with increasing precision of the instruments. The construction of the world's most precise laser gyroscope at the Geodetic Observatory Wettzell requires utmost orientation stability of the observation pillar. A detailed site investigation and records of natural tilts at different depths as well as environmental parameters were performed in order to assess the magnitude and origin of tilt variations and to develop strategies to minimize them under the given geological, hydrological, and financial conditions.

Site investigation

The Geodetic Observatory Wettzell is located in the Bavarian Forest 610 m above sea level on a flat saddle between two hilltops. The investigated area is a meadow with a slight slope of 4-6° towards west. A total of 6 boreholes reveal a strongly varying degree of weathering of the bedrock consisting of metamorphic crystalline rock (gneiss). The uppermost 2 m mainly consist of sandy loam, which is the result of the total decomposition of the bedrock. Below 2 m an increasing number of boulders of different size (up to 1-2 m) occur, which are remnants of the weathering process. The transition of weathered rock to solid rock is smooth and at varying depth; solid rock is present below 7-14 m. But even the solid rock is crossed with joints and fractures, where weathering might have produced zones of low strength and good permeability.

As a consequence of the geological conditions, the hydrological situation of the underground is very inhomogeneous. The sandy loam close to the surface is a pore aquifer with low permeability. The zone of weathered and partly weathered rock consists of pore aquifer zones with medium permeability and zones of no permeability in between (rock boulders). The fractured solid rock can be characterised as a cleft aquifer with strongly varying permeability. The records of 4 different groundwater gages match the complex hydrological situation. Although being no more than 100 m apart, every gage shows somewhat different behaviour. Three gages show groundwater levels of about 3-7 m below the surface, one gage show a very different level of 9-12 m. The maximum level difference is between 2.3 and 3.8 m in all 4 gages.

Tilt records

Tilt variations were recorded using two Applied Geomechanics type 722A borehole tiltmeters in a geodetic survey pillar close to the surface and in boreholes at 6 m and 13 m depth, and using an Askania pendulum at 30 m depth.

The survey pillar (Fig. 1) shows tilts after rainfall or snow melting up to 20 µrad. A strong and rapid tilt of the pillar up to 40 µrad may occur when the soil is freezing and thawing (e.g. January 2001). There is a linear drift of about 80 µrad/y towards WNW, but no seasonal wave can be observed.

At a depth of 6 m (Fig. 2), where is the transition between the unsaturated zone and the groundwater, the most prominent tilt signal is a seasonal wave with a double amplitude of 40 µrad. An thermal effect of the instrument does not seem to play a major role, because the tilt signal and the temperature are not exactly in phase. The short term tilt variations are due to rain and show amplitudes up to a few µrad per event. The highest value of 7 µrad occured after heavy rain on dry soil in October 1998. There is nor a clear temporal neither a quantitative correlation between tilt and rainfall or groundwater level. Time, direction, and amount of tilt after rain depends on the actual condition of the soil like humidity and temperature. In the winter when the soil is wet, even small amounts of rain or snow melt quickly migrate downwards and reach the tiltmeter level to produce soil deformations. But in the spring and summer, when the soil is dry and the vegetation needs a lot of water, the water migrates to deeper levels only after intense rain.

The instrument at 13 m depth, that is below the groundwater table, shows a weaker reaction after hydrological events, but there is a certain correlation with the groundwater level. A coefficient of roughly 10 nrad/cm can be deduced.

The Askania pendulum at 30 m depth (Fig. 3) shows a hydrologically induced seasonal signal of about 0.4 µrad, a seasonal thermoelastic wave of less than 0.2 µrad, and a linear drift of about 0.8 µrad towards NNW. The dominant hydrological signal occurs in late winter and spring when rain and snow melt penetrate deep soil layers. This signal correlates with the groundwater record at gage BK1, where the groundwater level is deeper than at the other gages. Short term hydrological tilts in the order of 0.1-0.2 µrad rather tend to correlate with gage BK3. This behaviour underlines the complexity of the hydrological system. But it is clear that beside the earth tides, the strongest signal at this depth is of hydrological origin.

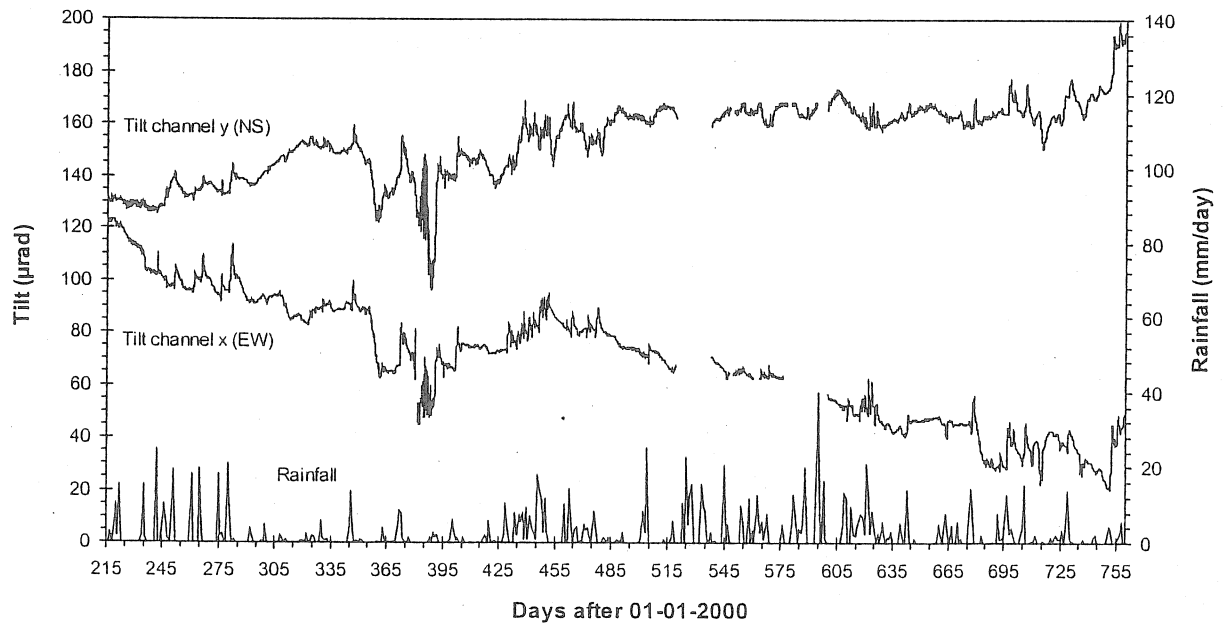

Figure 1: AGI borehole tiltmeter in a geodetic survey pillar; record over 540 days.

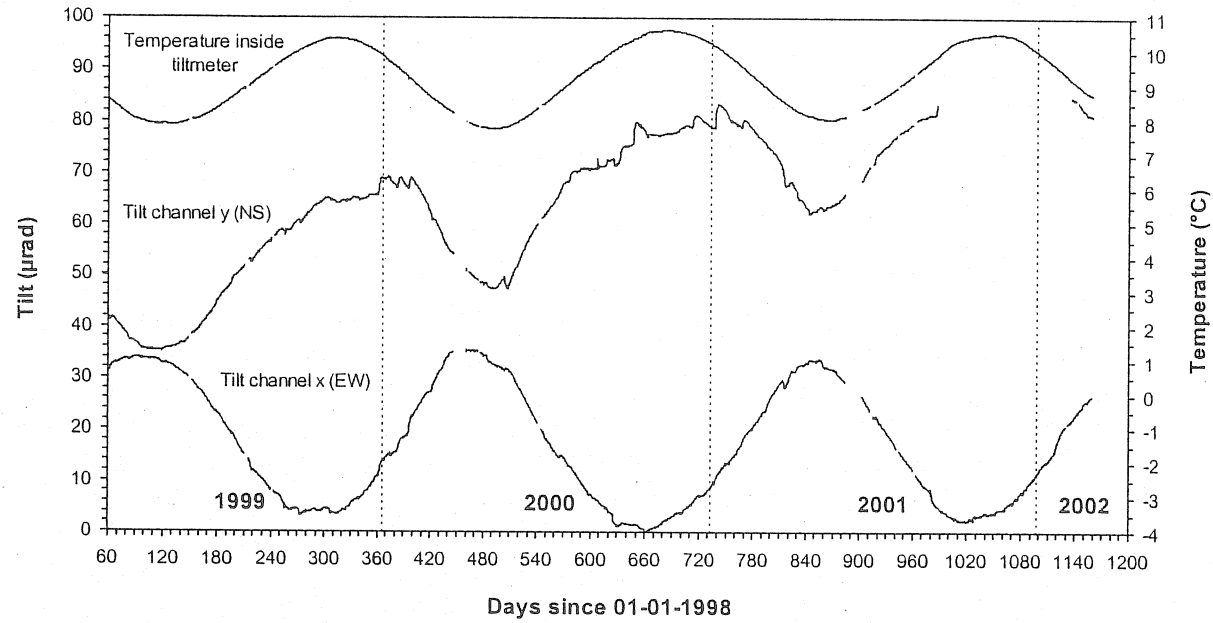

Figure 2: AGI borehole tiltmeter in 6 m depth; record over 3 years.

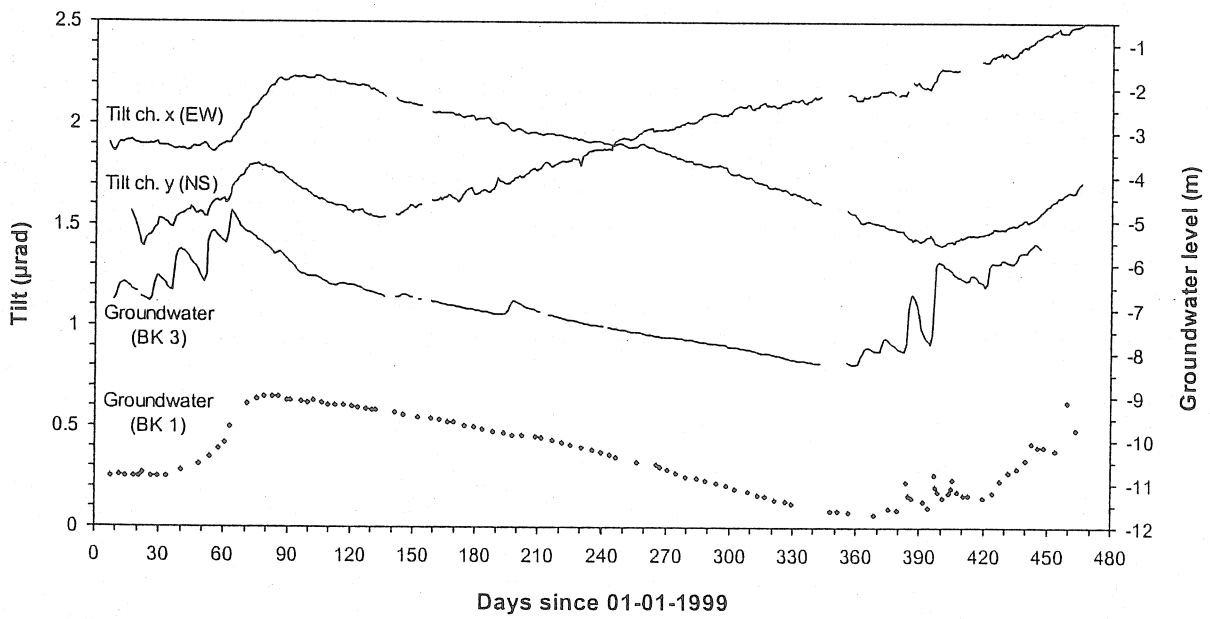

Figure 3: Askania pendulum in 30 m depth, earth tides removed; record over 460 days.

Results

Tilt records close to the earth's surface are mainly affected by thermoelastic and hydrologically induced, local soil deformations. The propagation of a thermal wave into the underground can be described by the formula for one-dimensional heat conduction:

$$T(z,t) = A \exp(-z \sqrt{\omega} / (\sqrt{2}\, a)) \sin(\omega t - z \sqrt{\omega} / (\sqrt{2}\, a))$$

where A is the amplitude at the surface, z is the depth, ω is the frequency and a is the thermal diffusivity. The amplitudes decrease exponentially with depth and $\sqrt{\omega}$, that diurnal thermal waves are detectable only in the upper 2 m. The annual thermal wave reaches in Wettzell double amplitudes of 2.8 °C at 6 m and 0.1 °C at 17 m depth. The temperature field is assumed to be stratified parallel to surface, that lateral inhomogeneities or an uneven surface are required to produce vertical tilts. The absence of seasonal tilts near the surface thus indicates that lateral inhomogeneities are small in the uppermost soil layer. However, there are strong seasonal tilts in 6 m depth being the consequence of major lateral strength contrasts between solid rock (boulders) and weathered rock (soil). In 30 m depth the thermoelastic seasonal tilts are very weak, which can be due to very small temperature amplitudes or small inhomogeneities in the solid rock.

Hydrological tilts occur immediately after rainfall or snow melt close to the surface. Near the groundwater table, tilts may be temporally correlated with either rain or groundwater. The seasonally varying direction indicates that thermoelastic strains due to heat transfer by downward migrating water seems to play a certain role. Below the groundwater table, tilts tend to correlate with changes of the groundwater level. These variations in hydrostatic pressure give rise to deformations even in 30 m depth.

The results entered into the design of the pillar and the observation lab, which depth was limited by the groundwater table. A drainage system below the lab keeps the groundwater level constant. The pillar is founded 5.5 m below the lab on solid rock and is shielded from deformations at shallower depth by a system of concrete rings. A thick thermal isolation and a mound on top keep the temperature in the lab constant at a 1/100 °C-level. A surface water seal prevents seeping water to migrate to deeper levels. High resolution platform tiltmeters being installed on top of the laser gyroscope prove the stability of the construction. However, after heavy rain a movement of the pillar of some hundred nanoradian can be observed.

Conclusions

The comparison of tilt measurements at different depths with environmental data reveal that thermoelastic deformations strongly decrease with depth and highly depend on the presence of lateral inhomogeneities. The influence of such deformations can be strongly reduced by increasing the depth of foundation and by thermal isolation. Hydrological tilts occur at every depth where meteorological water is present. They might be reduced by a deep, stable foundation and proper water draining, but cannot be prevented. Monitoring of tilt variations with high resolution tiltmeters placed on top of the laser gyroscope is required.

Environmental effects in tilt data of Nokogiriyama Observatory
extended abstract

Gerhard Jentzsch[1], Steffen Graupner[1], Adelheid Weise[1], Hiroshi Ishii[2] and Shigeru Nakao[3]

1. Tilt measurements at the Geodynamic Observatory Nokogiriyama, Japan

Nokogiriyama Observatory of Tokyo University, Earthquake Research Institute (ERI), established in summer 1993, is situated on the eastern side of the entrance to the Tokyo Bay, located at the foot of a hill at about 600 m distance east from the coastline. It comprises underground galleries and a building for data acquisition (Chen & Ishii, 1994). In connection with several neighbouring observatories the purpose is the monitoring of seismicity and crustal deformation in the earthquake area around Tokyo Bay, as well as the testing of new sensors (Ishii, 1995; Nakao et al., 2000). Thus, the instrumentation includes quartztube extensometers, water tube tiltmeters (ERI), a LaCoste-Romberg gravimeter, borehole strainmeters, various seismometers, meteorological instruments and a tide gauge station. In addition to the already existing water tube tiltmeters, the borehole tiltmeter No. 106 of the Askania type (Graf, 1964; Jacoby, 1966) was installed in a 10 m deep borehole inside the gallery close to the ERI tiltmeters, in April 1997. It operated with only a small drift until June 1999. First results of this comparison show a good correspondence between the signals of the two instruments. During the Earth-Tide Symposium in Mizusawa in 2000 we presented some results of the comparison of these tiltmeters (Ishii et al., 2001; Graupner, 2001).
In this extended abstract we provide additional information about environmental effects and ocean loading observed with the two tiltmeters. A more comprehensive paper including all results from Nokogiriyama as well as a comparison to other tilt measurements is in preparation.

2. Tidal results and drift

The tidal amplitude factors γ shown in Fig. 2 (from Ishii et al., 2001) are of an unusual order of magnitude: Instead of the theoretical value of around 0.7 we observe values of up to 10 due to ocean loading. Furthermore, there are significant differences between diurnal and semidiurnal tidal constituents. In E-W direction both instruments provide similar γ – factors, while in N-S direction the observed γ – factors for the water tube tiltmeter is generally about 30 % above the values for the Askania tiltmeter with slight deviations in the diurnal and semidiurnal bands. The phases fit well in both directions (not shown). The spectra (Fig. 1; Ishii et al., 2001) show tidal amplitudes well above the noise levels. The N-S noise levels are in the same order of magnitude as in previous observations at other sites (Weise et al., 1999), but due to the near coast, in connection with environmental influences, the noise levels in E-W direction are higher by a factor of 3 (note: The data of the ASKANIA tiltmeter, azimuth of 41° from the North, are transformed to N-S and to E-W, whereas the watertubes are constructed in these directions). In Tab. 1 the observed main tidal amplitu-des, the noise levels in the tidal bands as well as the signal/noise-ratios are given. The high tidal amplitudes are caused by strong ocean tidal loading. Since the noise levels in E-W are also bigger than in N-S, the signal-to-noise ratios are similar in both directions (up to 560).

The long-term drifts of the curves point to more local deformations than to instrumental effects. In our published paper (Ishii et al., 2001) the time series show a very good correlation in N-S for all periods and the same in E-W for medium periods at a week to months, but there is a general different aperiodic drift (Fig. 1 in Ishii et al., 2001). The reason is not quite clear, but it may be related to the difference inside the gallery of more than 50 m, whereas the east-west component is quite adjacent.

1) Institut für Geowissenschaften, Friedrich Schiller Universität Jena, Burgweg 11, 07749 Jena, Germany
2) Tono Research Institute of Earthquake Science, 1-63 Yamanouchi, Akiyo-cho, Mizunami City, Gifu 509-6132, Japan
3) Earthquake Research Institute, Uni Tokyo, No. 1-1, Yayoi 1-chome, Bunkyo-ku, Tokyo 113, Japan

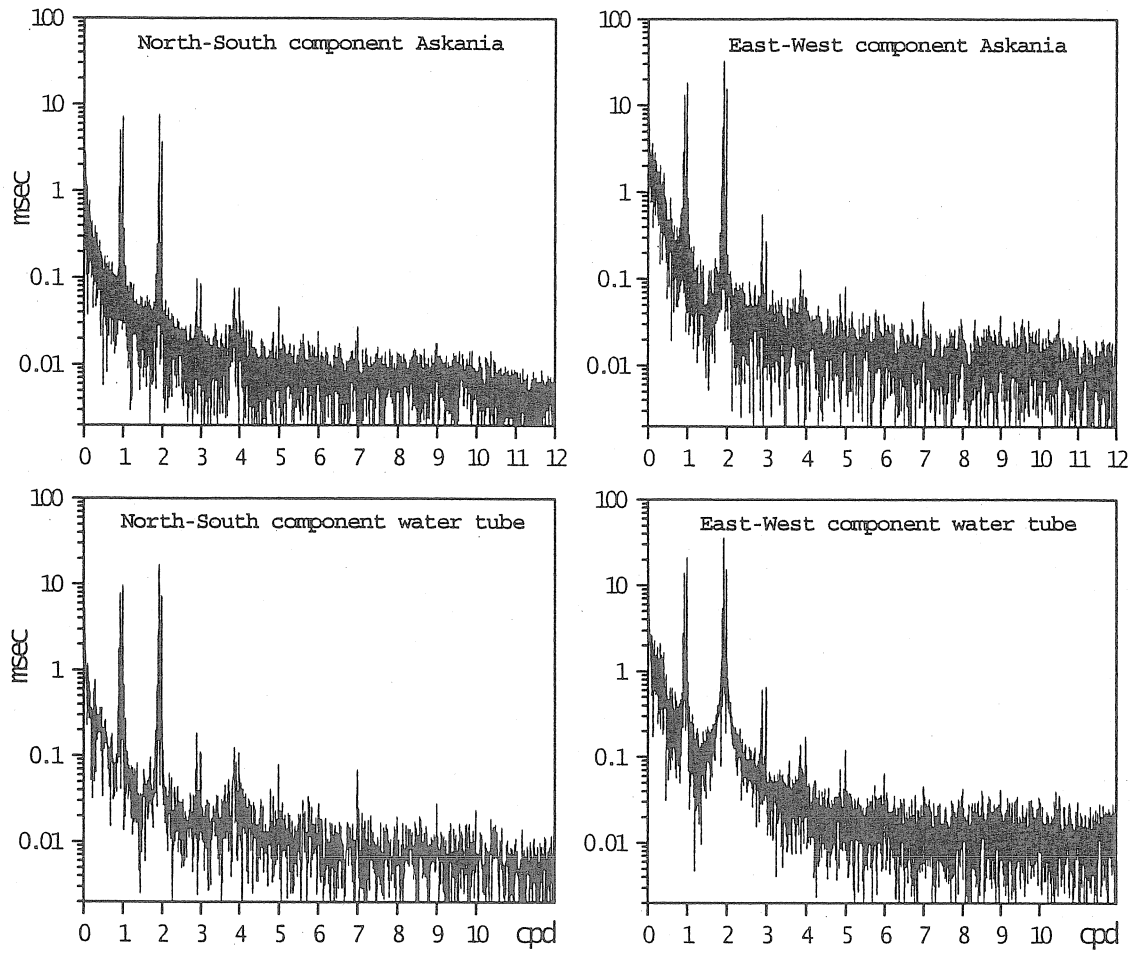

Figure 1. Amplitude spectra of hourly data for both tiltmeters and N-S and E-W components.

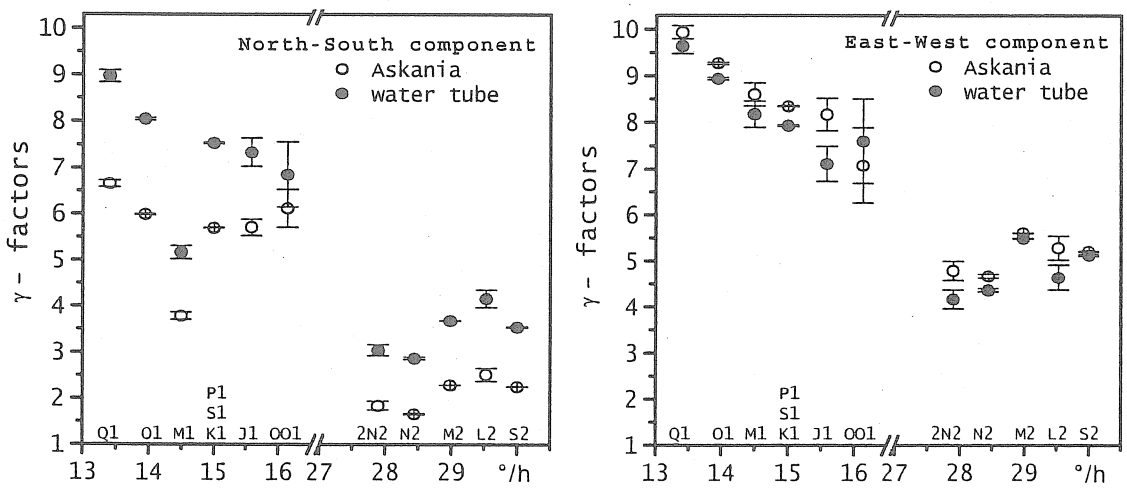

Figure 2. Amplitude factors of both tiltmeters for the major tidal constituents: The error bars indicate the least square deviations as given from the program ETERNA (Wenzel, 1994; 1997).

2. Environmental effects

Air pressure and rain induced tilt signals are prominent and also highly reproduceable features in both data sets. A particular strong rain event is plotted in detail (Fig. 3) and illustrates the simultaneous and equally strong reaction of both tiltmeters. Such rain events describe an unclosed loop in the projection plane, while pressure events are characterized by a prevailing forward/backward deflection in E-W direction (comp. Weise et al., 1999).

Because of their characteristic tilt patterns, it is possible to seperate the effects of air pressure and rain (Fig. 4). If rain and pressure changes occur at the same time, the

Table 1. Observed amplitudes of the main tidal waves, the noise level and s/n ratios.

tidal band		ASKANIA-borehole tiltmeter		ERI-type watertube tiltmeters	
		N-S	E-W	N-S	E-W
diurnal	K_1 [msec]	17.9	43.6	23.5	41.6
	noise [msec]	0.045	0.174	0.070	0.161
	S/N ratio	398	250	335	258
semi-diurnal	M_2 [msec]	17.2	71.8	27.5	70.7
	noise [msec]	0.043	0.128	0.054	0.161
	S/N ratio	400	561	509	439
ter-diurnal	M_3 [msec]	0.21	0.97	0.34	0.95
	noise [msec]	0.019	0.058	0.035	0.072
	S/N ratio	11	17	8	13
standard deviation	m_0 [msec]	0.94	2.96	1.17	2.42

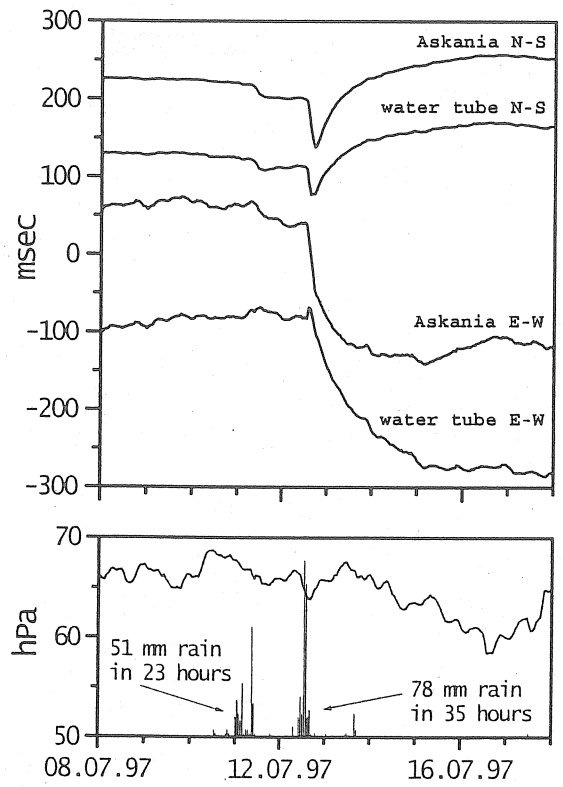

Figure 3. Rain event, air pressure of July 12, 1997, tilt signals, tides removed.

resulting figure is a superposition of both individual responses (comp. Braitenberg, 1999, for a review on the hydrologic induced strain-tilt signal and Dal Moro and Zadro, 1998).

Again, the general shape of the tilt changes is similar for the two instruments. For air pressure induced tilts a quantization attempt has been undertaken and yields regression coefficients of about 3.7 and 2.2 msec/hPa for the Askania and the water tube tiltmeter, respectively. These values are valid only for the predominant E-W direction. Tilt changes caused by rain are not that clearly correlated to the amount of rainfall. However, there seems to be a treshold at about 20 mm of rain within 24 hours for any rain induced tilt signal to be identifiable.

There is no ground water sensor in the vicinity of the tiltmeters, because the water level is far below. Therefore, we cannot give an interpretation of the tilt source. But one can conclude that changes of pore pressure due to rain leaking into the highly porous rock may be one reason. In addition, there might also be a stress component due to different temperatures of the water and the rock.

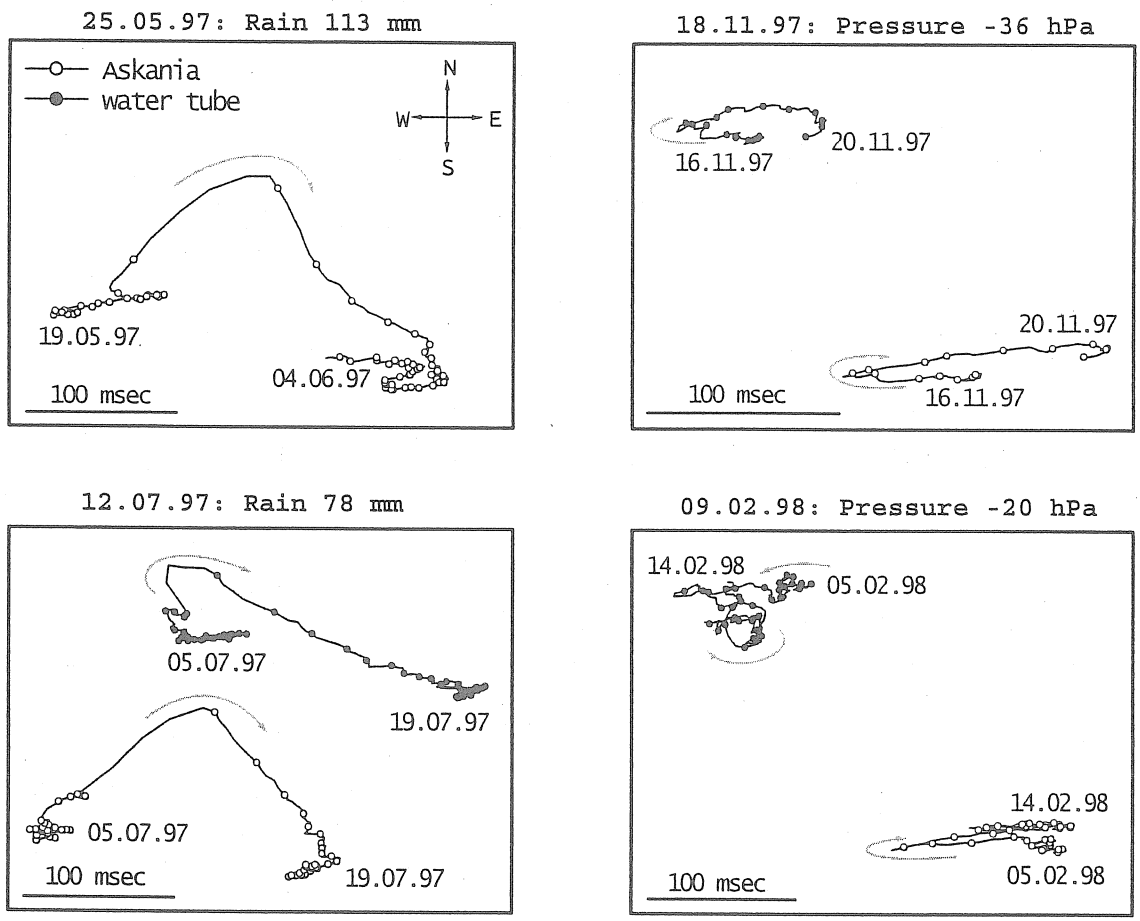

Figure 4. Classification of air pressure and hydrologically induced typical tilt patterns; general trend shown by arrows.

3. Loading tides

The observatory is situated on Boso peninsula forming the eastern margin of Tokyo Bay, about 600 m East of the shore line. Therefore, the tidal parameters are strongly disturbed by the loading tides of the adjacent Bay of Tokyo and the Pacific Ocean. Amplitude factors are amplified up to values of 10 and phases are shifted between 150° and 360° (N-S) and 40° and 120° (E-W), respectively.

The loading computations were carried out using the ocean tidal model of the National Astronomical Observatory NAO99b and NAOJb (global and for the Japanese area, resp., Matsumoto etal., 2000), and the software GOTIC2 (Matsumoto et al., 2001) based on GOTIC (Sato and Hanada, 1984). For the adjacent area the sea is gridded with a net of 2.25" N x 1.5" E, corresponding to a mesh of only about 50 m x 50 m. The evaluation of the results was performed according to Farrell (1972), Jentzsch (1997) and Jentzsch et al. (2000). Loading corrections for tilt measurements under similar conditions in the fjord region of southern Norway were applied by Jentzsch and Koß (1997).

The results of the loading computations are presented for the two main tidal waves both in the diurnal and the semi-diurnal tidal bands. The results in terms of vector diagrams reveal that the theoretical tides are the smallest signal for all waves and the loading tides are by far the biggest (Fig. 5). Therefore, it was to expect that the remaining residuals are still fairly big after subtraction of the tidal model and loading tides. But, since the tidal parameters obtained for both tiltmeters correlate quite well (esp. in the phase differences) also the residuals show a very good correlation.

The loading signals in E-W are bigger than in N-S by a factor of about 2 to 3. In N-S the observed loading is explained by the models by about 60% to 90%, whereas in E-W the results are between 40% and 50%. We do not assume that the existing discrepancy between

computed and observed loading tides are due to a misfit of the models; we rather suggest another explanation: First, the short distance to the sea is a great disadvantage, because from experience it seems to be impossible to model the tides at this small scale, esp. for tilt. Second, we must take into account another possible effect: strain-tilt coupling due to the strong ocean loading and the rough topography (comp. the basic work of Harrison, 1976).

In Fig. 5 the long solid arrows denote the observations, the small light errors in the center denote the theoretical tides, the thin solid arrows ending at the head of the observations show the oceanic load. The remaining two arrows are the residual vectors after subtraction of the ocean loading (dark) and after subtraction of ocean and theoretical tides (light), respectively.

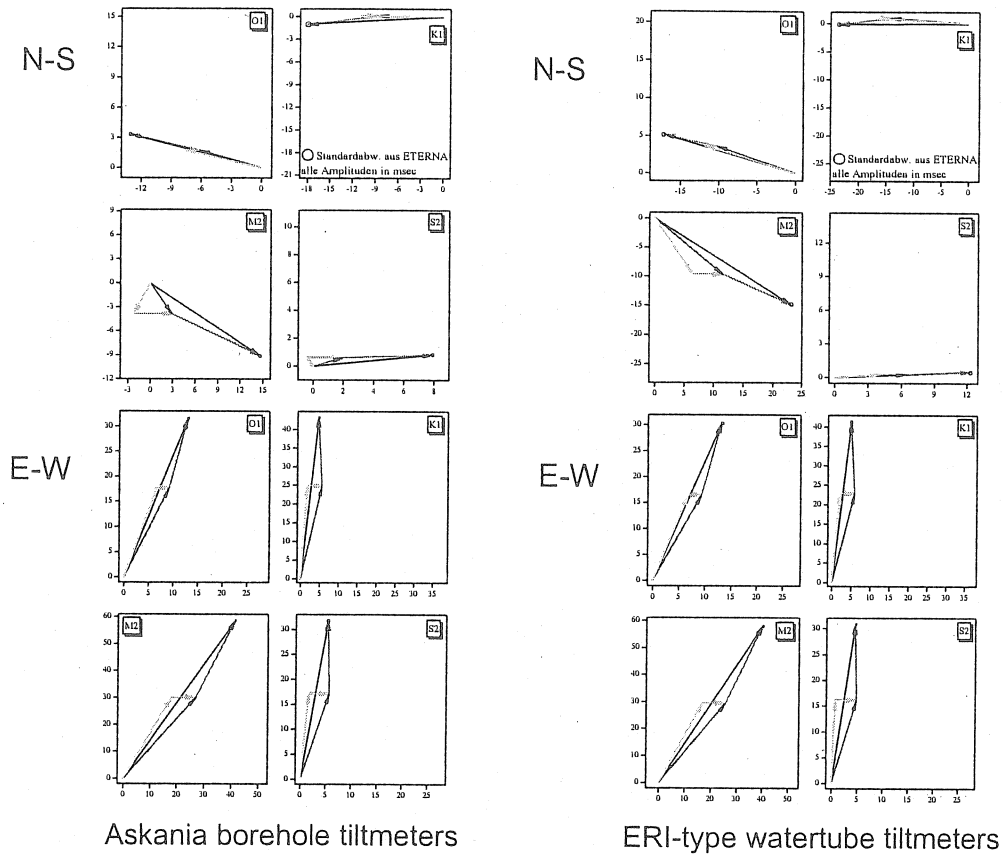

Figure 5. Phasor plot of tidal and loading vectors for constituents O1, K1 (upper row) and M2, S2 (lower row) for directions N-S and E-W: See text for explanation; the small circles at the heads of the arrows denote errors from ETERNA-Analyis. (from Graupner, 2001)

4. Acknowledgements

The idea of this work was realised during a stipendium of the Japanese Society for Promotion of Sciences (JSPS) offered to co-author Jentzsch. During this visit the borehole was prepared with the help of ERI. Later, the co-worker of Jentzsch, M. Ramatschi, installed the tiltmeter in the observatory. The analyses of the data were mainly carried out by co-auther Graupner (2002) in the frame of his thesis work. Parts of the project were funded by the German Research Society (Deutsche Forschungsgemeinschaft) and by the European Union (research grant CT960205). All this is gratefully acknowledged.

5. References

Braitenberg, C., 1999. The hydrologic induced strain-tilt signal – a review. Bull. d'Inf. Marées Terrestres, 131, 10171-10181.

Chen, G. and H. Ishii, 1994. Inversion of Initial Stresses from Deformations of Tunnel Surface during Tunneling - Modeling by Using SRM Combined with BEM. Proc. 8th Int. Symp. on Recent Crustal Movements, Kobe, Dez. 6-11, 1993, 285 - 291.

Dal Moro, G. and M. Zadro, 1998. Subsurface deformations induced by rainfall and atmospheric pressure: tilt/strain measurements in the NE Italy seismic area. Earth and Planetary Science Letters, 164, 193 - 203.

Farrell, W. E. (1972): Deformation of the earth by surface loads. Rev. Geoph. and Space Physics 10, No. 3, 761 - 797.

Graf, A., 1964. Erste Neigungsmessungen mit dem Vertikalpendel in einem 30 m Bohrloch. Comm. Obs. Roy. Bel., 236, Ser. Geophys. Nr. 69, 5ieme Symp. Int. sur la marées terrestres, Brüssel, 249 - 254.

Graupner, S., 2001. Hochpräzise Neigungsmessungen im geophysikalischen Observatorium Nokogiriyama/Tokyo. Diploma thesis, Institute of Geosciences, University of Jena, 191 p. (unpublished)

Harrison, J. C., 1976. Cavity and topographic effects in tilt and strain measurements. J. Geophys. Res., 81, 319 - 328.

Ishii, H., 1995. Developments of multi-component borehole instruments and application for earthquake prediction study. Abstract/Poster SA31G-17, XXI. General Assembly of the IUGG, Boulder.

Ishii, H., Jentzsch, G., Graupner, S., Nakao, S., Ramatschi, M. and Weise, A., 2001. Observatory Nokogiriyama / Japan: Comparison of different tiltmeters. Proc. 14th International Symposium on Earth Tides, Special Issue of the Journal of the Geodetic Soc. of Japan, 47/1, 155 – 160.

Jacoby, H. D., 1966. Das neue Bohrloch-Gezeitenpendel nach Graf. – Askania-Warte, 67, 12 - 17.

Jentzsch, G., 1997. Earth Tides and Ocean Tidal Loading. In: Wilhelm, H., Zürn, W. and H.-G. Wenzel (Eds.): Tidal Phenomena. Lecture Notes in Earth Sciences, 66, Springer, Berlin, 398 S.

Jentzsch, G. and S. Koß, 1997. Interpretation of long-period tilt records at Blasjö, Southern Norway, with respect to the variations in the lake level. Phys. Chem. Earth, V 22, Nr. 1, 25-31.

Jentzsch, G., Knudsen, P. and M. Ramatschi, 2000. Ocean tidal loading affecting precise geodetic observations on Greenland: Error account of surface deformations by tidal gravity measurements. Phys. Chem. Earth (A), Vol. 25, No. 4, 401 - 407.

Matsumoto, K., Takanezawa, T., and M. Ooe, 2000. Ocean tide models developed by assimilating TOPEX/Poseidon altimeter data into hydrodynamical model: A global model and a regional model around Japan. J. of Oceanography, 56, 567 - 581.

Matsumoto, K., Sato, T., Takanezawa, T., and M. Ooe, 2001. GOTIC2: A program for computation of oceanic tidal loading effect. Spec. Issue of the J. Geod. Soc. of Japan for the 14th Int. Symp. on Earth Tides, 243 - 248.

Nakao, S., Hirata, Y., Jentzsch, G., Ramatschi, M. and A. Araya (2000): Comparitive observation of pendulum type tiltmeters in Nokogiriyama observatory. (Abstract) 14th Int. Sym. on Earth Tides, Mizusawa.

Sato, T. and H. Hanada, 1984. A program for the computation of oceanic tidal loading effects "GOTIC". Pub. Int. Lat. Obs. Mizusawa, 18, No. 1, 29-47.

Weise, A., G. Jentzsch, A. Kiviniemi and J. Kääriäinen (1999): Comparison of long-period tilt measurements: results from the two clinometric stations Metsähovi and Lohja, Finland. Journal of Geodynamics, 27, 237 - 257.

Wenzel, H.-G., 1994. Earth Tides Analysis Package ETERNA 3.0. Bull. d'Inf. Marées Terrestr., 118, 8719 - 8721.

Wenzel, H.-G., 1997. Analysis of Earth Tide Observations. In: Wilhelm, H., Zürn, W. and H.-G. Wenzel (Eds.): Tidal Phenomena. Lecture Notes in Earth Sciences, 66, Springer, Berlin, 398 S.

Two Feedback Systems to the Gs 15 No. 228 Gravimeter

Jaroslav Brož, Zdeněk Šimon

Research Institute of Geodesy, Topography and Cartography
CZ 250 66 Zdiby 98

Jan Dupač
Papouch - Elektronika, Soběslavská 15, CZ 130 00 Praha 3

Antonín Zeman
Faculty of Civil Engineering, Czech Technical University Prague
Thákurova 7, CZ 166 29 Praha 6

Summary:

Two feedback systems were constructed for the tidal gravimeter Gs 15 No. 228. Both systems were based on the use of the gravimeter´s electro-magnetic record calibration device.

The first system was analog. It improved significantly accuracy of observations. The mean-square error (MSE) of an hourly ordinate from an analysis of observed data using the program ETERNA was 0.091 μGal. The results showed, however, that coils of the calibration device produced heat depending on magnitude of the compensation current. This heat can disturb the observations.

The second system was digital. In this case, an alternating current of 50 Hz was added to the compensation current. Its amplitude can be changed so that the total heat produced by the coils remained at the same level. This digital feedback system did not cause any time delay of the observed signal. According to performed observations, the MSE of the hourly ordinate was the same as in the case of the analog system. The reproduction of results had, however, significantly improved. Amplitude factors δ of major tidal waves derived from monthly observation series are stable at 0.1% level.

1. Introduction

The gravimeter Gs 15 No. 228 has been used for tidal observations at the Geodetic Observatory Pecný since 1975. The analog recording system was replaced by the digital system in 1995. This operation improved the accuracy of observed data from 0.48 μGal to 0.15 μGal (based on the MSE of the hourly ordinate from the data analysis using the program ETERNA), (Brož et al., 1997).

Further improvement of the gravimeter Gs 15 was achieved by the feedback system that according to (Orejana and Vieira, 1984), (Chen Yi Hui et al., 1986) employed a device for the electro-magnetic calibration of gravimeter's record (Schulze 1965). In this approach,

the compensation current in the coils of the calibration device, that is regulated to keep the beam in the zero position, is measured. This is contrary to the standard approach that is based on observations of beam's deviations from the zero position using a capacity sensor. The compensation current is directly proportional to the gravity variations, or better to changes of the vertical component of the tidal force. The capacity sensor (CPI) is used only as a balance indicator.

2. Analog feedback system

The analog feedback system for the gravimeter Gs 15 No. 228 was built in 1997. The diagram of the system is shown in Fig. 1. The feedback circuit consists of a differential amplifier and a proportional - integral regulator. The compensation current goes through a parallel adder into the coils of the electro-magnetic calibration device of the gravimeter. The parallel adder gives the possibility to feed the coils with both the compensation current and a step signal. Accurate determination of instrumental damping of the gravimeter is possible in this way (Wenzel, 1994). The current I from the PI regulation and that from the calibration unit are inverted into the voltage U and then recorded.

Fig. 1. Block diagram of the analog feedback device

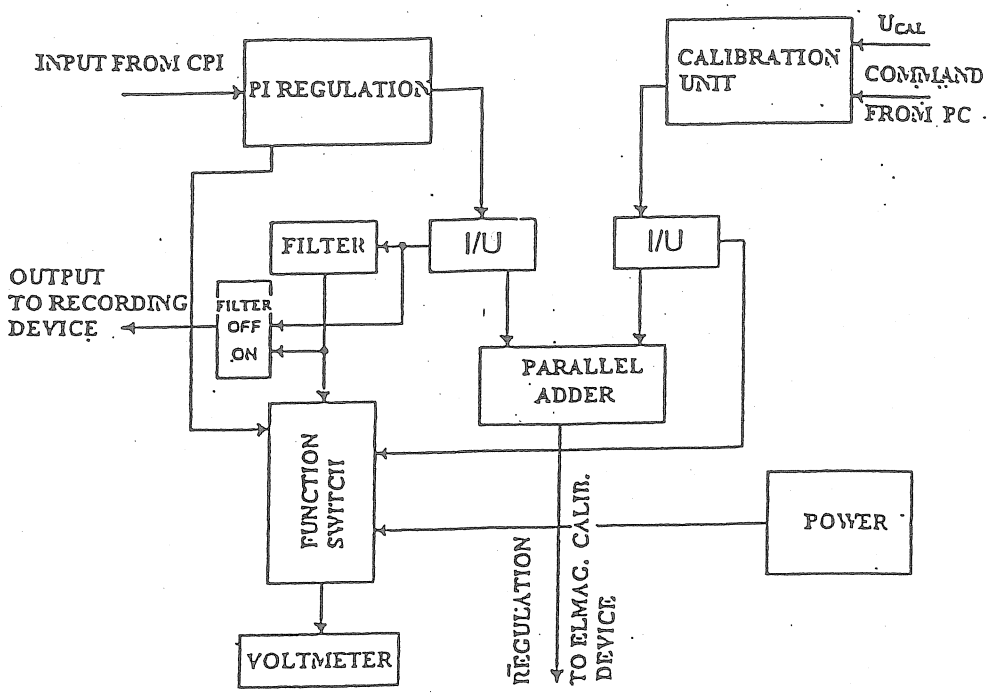

The output voltage of the feedback system was filtered at the station by the Butterworth filter of the 2nd order with the time constant of 16 sec. The filter was in a series connection with an amplifier that increased the output voltage three times.

The registration (PC board AD 18P) recorded and digitalized data at a sampling rate of 1 sec. These data were later re-sampled to one-minute samples (Brož et al., 1997). The scale of the record was approximately 1.093 mGal / V that corresponds approximately to the current scale of 0.328 mGal / mA in the coils of the electro - magnetic calibration device. To avoid greater changes of the micrometer reading when calibrating the record using the measuring screw of the gravimeter, the range of the feedback system was set to ± 2.5 mGal. This corresponds to ± 2.29 V in the digital record or to ± 7.62 mA in the coils of the calibration system. It is preferred to calibrate the record in this range since the micrometer non-linearity causes large errors in the calibration results (Šimon and Brož, 1993).

A series of tests was performed using the tidal gravimeter with the analog feedback system. Special attention was paid to eventual noisy effect of the heat generated by the Helmholtz coils of the electro-magnetic calibration device. A series of record calibrations using the measuring screw of the gravimeter was completed. The measuring screw was reset in the following three ways:

A) Symmetrically by ± 50 micrometer divisions around the zero of the system (zero signal of the feedback system). The resulting scale of the record was k = 1.093 mGal / V.

B) Between zero and + 50 micrometer divisions (between the zero and negative signal of the feedback system), k = 1.132 mGal/V.

C) Between zero and -50 micrometer divisions (between the zero and positive signal of the feedback system), k = 1.055 mGal/V.

Large changes of the record scales in the cases B and C are due to the effect of the heat generated by the coils of the electro-magnetic calibration device. This heat is rather small when the measuring screw is set to signal magnitude close to zero. In the extreme settings of the measuring screw in the cases B and C, the same current is circulating in the coils but in opposite directions. The same amount of heat is generated. It is quite large since it increases with the current squared. Changes of the scale are also approximately the same in both cases but they have an opposite sign. This can be explained in the following way: the disturbing heat affects the elastic system of the gravimeter by a moment in direction of larger magnitude of gravity. Recorded voltage changes in the extreme settings of the measuring screw by about the same value in the positive direction. In the case B, a smaller difference of voltage is observed between the zero and extreme setting. As a consequence, the value of k is larger. The situation is reversed in the case C.

The linearity of the entire equipment was also checked as well as the possibility of its damping determination using step changes on the input of the gravimeter via the parallel adder.

Six short recordings were performed at last. The measuring screw was set to different settings so that the entire range ±2.5 mGal of the feedback was covered. The data of each recording were analysed by the program ETERNA with an unique record scale k = 1.094 mGal/V. This scale was obtained from several calibrations symmetric around the zero of the system.

Results of the analyses change significantly based on mean magnitude of the measured signal (distance from the zero of the system) in the particular recording. An apparent change of the record scale is shown in Fig.2. It was derived from changes of the amplitude factors δ

of the major tidal waves between individual recordings. Changes of the phase delay κ of the wave M_2 only for the four recordings close to zero are shown in Fig. 3.

Fig. 2. Changes of the scale values *k* with distance of the record from zero (100% - prior measurement without feedback)

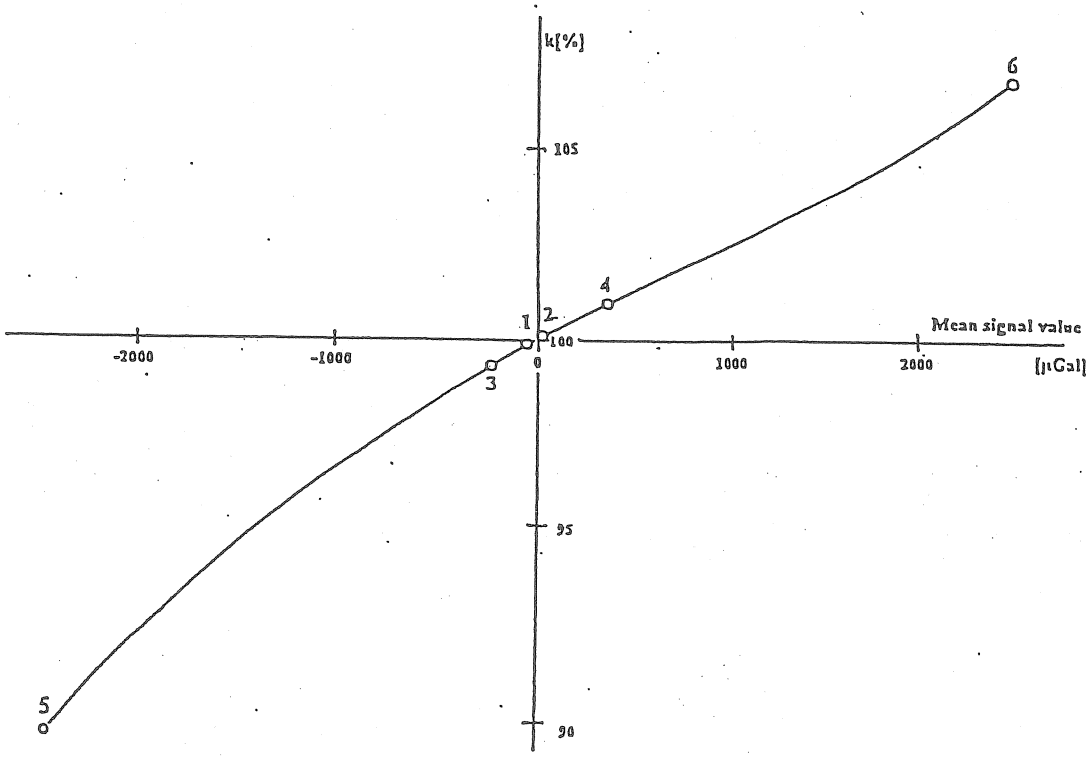

Fig. 3. Changes of the phase lags κ of the M2 wave with distance of the record from zero (0° - prior measurement without feedback)

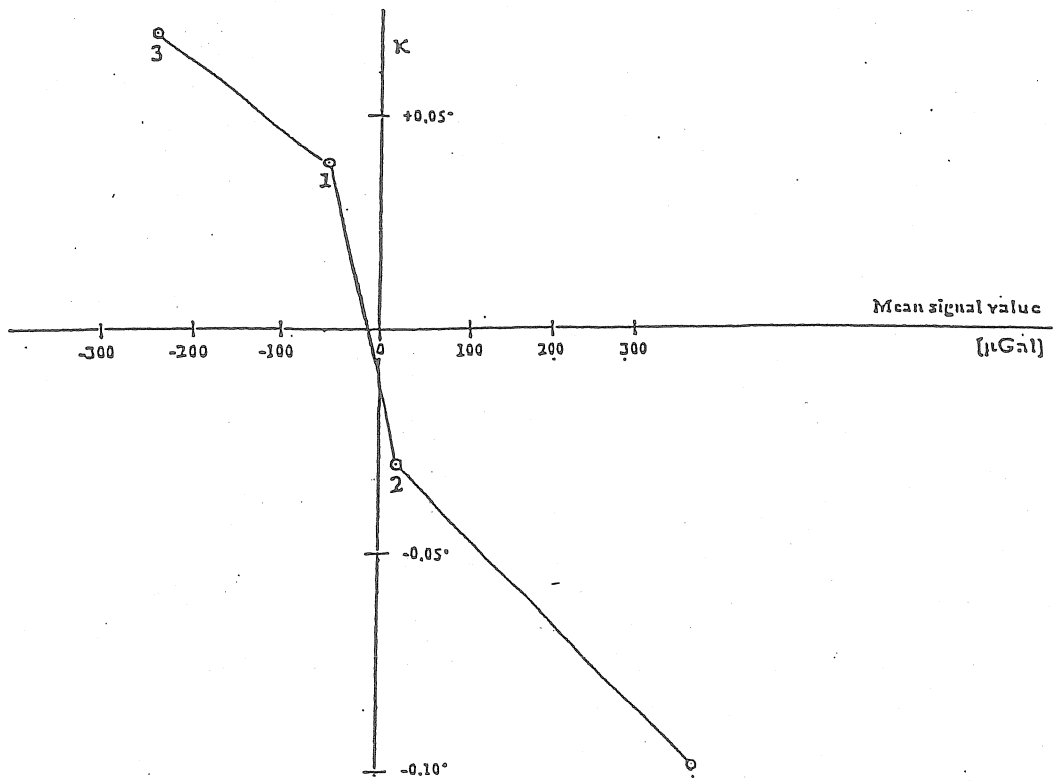

These results also indicate that the disturbing heat is generated in the coils of the electro-magnetic calibration device. This heat depends on magnitude of tides. Its disturbing effect is more pronounced with the larger distance of the record from the zero position. Each tidal wave is thus responsible for a disturbing heat wave that has the same frequency but certain phase delay. The amount of the generated heat increases with the square of the compensation current in the coils. The amplitude of the disturbing wave is thus proportional not only to the amplitude of the tidal wave but also to the average absolute magnitude of the feedback's signal. If the signal is positive (larger gravity than by the zero signal), the disturbing and tidal waves are added as two vectors. If the signal is negative (smaller gravity), the disturbing wave is subtracted. Parameters of the recorded wave change in this way.

One may conclude from all these performed tests that the tidal observations with the analog feedback system have reasonable quality only when the recording is done at the vicinity of the zero setting of the system. The record calibration must be performed symmetrically around the zero.

Tidal observations had been performed with the above described apparatus at the station Pecny since October 31, 1997 till January 3, 1999. The record was calibrated twice. The scale k was at the beginning equal to 1.0937 mGal/V and at the end to 1.0948 mGal/V. Corrections of the phase delay for damping of the system reached the value of 0.319° for the wave O1 and 0.663° for the wave M2. Results of the data analysis using the program ETERNA are in Table 1. The MSE of the hourly ordinate was estimated as 0.091μGal, i.e., the feedback system further improved the observation accuracy. Estimated values of the amplitude factors δ and the phase delays κ are in good agreement with previous results (Brož et al., 1997).

Due to the above described disturbing heat effect, analyses of monthly observation blocks were also performed. Deviations of the factors δ from the values obtained in a complete analysis of all data for the waves O1, K1 and M2 are shown in Fig. 4 together with the mean values of the signal. The values are obviously correlated although the variations of the factors δ are small. This dependency is not so significant in case of the values κ.

Fig. 4. Variations of the amplitude factors δ from one-month periods of measurement with the analog feedback device (zero - results of common analysis)

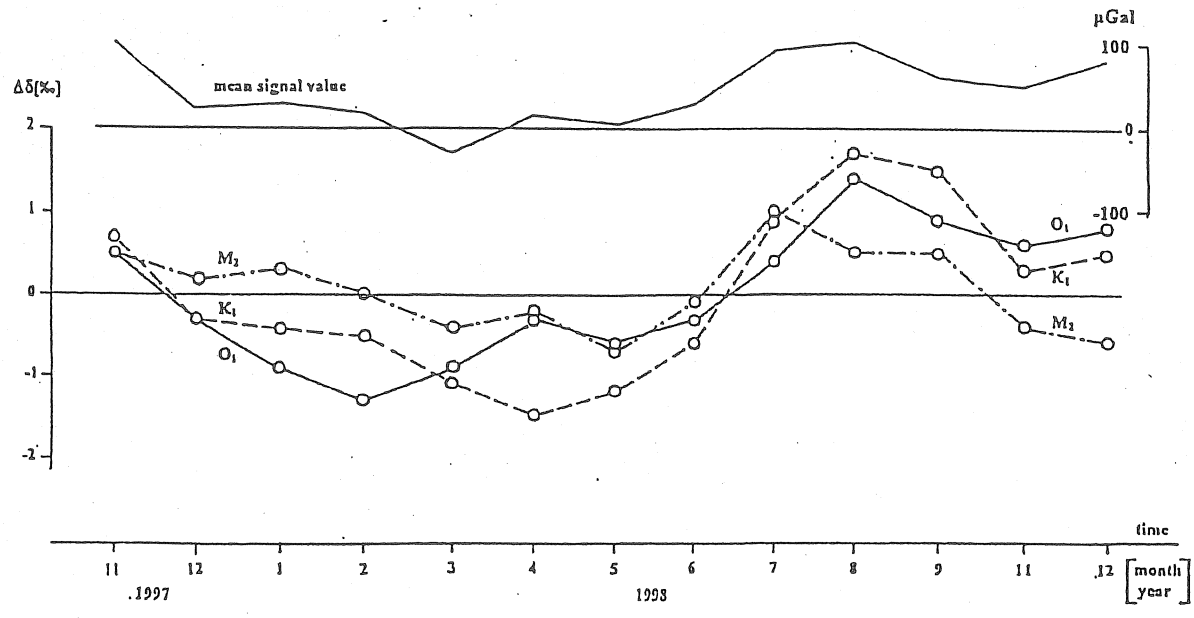

Table 1.

```
 Program ETERNA, version 3.21 950117 Fortran 77,  file: 1998-sst.prn
########################################################################
# GRAVIMETRIC EARTH TIDE STATION  PECNY  NO.0930,  CZECH REPUBLIC      #
# RESEARCH INSTITUTE OF GEODESY,TOPOGRAPHY AND CARTOGRAPHY, ZDIBY      #
#  49.92 N  14.78 E  H 534 M  P 2 M 'D 400 KM  VERTICAL COMPONENT      #
# GRAVIMETER ASKANIA GS15 - NO.228  (TECHNICAL UNIVERSIITY PRAHA)      #
# CALIBRATION ELEKTROMAGNETIC; DIGITAL RECORD, ANALOG FEEDBACK         #
# 1997.10.31 - 1999.01.03    412 DAYS                                  #
# INSTALLATION   Z.SIMON, J.BROZ; MAINTENANCE  J.BROZ                  #
# CALIBRATED TO CZECH GRAVITY BASELINE                                 #
# INSTRUMENTAL LAG CORRECTED FOR 0.32 DEG O1 AND 0.66 DEG M2           #
# WITHOUT INERTIAL CORRECTION                                          #
########################################################################

 Latitude: 49.9200 deg, longitude: 14.7800 deg, azimuth:  0.000 deg.

 Summary of observation data :
 19971031140000...19980929160000  19981015 80000...19981126230000
 19981128 80000...19990103160000
 Initial epoch for tidal force     : 1997.10.31. 0
 Number of recorded days in total :   412.17

 TAMURA 1987   tidal potential used.
 WAHR-DEHANT-ZSCHAU inelastic Earth model used.
 UNITY window used for least squares adjustment.
 Numerical filter is PERTZEV 1959 with  51 coefficients.

 Estimation of noise by FOURIER-spectrum of residuals
 0.1 cpd band99999.9990 nm/s**2       1.0 cpd band    0.0463 nm/s**2
 2.0 cpd band    0.0344 nm/s**2       3.0 cpd band    0.0233 nm/s**2
 4.0 cpd band    0.0203 nm/s**2       white  noise    0.0215 nm/s**2

 adjusted tidal parameters :
 from       to       wave   ampl.  ampl.fac.     stdv. ph. lead     stdv.
 [cpd]      [cpd]       [nm/s**2 ]                        [deg]     [deg]

 0.721500 0.906315 Q1     67.125   1.14512  0.00058   -0.0567    0.0332
 0.921941 0.940487 O1    351.768   1.14896  0.00011    0.0867    0.0064
 0.958085 0.974188 M1     27.776   1.15354  0.00104    0.1602    0.0595
 0.989049 0.998028 P1    163.983   1.15111  0.00020    0.1825    0.0113
 0.999853 1.000147 S1      3.667   1.08852  0.01184   -4.3632    0.6780
 1.001825 1.003651 K1    489.326   1.13643  0.00007    0.1464    0.0043
 1.005329 1.005623 PSI1    4.252   1.26222  0.00858    3.7639    0.4906
 1.007595 1.011099 PHI1    7.158   1.16743  0.00453    0.8187    0.2596
 1.013689 1.044800 J1     27.776   1.15362  0.00135    0.0863    0.0776
 1.064841 1.216397 OO1    15.267   1.15882  0.00331   -0.0699    0.1895
 1.719381 1.872142 2N2    11.153   1.17080  0.00164    2.0695    0.0941
 1.888387 1.906462 N2     70.363   1.17962  0.00033    1.6217    0.0190
 1.923766 1.942754 M2    368.860   1.18397  0.00006    1.2030    0.0037
 1.958233 1.976926 L2     10.378   1.17856  0.00255    0.0789    0.1463
 1.991787 2.002885 S2    171.025   1.17991  0.00015   -0.0130    0.0085
 2.003032 2.182843 K2     46.655   1.18404  0.00070    0.1518    0.0400
 2.753244 3.081254 M3      4.153   1.05166  0.00320   -0.4170    0.1832
 3.791964 3.937897 M4      0.004   0.09621  0.23271  143.8727   13.3332

 Adjusted meteorological or hydrological parameters:
 no. regr.coeff.       stdv.  parameter   unit
   1    -4.89812     0.01319  airpress.   nm/s**2 /hPa

 Standard deviation of weight unit:     0.908
 degree of freedom:                     9705
 Standard deviation:                    0.908  nm/s**2
```

3. Digital feedback system

It was concluded in Section 2 that there is a small disturbing effect of the heat generated by the coils of the analog feedback system on the tidal observations. This effect remains despite all efforts to perform the recording as close to the zero of the system as possible. Should this effect completely be eliminated, the feedback device with the coils generating constant heat independent on magnitude of the compensation current would have to be constructed.

For this reason, the gravimeter Gs 15 No. 228 was equipped in 1999 by a new digital feedback system. The requirement for a stable heat output generated by the coils is satisfied using alternating current of higher frequency that is added to the compensation current I_C. The amplitude A of this alternating current changes so that the total heating of both components has a stable mean value P, i.e.,

$$P = \frac{1}{T}\int_0^T R\left(I_C + A\sin 2\pi ft\right)^2 dt,$$

A stands for the amplitude of the alternating current, T for its period and f for its frequency. R is the effective resistance of the coils. The compensation current I_C can be assumed constant during one period of the alternating current. Then the amplitude A satisfies

$$A^2 = 2\left(I_0^2 - I_C^2\right),$$

where the constant $I_0 = P/R$ determines the range of heat compensation. For technical reasons, the value $I_0 = 7$ mA was used. For the constant of the electro-magnetic device equal to 0.328 mGal/mA this range should be ±2.3 mGal.

The amplitude A depends only on I_0 and I_C. It reaches its maximum of 9.9 mA for $I_C = 0$, which corresponds to the amplitude of acceleration 3.25 mGal.

The frequency of the alternating current was chosen at level of 50 Hz. This current does not deflect the gravimeter's beam. It causes only slight vibration of the beam with this frequency. The mechanical measuring system of the gravimeter damps these vibrations by-70 dB, i.e., with a coefficient of 3.2×10^{-4}.

The block diagram of the digital feedback system is depicted in Fig. 5. Its key component is the 16-bit processor ADSP-2181 made by Analog Devices. To measure the output voltage of the gravimeter, the sigma-delta converter AD7712 is used. The 16-bit DA converter is used to regulate the gravimeter. It is followed by the voltage - current converter. The output current, that is directly proportional to the gravity changes, is read by the resistor of 100 Ω and measured by another converter AD7712. The voltage output with a filter of 2nd order (to suppress the alternating component of the signal) can be used for eventual analog recording. The processor is connected to a PC via modules TTL/RS485 and UC485.

The regulation is solved in such a way that the transfer function of the gravimeter is preserved, i.e., the feedback system does not cause any time delay of the signal. Sampling frequency is 25 Hz. The used AD converter is equipped with the digital filter that suppresses any signal with frequency equal to multiplication of the frequency 25 Hz. The regulator computes 5 second averages of the compensation current.

Software consists of two programs. A service program is in the EPROM, a regulation program is in the FLASH memory.

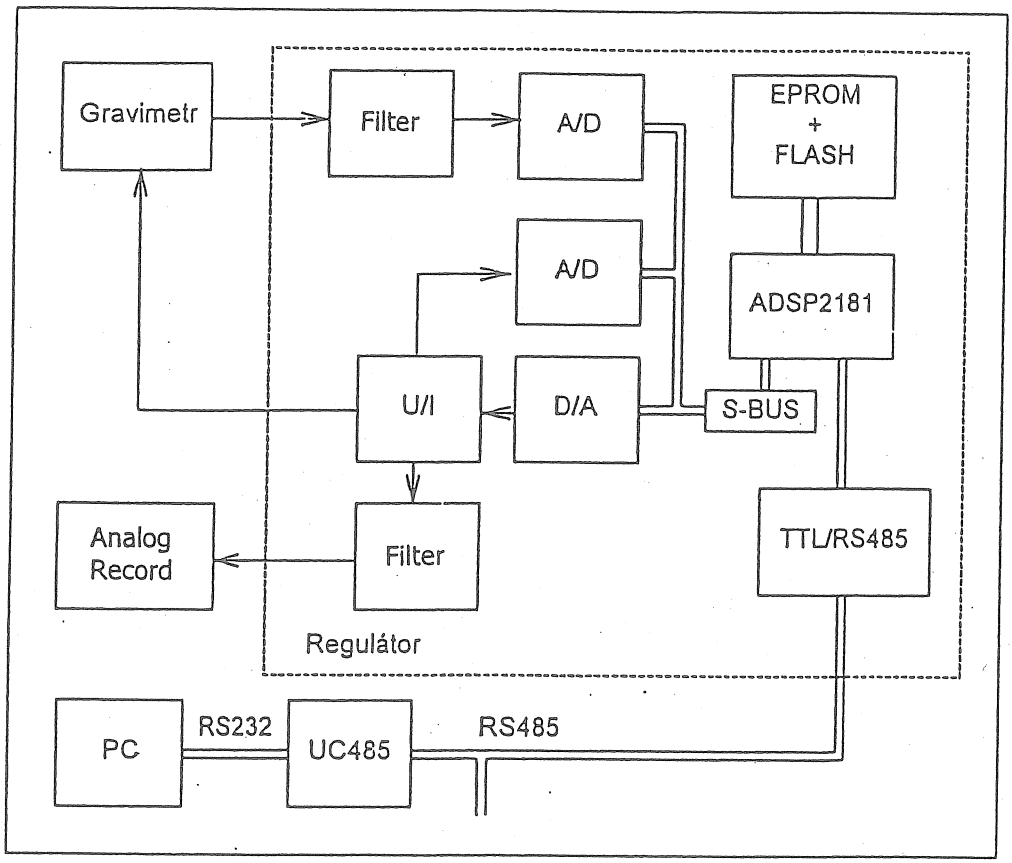

Fig. 5. Block diagram of the digital feedback device

The PC reads, after each 30th second UT, 13 five second averages of the compensation current I_C from the feedback. It estimates at the same time a correction of the regulator's clock. From these data, a value corresponding to each minute UT is computed by weighted averaging. The internal clock in the PC is controlled by DCF-77. The scale of the record is approximately 0.329 μGal / μA. Additional data are recorded together with the gravimetric data. The data are stored in the computer as the following four files:

The file rrrrmmdd.log contains five second averages of the tidal signal in μA .

The file rrrrmmdd.sut contains minute averages of the tidal signal and their MSE. This file is used for computation of the record calibration.

The file rrrrmmdd.sgt contains minute averages of the tidal signal in μA as well as minute samples of air pressure in hPa. These data are used after pre-processing in the tidal analysis.

The file rrrrmmdd.met contains hourly values of additional data such as the air pressure in hPa, air temperature in the chamber with the gravimeter and in the recording room in degree Celsius (°C), air humidity in the chamber in %, and the elevation of ground water level in m.

Tests of the digital feedback system showed that the actual range of heat compensation, i.e., the interval in μGal around the zero of the system with the constant heat power of the Helmholtz coils, is different from the expected range.

If the measuring screw is set to smaller values on its scale z (smaller than a value corresponding to the zero of the system), the recorded signal is positive. The heat compensation is effective for settings of the values z within the range of ± 0.6 scale division. No disturbances in the drift of the system can be observed, see Fig. 6. Note, that the settings from z = 42.66 to z = 42.96 indicated in Fig. 6 are too large, i.e. they are outside the sensing range of the system. The difference in y between the first and the last setting z = 43.66 is due to not exact setting of the screw.

Fig. 6. Output signal *y* with different settings of the measuring screw *z* in which the signal has positive values (tidal corrections introduced, reduced).

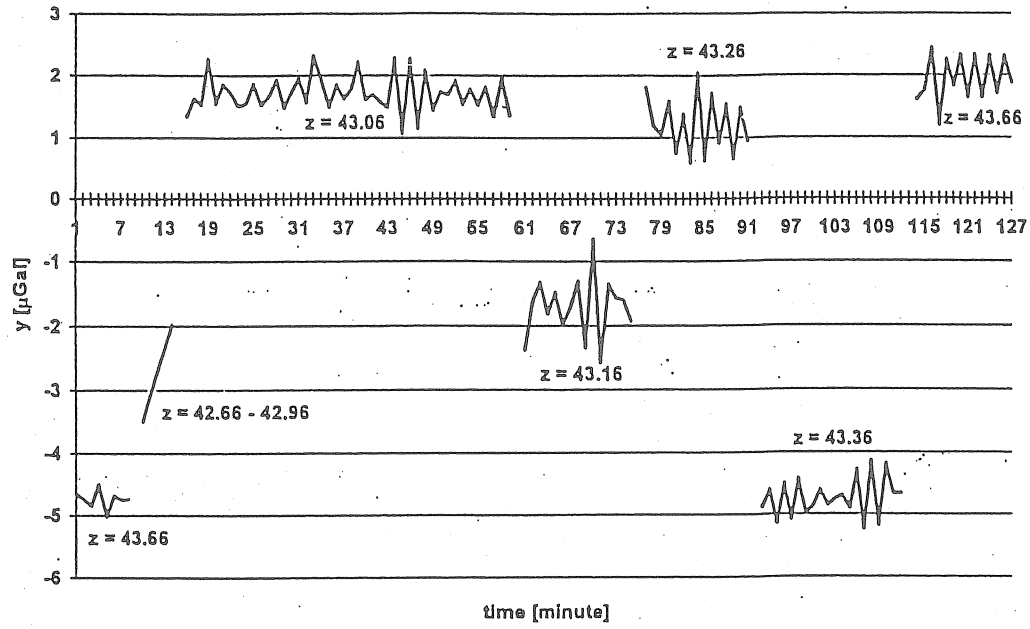

Fig. 7. Output signal *y* with different settings of the measuring screw *z* in which the signal has negative values (tidal corrections introduced, reduced)

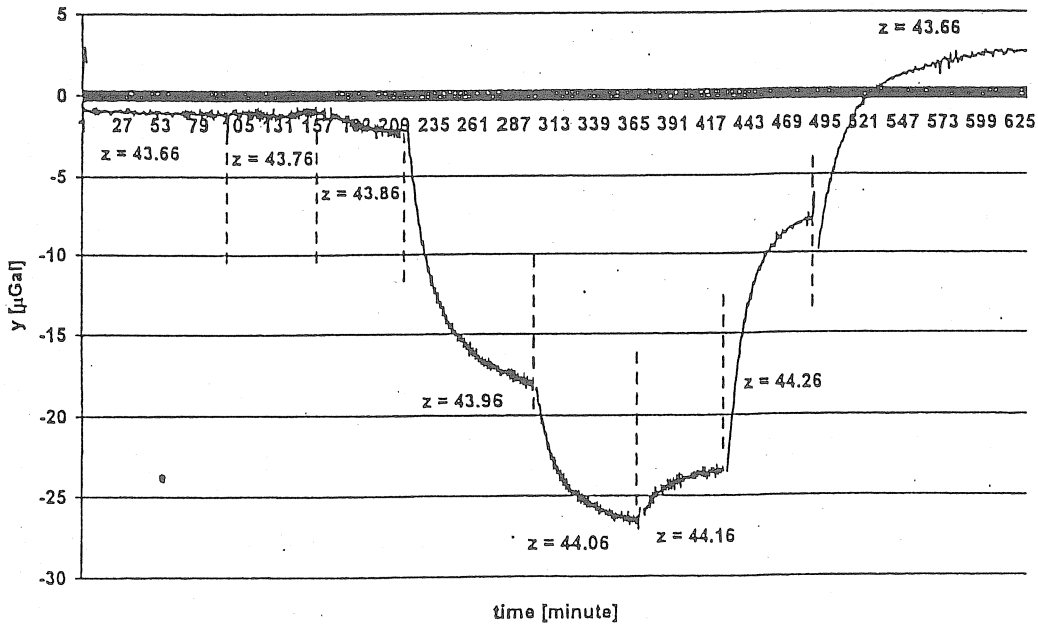

From Fig. 6 it is obvious that all the records with different settings of the measuring screw between 43.66 and 43.06 are parallel i.e. heat compensation is effective.

If the measuring screw is set to larger values, i.e., the recorded signal is negative, the drift of the system is not disturbed for increasing of the value z only up by approximately 0.2 scale division. In the case of further increase of the value z up to approximately 0.4 scale division, transition effects in the direction of the further decrease of the signal can be observed. This corresponds to the loss of the heat produced by the coils, see Fig. 7. For values of z increased up to 0.6 scale division the transition effect is reversed. It corresponds to the repeated increase of the heating in the coils. The disturbances of the drift may reach values up to 25 μGal. The transition effects are stabilised approximately after 90 minutes. The damping of the system does not contribute anything since its time constant is negligibly small (see below) as is also obvious for example from Fig. 6.

Described behaviour of the feedback system has not been eliminated yet. The observation technique must thus be adjusted: registration of the tides must be performed within the range of complete heat compensation, i.e., using the positive signal of the device.

Determination of the proper record scale is more difficult when the non-linearity of the micrometer should be eliminated by resetting the measuring screw during calibration by one scale division. Transition curves of the record for the measuring screw previously set to values larger by 0.5 scale division with respect to the zero with different time intervals can be found in Fig. 8.

Fig. 8. Output signal *y* with the measuring screw settings in which the signal is near zero. Each prior setting was for different period by 0.50 scale division higher.

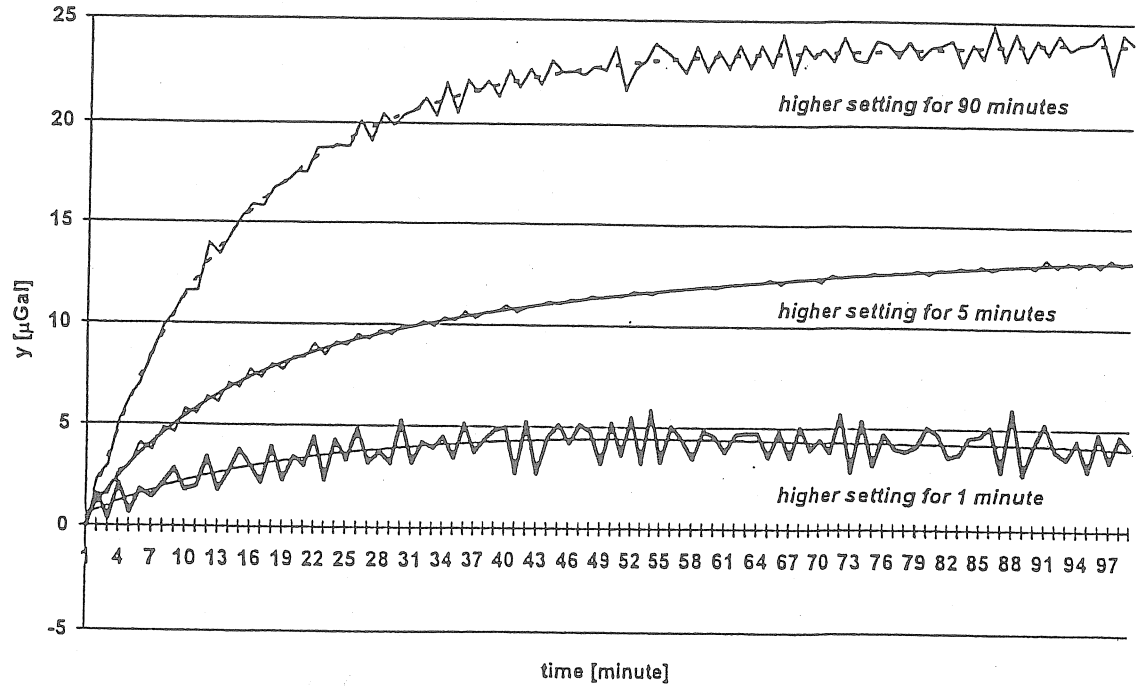

It is obvious that the disturbance is significantly dependent on the time interval during which the larger values were set. If this interval is shorter than 2 minutes, the disturbance reaches approximately 5μGal and disappears completely after 40 minutes. If the measuring screw is reset during the record calibration by 5000 μGal, there will be an error in the record scale up to 0.1 %. If the reading z is increased during the calibration by 0.6 scale division and

decreased by 0.4 scale division, the disturbance is smaller. It may reach only about 2 μGal because, as we can see from Fig. 7, the disturbance with the setting 44.26 is much smaller than that with the setting 44.16.

To establish a methodology for record calibration one has also to take into account that the used one-minute averages of the signal are derived from 13 five-second values distributed in the interval approximately -30 s, +30 s centred at the full minute. The record calibration then consists of the following steps:

1) A reading z_1 is made on the scale of the measuring screw when the signal is close to zero. The record is left to balance for about 40 minutes. The last minute ordinate y_1 is used for the calibration.
2) The measuring screw is set to a reading z_2 smaller by 0.4 of the scale division 5 to 15 seconds after the full minute (the signal is positive). The following minute ordinate y_2 is used for the calibration.
3) We return the measuring screw 40 to 55 seconds after this full minute back to a reading z_3 for which the signal is again near to zero. The recording is performed for 5 minutes. The last minute ordinate y_3 is used for the calibration.
4) The measuring screw is set to a reading z_4 larger by 0.6 of the scale division 5 to 15 seconds after the full minute (the signal is negative). The following minute ordinate y_4 is used for the calibration.
5) 40 to 55 seconds after this full minute, the measuring screw is set to a reading z_5 for which the signal is close to zero. The record is left to balance for 40 minutes and the last ordinate y_5 is used for the calibration.

Further calibrations follow that use the same procedure.

The reading scale k is determined twice from data obtained from the above five steps, i. e. from the pairs (z_1, y_1), (z_2, y_2), (z_3, y_3) and from the pairs (z_3, y_3), (z_4, y_4), (z_5, y_5).The ordinates y are corrected for the tidal effect using preliminary sooner estimated parameters of the tidal waves. The average value k computed from the two estimates is corrected for the non-linearity of the micrometer. The effect of incomplete heat compensation for the negative signal is practically eliminated. Since the steps of the calibration procedure do not proceed uniformly in time, the drift of the apparatus is not excluded from the results. However the drift may reach values at the level of 1 μGal/day and can be neglected.

The damping of the apparatus is difficult to check because it is very small. Introducing a step change on the input using the measuring screw, the transition on the output vanishes in 5 seconds during which the feedback reads and averages the signal. Only seldom there is a transition between two 5 second intervals that allows one to determine approximately the time constant of the apparatus τ.

The feedback systems outputs in the instants t_1 to t_4 average values of the signal from previous five seconds y_1 to y_4. The values y_1 and y_4 are stable but the values y_2 a y_3 are affected by the step, see Fig. 9. Assuming that the step response may be written as follows

$$y=(y_4-y_1)\left(1-e^{-\frac{T}{\tau}}\right),$$

differences (y_2 - y_1) and (y_4 - y_3) may be derived. T denotes an instant measured from the beginning of the step and T_1 corresponds to an instant t_2 .From the ratio of the differences (y_2 - y_1) and (y_4 - y_3) the time constant τ can be determined. From many realised steps only 10 could be used. The estimated value of τ is 0.64 ± 0.02 second.

Fig. 9. Supposed response of the signal after a step change on the input

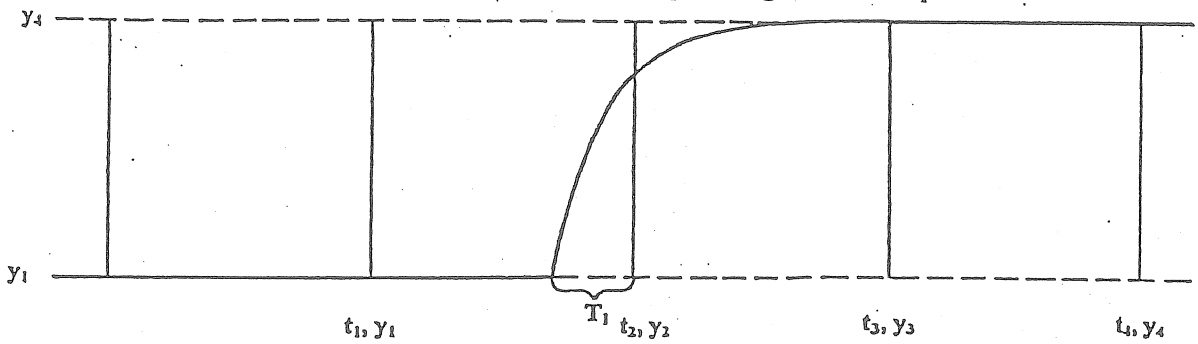

The tidal variations had been recorded using the gravimeter with the feedback system since 20.4. 2000 to 18.9. 2001. Results of the data analysis using the program ETERNA can be found in Table 2. The MSE of the observed hourly ordinate is 0.096 μGal despite many interruptions of the recording caused by frequent tests of the apparatus as well as of the observation methodology. The record was calibrated three times and the analysis was performed with the constant record scale of 0.329316 μGal/μA. No corrections for the damping of the system were introduced. Final values of the amplitude factors δ and the phase delays κ of the tidal waves agree well with previous results at the station. The comparison of the results of all tidal observations at the station Pecný for the main waves is in Table 3. The values κ from the analog recording system are burdened by systematic errors originating in visual reading of the ordinates.

The data were also divided in 17 one-month periods that were analysed individually. The comparison of resulting parameters δ with the results from the analysis of the complete period can be found for the waves O1, K1, M2 and S2 in Fig. 10. No correlations are visible. While the gravimeter without any feedback system suffered from the systematic effect caused by the non-linearity of the capacity sensor of the beam's position and the gravimeter with the analog feedback system by the heat produced by the coils of the calibration system, there are no such effects in the case of the gravimeter with the digital feedback system.

Fig. 10. Variations of the amplitude factors δ from one-month periods of measurement with the digital feedback device (100/% - result of the common analysis)

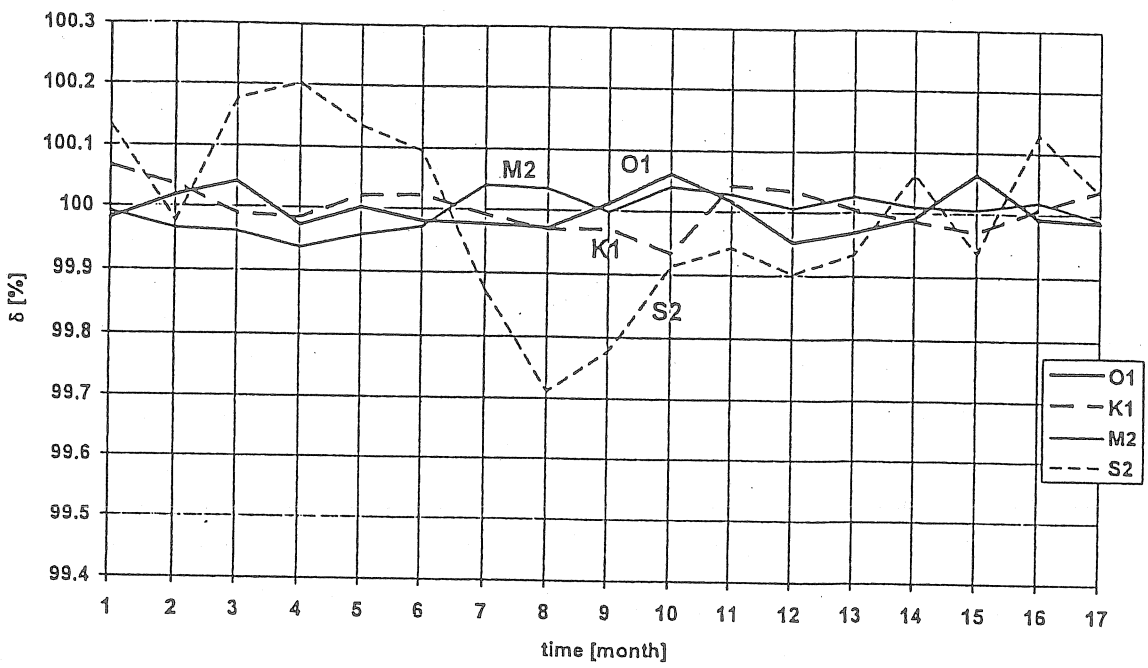

Table 2.

```
Program ETERNA, version 3.21 950117 Fortran 77,    file: 41-00-09
#########################################################################
# GRAVIMETRIC EARTH TIDE STATION  PECNY  NO.0930,  CZECH REPUBLIC      #
# RESEARCH INSTITUTE OF GEODESY, TOPOGRAPHY AND CARTOGRAPHY,ZDIBY      #
#  49.92 N  14.78 E  H 534 M  P 2 M  D 400 KM  VERTICAL COMPONENT      #
# GRAVIMETER ASKANIA GS15 - NO.228   (TECHNICAL UNIVERSITY PRAHA)      #
# DIGITAL FEEDBACK, DIGITAL RECORD                                     #
# CALIBRATION MEASURING SCREW, WITHOUT MICROMETER USE                  #
# INSTRUMENTAL LAG CORRECTED FOR 0.00 DEG O1 AND 0.00 DEG M2           #
# 2000.4.20 - 2001.9.18     513 DAYS                                   #
# INSTALLATION   Z.SIMON, J.BROZ,   MAINTENANCE   J.BROZ              #
# WITHOUT INERTIAL CORRECTION                                          #
#########################################################################

Latitude: 49.9200 deg, longitude:14.7800 deg, azimuth:  0.000 deg.

 Summary of observation data :
20000420 80000...20000825130000  20000828210000...20001031110000
 20001031120000...20010918160000

 Initial epoch for tidal force     : 2000. 4.20. 0
 Number of recorded days in total :   513.08
 TAMURA 1987  tidal potential used. WAHR-DEHANT-ZSCHAU inelastic
 Earth model used. UNITY window used for least squares adjustment.
 Numerical filter is PERTZEV 1959 with  51 coefficients.
 Estimation of noise by FOURIER-spectrum of residuals
 0.1 cpd band99999.9990 nm/s**2       1.0 cpd band    0.0367 nm/s**2
 2.0 cpd band    0.0298 nm/s**2       3.0 cpd band    0.0236 nm/s**2
 4.0 cpd band    0.0225 nm/s**2       white  noise    0.0222 nm/s**2

 adjusted tidal parameters :
 from      to       wave   ampl. ampl.fac.    stdv. ph. lead    stdv.
 [cpd]     [cpd]      [nm/s**2 ]                      [deg]     [deg]

 0.721500 0.906315 Q1    67.098   1.14466  0.00034  -0.1517   0.0195
 0.921941 0.940487 O1   351.560   1.14829  0.00007   0.1436   0.0040
 0.958085 0.974188 M1    27.637   1.14779  0.00119   0.3725   0.0680
 0.989049 0.998028 P1   163.818   1.14996  0.00015   0.1475   0.0085
 0.999853 1.000147 S1     3.763   1.11732  0.00886   0.8597   0.5074
 1.001825 1.003651 K1   488.673   1.13492  0.00005   0.1630   0.0029
 1.005329 1.005623 PSI1   4.129   1.22586  0.00629   0.0913   0.3608
 1.007595 1.011099 PHI1   7.205   1.17516  0.00341  -0.4287   0.1962
 1.013689 1.044800 J1    27.781   1.15382  0.00077   0.1267   0.0442
 1.064841 1.216397 OO1   15.139   1.14919  0.00186   0.1652   0.1064
 1.719381 1.872142 2N2   11.032   1.15810  0.00118   2.0204   0.0676
 1.888387 1.906462 N2    70.035   1.17413  0.00025   1.5910   0.0143
 1.923766 1.942754 M2   368.527   1.18289  0.00005   1.2314   0.0030
 1.958233 1.976926 L2    10.526   1.19530  0.00258   1.6073   0.1478
 1.991787 2.002885 S2   170.718   1.17779  0.00012   0.0806   0.0069
 2.003032 2.182843 K2    46.540   1.18115  0.00045   0.1380   0.0258
 2.753244 3.081254 M3     4.265   1.08019  0.00305   0.0300   0.1748
 3.791964 3.937897 M4     0.018   0.39053  0.24192 -35.1252  13.8605

 Adjusted meteorological or hydrological parameters:
 no. regr.coeff.       stdv.  parameter   unit
   1    -3.79874     0.01539  airpress.   nm/s**2 /hPa
 Standard deviation of weight unit:      0.958
 degree of freedom:                      12127
 Standard deviation:                     0.958  nm/s**2
```

Table 3. Comparison of the results of tidal measurements at the Pecný station

Gravimetr	Gs 11 No.131		BN-26		Gs 15 No.228		Gs 15 No.228				Gs 15 No.228 analog feedback digital		Gs 15 No.228 digital feedback digital		LCR 137 analog feedback digital	
Record	analog		analog		analog		digital									
Period	70 09 - 80 02		83 04 - 88 03		76 04 - 95 03		95 12 - 96 09		99 02 - 99 10		97 10 - 99 01		00 04 - 01 09		01 01 - 01 04	
Days	1372		1326		4555		284		233		412		513		90	
Analysis	M 74		M 74		ETERNA 2.1		ETERNA 3.20		ETERNA 3.20		ETERNA 3.20		ETERNA 3.20		ETERNA 3.20	
vlna	$\delta \pm m_\delta$	$\kappa \pm m_\kappa$	$\delta \pm m_\delta$	$\kappa \pm m_\kappa$	$\delta \pm m_\delta$	$\kappa \pm m_\kappa$	$\delta \pm m_\delta$	$\kappa \pm m_\kappa$	$\delta \pm m_\delta$	$\kappa \pm m_\kappa$	$\delta \pm m_\delta$	$\kappa \pm m_\kappa$	$\delta \pm m_\delta$	$\kappa \pm m_\kappa$	$\delta \pm m_\delta$	$\kappa \pm m_\kappa$
O_1	1.1490	0.15	1.1486	-0.02	1.1479	-0.01	1.1491	0.09	1.1489	0.11	1.1490	0.09	1.1483	0.14	1.1484	0.06
	11	0.06	12	0.06	2	0.01	2	0.01	2	0.01	1	0.01	1	0.00	2	0.01
K_1	1.1362	0.42	1.1362	0.21	1.1348	0.06	1.1354	0.18	1.1365	0.19	1.1364	0.15	1.1349	0.16	1.1353	0.17
	7	0.04	8	0.05	2	0.01	1	0.01	1	0.01	1	0.00	1	0.00	2	0.01
M_2	1.1847	1.28	1.1844	1.08	1.1849	1.03	1.1839	1.22	1.1836	1.21	1.1840	1.20	1.1829	1.23	1.1829	1.21
	6	0.03	6	0.03	2	0.01	1	0.01	1	0.01	1	0.00	1	0.00	1	0.01
S_2	1.1805	0.88	1.1792	-0.04	1.1798	0.14	1.1807	-0.04	1.1784	0.09	1.1799	-0.01	1.1778	0.08	1.1806	0.07
	13	0.07	12	0.07	3	0.01	2	0.01	2	0.01	2	0.01	1	0.01	3	0.02
m_o [μGal]					0.474		0.149		0.121		0.091		0.096		0.073	

References:

BROŽ, J. - ŠIMON, Z. - VANKA, P. - ZEMAN, A. (1997): High Accurate Tidal Data from a Gs 15 Gravimeter. B.I.M. No. 128, pp 9893 - 9905.

CHEN YI HUI - ZHU HAN YUN - GUO ZI QIANG - LEI YU TIAN (1986): Magnetic Feedback of GS 15 Gravimeter and Digital Record. Proceedings of the 10th Intern. Symp. Earth Tides, pp 21 - 26. Consejo Sup. de Invest. Cientific., Madrid.

OREJANA, M. - VIEIRA, R. (1984): Transforming an Askania Gs 15 Gravimeter into a Zero Gravimeter. Proceedings of the 9th Intern. Symp. Earth Tides, pp 311 - 313. Schweizerbart'sche Verlagsbuchhandlung, Stuttgart.

SCHULZE, R. (1965): Eine neue Eicheinrichtung im Gezeitengravimeter. Askania - Warte, H.66.

ŠIMON, Z. - BROŽ, J. (1993) : Calibration of Askania Gravimeter Record. B.I.M.No 115, pp. 8478 - 8483.

WENZEL, H.-G. (1994): Accurate Instrumental Phase Lag Determination for Feedback Gravimeters. B.I.M. No. 118, 8735-8752.